

2021

Coaxially Electrospun fibrous Polymer Scaffolds for Tissue Regeneration and Drug Delivery

Matthew Michael Kleszynski
mmkleszynski@gmail.com

Follow this and additional works at: <https://huskiecommons.lib.niu.edu/allgraduate-thesedissertations>



Part of the [Materials Science and Engineering Commons](#), [Mechanical Engineering Commons](#), and the [Polymer Chemistry Commons](#)

Recommended Citation

Kleszynski, Matthew Michael, "Coaxially Electrospun fibrous Polymer Scaffolds for Tissue Regeneration and Drug Delivery" (2021). *Graduate Research Theses & Dissertations*. 7258.
<https://huskiecommons.lib.niu.edu/allgraduate-thesedissertations/7258>

This Dissertation/Thesis is brought to you for free and open access by the Graduate Research & Artistry at Huskie Commons. It has been accepted for inclusion in Graduate Research Theses & Dissertations by an authorized administrator of Huskie Commons. For more information, please contact jschumacher@niu.edu.

ABSTRACT

COAXIALLY ELECTROSPUN FIBROUS POLYMER SCAFFOLDS FOR TISSUE REGENERATION AND DRUG DELIVERY

Matthew Kleszynski, MS
Department of Engineering
Northern Illinois University, 2021
Sahar Vahabzadeh, Advisor

A biomaterial is a substance that is specifically engineered to take on a role within the body, either alone or in conjunction with other materials, with the purpose of influencing the body. Using polymers as a biomaterial is an exciting field of study that has the potential to further our abilities to help those in need. Creating composite nanofibrous scaffolds composed of hydrophobic and hydrophilic polymers may outperform structures made of a single polymer in both *in vitro* and *in vivo* environments. Hydrophilicity governs the behavior of polymers in the body that and has influence over the mechanical properties of the polymer.

The polymers of interest in our current work are polycaprolactone (PCL) and Poly(lactic-co-glycolic acid) (PLGA). PCL is a synthetic polymer with hydrophobic properties and a relatively high degradation rate in the body that can be used to make biodegradable scaffolds. PLGA is also a synthetic polymer, but hydrophilic, which has excellent bio-adhesion. In the current work, polymers have been fabricated by electrospinning method to create fibrous scaffolds. Electrospinning as a fiber production method was first attempted in 1888 and since then has been used to create polymer fibers by controlling the voltage, concentration, feed rate, and plate distance. A composite fibrous scaffold composed of a hydrophobic and hydrophilic

polymer may result in better physical and mechanical properties and improve its performance in biological environment, as compared to non-composite scaffolds. The core-shell method is a composite electrospinning technique that creates a fiber out of two concentric components polymers. In this work the core-shell fabrication technique was used to create a concentric fiber with an outer layer composed of 7.5% w/v PCL and an inner layer composed of 35% w/v (50:50) PLGA. For the core-shell composite fibers, PCL was chosen as the shell material as its hydrophobic properties would act as a barrier prolonging drug release and reducing the initial burst. PLGA was used as the core material because its more hydrophilic nature gives it better drug encapsulation efficiency. This was achieved by first optimizing the electrospinning process of the individual polymers.

The results are considered optimized by first examining the electrospinning process, especially the Taylor cone, provided that the Taylor cone is stable and consistent. The fibers are then examined under an SEM where the fiber morphology is characterized and any abnormalities such as beading could be seen. The first step taken was optimizing monoaxial PCL fibers. This was done by electrospinning 7.5% (w/v) PCL in HFIP at various feed rates, voltages, and plate distances. Through experimentation it was determined that an applied voltage from 7.0-8.0 kV, a 1.5 mL/h feed rate, and a 10 cm plate distance resulted in the best fibers. Monoaxial PLGA fibers were then optimized using 35% (w/v) PLGA in HFIP and the PCL parameters. Using an applied voltage of 7.0-8.0 kV the feed rate had to be decreased to 1.1 mL/h to improve fiber consistency with a 10 cm plate distance. The production of core-shell composite electrospun fibers with a PLGA core and a PCL shell was successful under a 7.0-8.0 kV applied voltage, a

1.1-1.5 mL/h core-shell feed rate or a 0.9-1.5 mL/h core-shell feed rate, and a 10 cm plate distance.

This research did not find a clear relationship between core feed rate and overall core-shell fiber diameter. The impact of voltage outside the optimized range on core-shell fibers was found to increase the range of fiber diameters produced. Increasing relative humidity was studied and found to have a direct impact on core-shell fiber diameter. The core-shell scaffolds produced in this work can be used as drug delivery vehicles in tissue engineering or as composite scaffolds in soft tissue regeneration. Periodontal disease treatment, therapeutic reparation, and bone tissue regeneration have already found improvements using PCL based scaffolds. The successful electrospinning of these core-shell fibers opens future research to investigate the impact electrospinning parameters have on the mechanical, drug release, and degradation properties of PLGA-PCL core-shell fibers.

NORTHERN ILLINOIS UNIVERSITY
DE KALB, ILLINOIS

MAY 2021

COAXIALLY ELECTROSPUN FIBROUS POLYMER SCAFFOLDS FOR
TISSUE REGENERATION AND DRUG DELIVERY

BY

MATTHEW MICHAEL KLESZYNSKI

©2020 Matthew Michael Kleszynski

A THESIS SUBMITTED TO THE GRADUATE SCHOOL
IN PARTIAL FULFILLMENT OF THE REQUIREMENTS
FOR THE DEGREE
MASTER OF SCIENCE

DEPARTMENT OF MECHANICAL ENGINEERING

Thesis Director:

Sahar Vahabzadeh

ACKNOWLEDGEMENTS

Throughout this process I have been blessed by many of my colleagues and superiors lending their time, expertise, and resources to assist me on this project, without them I would have been lost. First, I would like to thank my primary thesis adviser, Dr. Sahar Vahabzadeh, without her there would have been no project. Under her tutelage I have learned more about biomaterials and more specifically biopolymers that not only allowed me to proceed with this research but has sparked a desire to continue future works as well. My co-thesis advisor Dr. Nicholas Pohlman also has my gratitude for assisting me with the research through these unprecedented times.

Next, I would like to thank Dr. Bobby Sinko who imparted me with some of his extensive knowledge working with polymers and gave insight on the relations between polymer properties and mechanical properties. I would also like to thank Stephen Binderup and Dr. Paige Bothwell who took time to introduce, demonstrate, and train me on the various machines that would be used throughout this project. Lastly, I would like to thank Jeannie Peterson who was always available to help me through the intricacies of the master's program as well as all the faculty and staff in the Mechanical Engineering program and the Thesis Department at Northern Illinois University for their help and commitment to learning. The assistance provided to me ensured that my research was focused and I remained diligent in keeping within the scope of the project, through this I have broadened my perspective on biomaterials and materials in general making me a better and more knowledgeable engineer.

DEDICATION

This thesis is dedicated to my parents, Michael and Sharon Kleszynski; Jon, Susan, and Kathrine Wright; and the family and friends who supported me throughout my education.

TABLE OF CONTENTS

	Page
LIST OF TABLES.....	vii
LIST OF FIGURES.....	viii
LIST OF ABBREVIATIONS	xiii
CHAPTER 1 INTRODUCTION	1
1.1 Research background and significance	1
1.2 Current scaffold production approaches.....	4
1.3 Current applications of fibrous scaffolds.....	6
1.4 Techniques for fiber fabrication	10
1.5 Introduction to electrospinning.....	10
1.6 Electrospinning techniques.....	12
1.6.1 Solution electrospinning.....	12
1.6.2 Melt electrospinning.....	13
1.7 Fabrication techniques.....	14
1.7.1 Monoaxial electrospinning	14
1.7.2 Collector selection	14
1.8 Composite electrospinning techniques	15
1.8.1 Blending	15
1.8.2 Layering.....	19
1.8.3 Multiaxial electrospinning.....	20
1.9 Previous work.....	23
1.9.1 Research goal and main tasks	26
CHAPTER 2 MATERIALS AND METHODS	28
2.1 Solution preparation.....	28
2.2 Electrospinning Process	30
2.3 Optimization process	31
2.4 Characterization process.....	33

	Page
2.5 Statistical analysis	34
CHAPTER 3 MONOAXIAL POLY(CAPROLACTONE)	36
3.1 Introduction	36
3.2 Results	37
3.2.1 Fiber optimization	37
3.2.2 SEM	38
3.2 ATR-FTIR bond analysis	44
3.3 Discussion.....	45
3.3.1 Fiber diameter.....	45
3.3.2 Tensile strength.....	46
3.3.3 Degradation rate	48
3.3.4 Drug release	49
3.4 Summary	50
CHAPTER 4 MONOAXIAL POLY(LACTIC-CO-GLYCOLIC) ACID.....	52
4.1 Introduction	52
4.2 Results	54
4.2.1 SEM	54
4.2.2 ATR-FTIR bond analysis	70
4.3 Discussion.....	72
4.3.1 Impact of feed rate	72
4.3.2 Impact of voltage	73
4.3.3 Impact of concentration	75
4.3.4 Fiber diameter.....	76
4.3.5 Mechanical strength	78
4.3.6 Degradation	80
4.3.7 Drug release	81
4.4 Summary	81
4.5 Future work.....	82
CHAPTER 5 COAXIAL CORE-SHELL.....	84

	Page
5.1 Introduction	84
5.2 Results.....	85
5.2.1 SEM	85
5.2.2 ATR-FTIR Bond Analysis.....	108
5.2.3 TEM	109
5.3 Discussion.....	110
5.3.1 Impact of feed rate	111
5.3.2 Impact of voltage	112
5.3.3 Impact of humidity.....	113
5.3.4 Fiber diameter.....	113
5.3.5 Core-shell integrity.....	114
5.3.6 Degradation	115
5.3.7 Drug release	116
5.4 Summary	116
5.5 Future work.....	117
REFERENCES.....	119
APPENDIX: ELECTROSPINNING SOP.....	138
A.1 Safety	140
A.2 Maintenance	140
A.2.1 Electrical	140
A.2.2 Hardware	140
A.3 Solution preparation.....	142
A.4 Electrospinning procedure	146
A.4.1 Parts of the electrospinner	146
A.4.2 Safe use of the NanoSpinner	149
A.4.3 Electrospinning quick start	149
A.4.4 Monoaxial electrospinning	151
A.4.5 Coaxial electrospinning.....	152

LIST OF TABLES

	Page
Table 1 Advantages and disadvantages of various fiber production techniques [17].....	6
Table 2 Polymer structure and properties	25
Table 3 Impact of voltage on monoaxial PCL fiber diameter at 1.5 mL/h and 10 cm	42
Table 4 Impact of feed rate on monoaxial PLGA (50:50) fiber diameter at 25% w/v 7.5 kV and 10 cm.....	57
Table 5 Impact of feed rate on monoaxial PLGA (50:50) fiber diameter at 25% w/v 8 kV and 10 cm.....	60
Table 6 Impact of feed rate on monoaxial electrospun (50:50) PLGA at 35% w/v 7 kV and 10 cm	65
Table 7 Impact of feed rate on monoaxial PLGA (50:50) fiber diameter at 35% w/v 7.5 kV and 10 cm.....	66
Table 8 Impact of feed rate on monoaxial PLGA (50:50) fiber diameter at 35% w/v 8 kV and 10 cm.....	67
Table 9 Impact of feed rate on coaxial fiber diameter at 7.5 kV and a 10 cm plate distance	87
Table 10 Impact of Feed Rate on Coaxial Fiber Diameter at 8 kV and a 10 cm plate distance ...	89
Table 11 Impact of feed rate on coaxial fiber diameter at 7.5 kV and a 15 cm plate distance	92
Table 12 Impact of feed rate on coaxial fiber diameter at 8 kV and a 15 cm plate distance	97
Table 13 Impact of feed rate on coaxial fiber diameter at 8.5 kV and a 15 cm plate distance ...	101

LIST OF FIGURES

	Page
Figure 1 Conceptual image of tissue-biomaterial interaction [7]	2
Figure 2 Polymeric scaffolds produced by electrospinning of A) Collagen, B) Polyacrylic acid, C) Polycaprolactone, D) Polyvinyl alcohol [15].....	4
Figure 3 A) Cell proliferation and regeneration on PVA-PCL-HAB scaffolds for bone regeneration B) In vivo ectopic bone formation on subcutaneous implantation after eight weeks [25].....	8
Figure 4 Images of scaffolds designed for various applications A) Diagram of multilayered aortic valve cusp using collagen fibers [29] B) SEM images of P(LLA-CL) and SF/P(LLA-CL) fibrous scaffolds for myocardial infarction [31] C) SEM images of PDL cells on honeycomb film (HF) for periodontal regeneration [35]	9
Figure 5 Taylor cone formation of electrospinning PEO/water at various voltages A) 0.47 kV/cm B) 0.53 kV/cm C) 0.60 kV/cm D) 1kV/cm [42] B stages of flow in electrospinning [43]	11
Figure 6 Diagram of a typical solution electrospinning setup, depositing onto a drum [48]	13
Figure 7 Effects of collector on pure PHB and PHB/plasticizer/PANI blended fibers A) stress- strain curves a) pure PHB 610rpm drum b) 79/20/1 blend 610rpm drum c) 79/20/1 blend plate d) 80/20 blend plate [55]	16
Figure 8 A) Conceptual image of the blended-fiber electrospinning process [57] B) Engineering stress vs. elongation curve for different blends of PCL:PET [58].....	18

Figure 9 FESEM images of PA-6 (35% w/v), EEP blended fibers A) 20% (w/v) EEP B) 30% (w/v) EEP C) 40% (w/v) EEP D) 50% (w/v) EEP [60].....	18
Figure 10 A) Conceptual image of a composite scaffold produced by layering B) Layered PCL scaffold for tubular structure formation [63]	20
Figure 11 A) Mechanical strength of coaxial silk fibroin/silk sericin to monoaxial silk fibroin B) Stress strain curve of coaxial silk fibroin/silk sericin to monoaxial silk fibroin [66].....	21
Figure 12 Diagram of standard coaxial electrospinning with Taylor cone [68]	22
Figure 13 Rhodamine B release graphs A) Cumulative release vs. time lines are experiment vs simulation B) Release dependence on layer thickness lines are different thicknesses (um) C) Effect of hydrophobicity lines are different partitions [71]	24
Figure 14 Phase diagram of research goals and tasks.....	26
Figure 15 Electrospinning decision tree	35
Figure 16 SEM images of 5% (w/v) PCL/HFIP electrospun at 1.2 mL/h 15cm 12kV A) 0.15k magnification, B) 0.5k magnification, C) Cutaway images of beading found in A D) 2k magnification	39
Figure 17 7.5% (w/v) PCL/HFIP electrospun at 1.5mL/h 15cm 7kV A) 0.5k magnification B) 1k magnification C) 2k magnification, C) 2k magnification.....	40
Figure 18 7.5% (w/v) PCL/HFIP electrospun at 1.5mL/h 10cm 7kV A) 0.5k magnification B) 1k magnification C) 2k magnification D) 2k magnification.....	41
Figure 19 SEM images of PCL electrospun fibers 10cm 1.5mL/h A) 7kV 2k B) 7.5kV 2k, C) 8kV 2k D) 8kV 11k.....	42

Figure 20 Phase diagram of PCL process	43
Figure 21 ATR-FTIR analysis of a pure PCL scaffold.....	44
Figure 22 SEM images of (50:50) PLGA electrospun at 8.0 kV, 15% w/v, 1.2 mL/h, and 15 cm plate distance imaged at 1k magnification A) Spot A B) Spot B	55
Figure 23 SEM images of (50:50) PLGA electrospun at 7.5 kV, 25% w/v, and 10 cm plate distance A) 0.9 mL/h 1k B) 0.9 mL/h 2k C) 1.1 mL/h 1k D) 1.1 mL/h 2k E) 1.3 mL/h 1k f) 1.3 mL/h 2k.....	56
Figure 24 SEM images of (50:50) PLGA electrospun at 8.0 kV, 25% w/v, and 10 cm plate distance A) 1.1 mL/h 1k B) 1.1 mL/h 2k C) 1.3 mL/h 1k D) 1.3 mL/h 2k E) 1.5 mL/h 1k F) 1.5 mL/h 2k.....	59
Figure 25 Phase diagram of the 25% (w/v) process	62
Figure 26 SEM imagery of electrospun (50:50) PLGA at 35% w/v 10 cm A) 7 kV 1.1 mL/h 1k B) 7 kV 1.1 mL/h 2k C) 7 kV 1.3 mL/h 1k D) 7 kV 1.3 mL/h 2k E) 7.5 kV 1.1 mL/h 1k F) 7.5 kV 1.1 mL/h 2k G) 7.5 kV 1.3 mL/h 1k H) 7.5 kV 1.3 mL/h 2k I) 8 kV 1.1 mL/h 1k J) 8 kV 1.1 mL/h 2k K) 8 kV 1.3 mL/h 1k L) 8 kV 1.3 mL/h 2k.....	64
Figure 27 Impact of voltage on monoaxial PLGA (50:50) fiber diameter at 35% w/v and 10 cm (*) p<.05 (**) p<.01.....	68
Figure 28 Impact of concentration on monoaxial PLGA (50:50) fiber diameter at 10 cm	69
Figure 29 Phase diagram of the 35% (w/v) process	70
Figure 30 ATR-FTIR analysis of (50:50) PLGA scaffolds	71

Figure 31 SEM imagery of 35% w/v PLGA (50:50) – 7.5% w/v PCL core-shell fibers electrospun at a plate distance of 10 cm with a 7.5 kV applied voltage A) 0.5-1.5 mL/h feed rate (core-shell) 1k B) 0.5-1.5 mL/h feed rate (core-shell) 2k C) 0.9-1.5 mL/h feed rate (core-shell) 1k D) 0.9-1.5 mL/h feed rate (core-shell) 2k E) 1.1-1.5 mL/h feed rate (core-shell) 1k 1.1-1.5 mL/h feed rate (core-shell) 2k.....	86
Figure 32 SEM imagery of 35% w/v PLGA (50:50) – 7.5% w/v PCL core-shell fibers electrospun at a plate distance of 10 cm with an 8 kV applied voltage A) 0.9-1.5 mL/h feed rate (core-shell) 1k B) 0.9-1.5 mL/h feed rate (core-shell) 2k C) 1.1-1.5 mL/h feed rate (core-shell) 1k D) 1.1-1.5 mL/h feed rate (core-shell) 2k E) 1.3-1.5 mL/h feed rate (core-shell) 1k 1.3-1.5 mL/h feed rate (core-shell) 2k.....	88
Figure 33 SEM imagery of 35% w/v PLGA (50:50) – 7.5% w/v PCL core-shell fibers electrospun at a plate distance of 15 cm with a 7.5 kV applied voltage A) 0.5-1.5 mL/h feed rate (core-shell) 1k B) 0.5-1.5 mL/h feed rate (core-shell) 2k C) 0.7-1.5 mL/h feed rate (core-shell) 1k D) 0.7-1.5 mL/h feed rate (core-shell) 2k E) 0.9-1.5 mL/h feed rate (core-shell) 1k F) 0.9-1.5 mL/h feed rate (core-shell) 2k G) 1.1-1.5 mL/h feed rate (core-shell) 1k H) 1.1-1.5 mL/h feed rate (core-shell) 2k I) 1.3-1.5 mL/h feed rate (core-shell) 1k J) 1.3-1.5 mL/h feed rate (core-shell) 2k.....	91
Figure 34 SEM imagery of 35% w/v PLGA (50:50) – 7.5% w/v PCL core-shell fibers electrospun at a plate distance of 15 cm with an 8 kV applied voltage A) 0.9-1.5 mL/h feed rate (core-shell) 1k B) 0.9-1.5 mL/h feed rate (core-shell) 2k C) 1.1-1.5 mL/h feed rate (core-shell)	

1k D) 1.1-1.5 mL/h feed rate (core-shell) 2k E) 1.3-1.5 mL/h feed rate (core-shell) 1k F) 1.3-1.5 mL/h feed rate (core-shell) 2k.....	96
Figure 35 SEM imagery of 35% w/v PLGA (50:50) – 7.5% w/v PCL core-shell fibers electrospun at a plate distance of 15 cm with an 8.5 kV applied voltage A) 0.9-1.5 mL/h feed rate (core-shell) 1k B) 0.9-1.5 mL/h feed rate (core-shell) 2k C) 1.1-1.5 mL/h feed rate (core-shell) 1k D) 1.1-1.5 mL/h feed rate (core-shell) 2k E) 1.3-1.5 mL/h feed rate (core-shell) 1k F) 1.3-1.5 mL/h feed rate (core-shell) 2k.....	99
Figure 36 SEM imagery of 35% w/v PLGA (50:50) – 7.5% w/v PCL core-shell fibers electrospun at a plate distance of 10 cm with a 1.1-1.5 mL/h feed rate (core-shell) A) 1k magnification 7.5kV 65% rel. humidity B) 2k magnification of A C) 1k magnification 7.5kV 25% rel. humidity D) 2k magnification of C	102
Figure 37 Impact of humidity on fiber diameter at 7.5 kV (*) p<.05 (**) p<.01	103
Figure 38 Impact of voltage on fiber diameter at 15 cm plate distance (*) p<.05 (**) p<.01	105
Figure 39 Impact of plate distance on fiber diameter at 7.5 kV (*) p<.05 (**) p<.01.....	105
Figure 40 Phase diagram of core-shell process with a 10 cm plate distance.....	107
Figure 41 Phase diagram of core-shell process with a 15 cm plate distance.....	108
Figure 42 ATR-FTIR of core-shell PLGA-PCL.....	109
Figure 43 TEM images A) 100 magnification B) 20k magnification 1.1 mL/h core feed rate C) 20k magnification 0.7 mL/h core feed rate.....	110

LIST OF ABBREVIATIONS

PCL	Polycaprolactone
PLGA	Ploy(lactic-co-glycolic) acid
PLA	Polylactic acid
PLLA	Poly-L-Lactic acid
PGA	Polyglycolic acid
PAA	Polyacrylic acid
COL	Collagen
PVA	Polyvinyl alcohol
PEO	Polyethylene oxide
PHB	Polyhydroxybutyrate
PANI	Polyaniline
F-127	Fibrinogen from bovine plasma
PET	Polyethylene terephthalate
NVP	1-vinyl-pyrrolidinone
BMA	n-butyl-methacrylate

CHAPTER 1

INTRODUCTION

1.1 Research background and significance

A biomaterial is a substance that is specifically engineered to take on a role within the body, either alone or in conjunction with other materials, with the purpose of influencing the body. Biomaterials can consist of polymers [1], ceramics [2], metals [3], or composites [4] depending on the intended application and desired material properties. Biomaterials are characterized by their interaction with living tissue; they can be bioinert, bioactive, or biodegradable. Bioinert materials do not interact with the tissues or functions of the host organism; these materials were some of the first biomaterials produced. The purpose of inert biomaterials is to fulfill a mechanical role or purpose and to improve the body's ability to function [5]. Bioactive materials interact directly with cells and tissues through pathways to elicit a biological response. Biodegradable materials can be further characterized by how they degrade in the body. Traditional degradable materials will lose their mechanical properties over time in the body. This degradation leads to the material releasing byproducts that are not absorbed into the body and may need to be removed by surgery. Bioresorbable material byproducts from degradation are absorbed into the body, eliminating the need for a second removal surgery [6]. Figure 1 shows a conceptual demonstration of how the body interacts with a biomaterial.

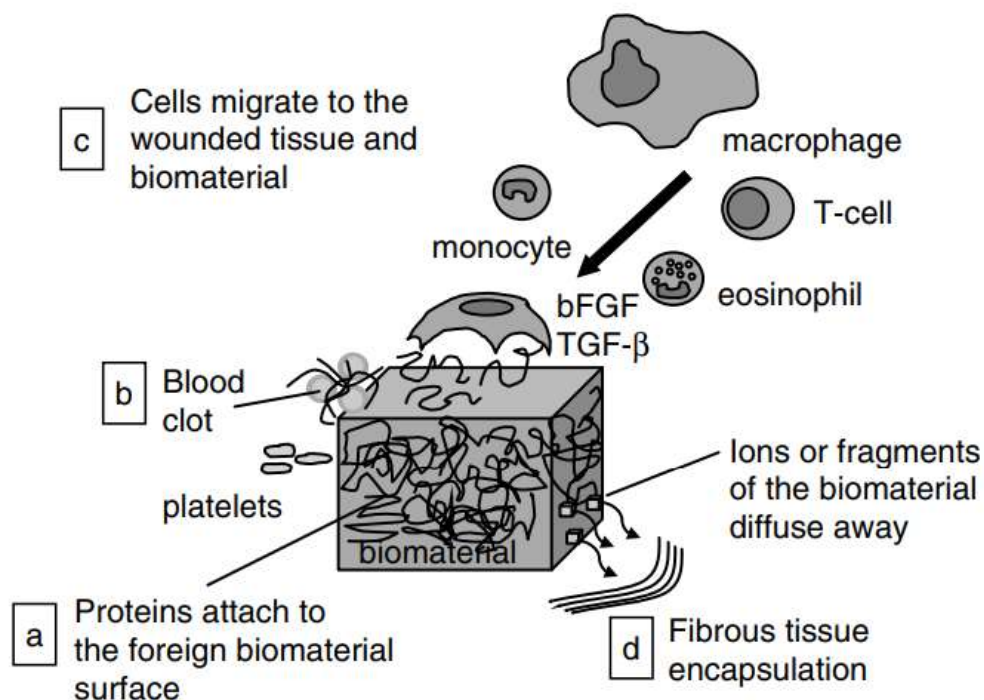


Figure 1 Conceptual image of tissue-biomaterial interaction [7]

Biomaterials can be natural or synthetic, based on where they are derived. Synthetic biomaterials include metals, ceramics, and polymers that have been produced by man. Synthetic biomaterials are easier to produce but do not mimic the structure and composition of the tissue they are implanted in, reducing their biocompatibility. Natural biomaterials can be protein-based, polysaccharide-based, and decellularized tissue. While these materials have to be harvested from living organisms, natural biomaterials have better bioadhesion and can further promote tissue repair in the body [8]. The most sophisticated biomaterials being researched are biomimetic; these materials are engineered to have the same or very similar mechanical, chemical, and morphological properties as the tissues they are replacing [9].

Biomaterials play an important role in modern medicine. They are used to assist, improve, or replace tissue or a biological function by acting as medical implants, tissue regenerators, biosensors, and drug delivery systems [10]. The use of biomaterials did not become practical until aseptic surgical techniques were developed to mitigate infection. The significance of biomaterials has been demonstrated through their uses in the skeletal, nervous, and muscular systems as well as their use in organ repair [11]. Polymeric biomaterials are commonly used as scaffolds (images of polymeric scaffolds are shown in Figure 2). These scaffolds are composed of collagen, polycaprolactone, polyacrylic acid, and polyvinyl alcohol. Scaffolds are defined as three-dimensional porous or solid biomaterials designed to perform tasks that fall under tissue engineering (TE) [12]. Tissue engineering is a common application for biomaterials. TE refers to any application where the goal is to repair, preserve, or enhance damaged tissue or organs. This is done by combining scaffolds, cells, and biologically active molecules into functional tissue [13]. Fibrous polymer scaffolds are being researched in part because the scaffolds should emulate the extracellular matrix (ECM) of the tissue it is to be implanted in, which is fibrous in nature [14]. The significance of this work is producing a micro-fibrous composite polymeric scaffold using a lower molecular weight core polymer than what has been attempted in research. The produced scaffold will be tunable for a multitude of tissue engineering applications.

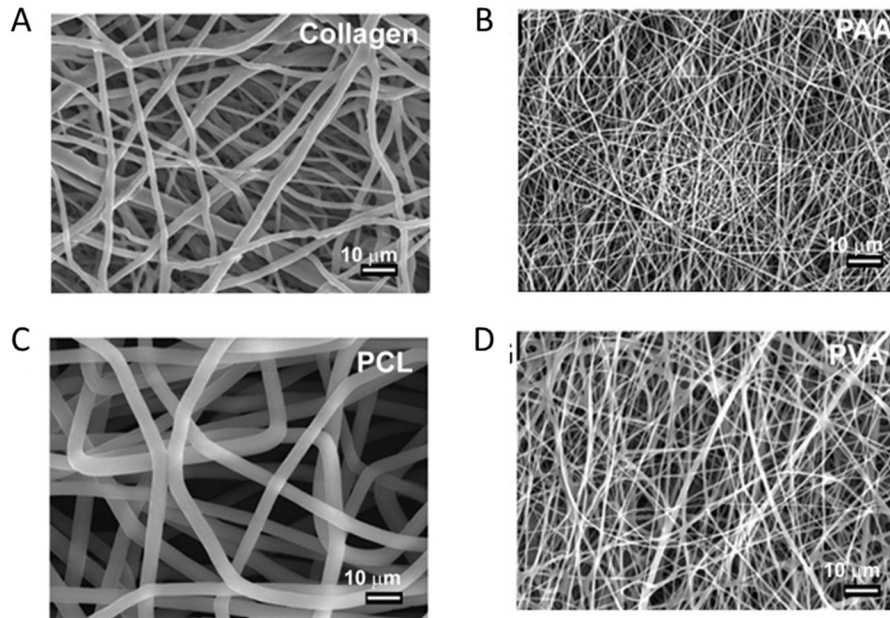


Figure 2 Polymeric scaffolds produced by electrospinning of A) Collagen, B) Polyacrylic acid, C) Polycaprolactone, D) Polyvinyl alcohol [15]

1.2 Current scaffold production approaches

Scaffolds act as a synthetic extracellular matrix (ECM), whose role is to expedite tissue regeneration or repair in the inserted area. An ideal scaffold will exhibit biodegradable or bioresorbable properties, good bioadhesion allowing existing tissue to easily bond with the scaffold and similar mechanical properties to the surrounding tissue to prevent stress shielding. Conventional scaffolds biological interactions can be improved by increasing the porosity of the material as is shown in scaffolds' used for bone osteogenesis [16]. Scaffolds can be produced by a variety of methods, including solvent casting, freeze drying, thermal-induced separation (TIPS), gas foaming, electrospinning, rapid prototyping, stereolithography, fused deposition modeling (FDM), and selective laser sintering (SLS) [17]. Solvent casting involves using a solvent combined with uniformly distributed salt particles of a predetermined size to dissolve the

polymer solution. The solvent then evaporates and the salt polymer matrix must be submerged in water to remove the salt. The resulting matrix has a high degree of porosity. Freeze drying is sometimes referred to as lyophilization and uses a synthetic polymer that is dissolved in a solvent. Once dissolved the solution is cooled under the freezing point and the solid solvent evaporates by sublimation. This results in a solid scaffold with interconnected pores.

TIPS uses low temperatures to force phase separation in high-temperature polymer solutions. This creates a polymer-rich phase and a poor-polymer phase and is used for creating thermoplastic crystalline scaffolds. Gas foaming involves using an inert gas foaming agent like carbon dioxide or nitrogen to pressurize the polymer with water or flouroform until it is saturated with gas bubbles. The technique produces sponge-like structures. Electrospinning requires a polymeric solution be exposed to a high voltage that induces a jet to spray the polymer onto a collector. Rapid prototyping, also referred to as solid free-form fabrication, is a process that generates objects from computer-aided design models. Rapid prototyping of scaffolds allows precise control over polymer structure, allowing for customized scaffolds. Stereolithography prints layers of ultraviolet-curable material. This is done by having a laser deposit photosensitive liquid resin in a layer-by-layer fashion. FDM uses a solid polymer that is melted and extruded on the surface of an object. The scaffold is created from multiple layers of microfilaments. This process is used on thermoplastic biopolymers and can produce porous scaffolds with controlled mechanical properties. SLS uses a laser to sinter powdered material in thin layers. This technique has been used with polymers, metals, and ceramics. The advantages and disadvantages of each method are listed in Table 1.

Table 1 Advantages and disadvantages of various fiber production techniques [17]

Method	Advantages	Disadvantages
Solvent Casting	Simple and low cost.	Time consuming, limited pore size.
Freeze-Drying	Uses water and ice crystals instead of organic solvents.	Difficult to produce hierarchical structured scaffolds ex. Vascular systems.
TIPS	Can produce nanofibrous scaffolds.	Only certain materials can be used in fabrication.
Gas Foaming	Produces structures with up to 85% porosity.	Can form closed pores or solid polymer skins.
Electrospinning	Simple and quick.	Cannot produce a homogenous pore distribution.
Rapid Prototyping	Precise spatial control.	Reliant on 3D printing, FDM, or SLS
Stereolithography	Reduces waste material compared to subtractive methods.	Requires large quantities of monomers and post polymerization treatment.
FDM	Can create structures with controlled mechanical properties.	Requires preformed, consistent sized fibers.
SLS	High control over microstructures of the produced scaffold.	Post fabrication procedures must be completed to remove injected powder at higher temperatures.

1.3 Current applications of fibrous scaffolds

Fibrous scaffolds have been used in virtually every medical application for tissue engineering. Fibrous scaffolds are used because of the incredible range of properties they can

exhibit, such as tensile strength [18]. Fibrous scaffolds are also used because they can be fabricated to have structures with interconnected pores similar to those found in a natural ECM [19]. The use of drugs and antibiotics in the medical field is very important to reduce the risk of infection. Drug release methods are characterized by their burst and sustained release patterns. A sustained release is generally favored and fibrous scaffolds can be tuned to modify the sustained release [20]. Fibrous scaffolds have been successfully used to deliver a sustained and targeted dosage of a drug into the body for cytotoxicity testing [21], diabetic wound treatment [22], and bone regeneration [23].

Looking more intensely at bone regeneration, fibrous scaffolds are used because good bone regeneration requires osteogenic and angiogenic potential [24]. Figure 3 A shows the cell proliferation on the PVA-PCL-HAB scaffold over a 15-day period. Figure 3 B shows successful ectopic bone formation and cell migration through the scaffold stained with haematoxylin and eosin (H&E), vimentin antibody (VM), collagen type 1 antibody, and sirius red F3BA [25]. Bone remodeling requires the scaffold provide both a good environment for cell seeding and good mechanical properties. Polymer scaffolds are engineered to fulfill these requirements by creating composite scaffolds with both hydrophobic and hydrophilic polymers [26]. The hydrophilicity or hydrophobicity of a polymer is important as it plays a crucial role in the body's response to the scaffold. Research has shown that the more hydrophobic (50:50) ratio PLGA produced scaffold's that more easily allow the formation of bone tissue within the scaffolds pores [27]. The explanation given is the (50:50) PLGA has a better balance between hydrophobic and hydrophilic attributes when compared to the (70:30) NVP:BMA it was

compared to. Research has been done combining computer-aided design and fibrous scaffold production techniques to further improve scaffold topography for bone regeneration [28].

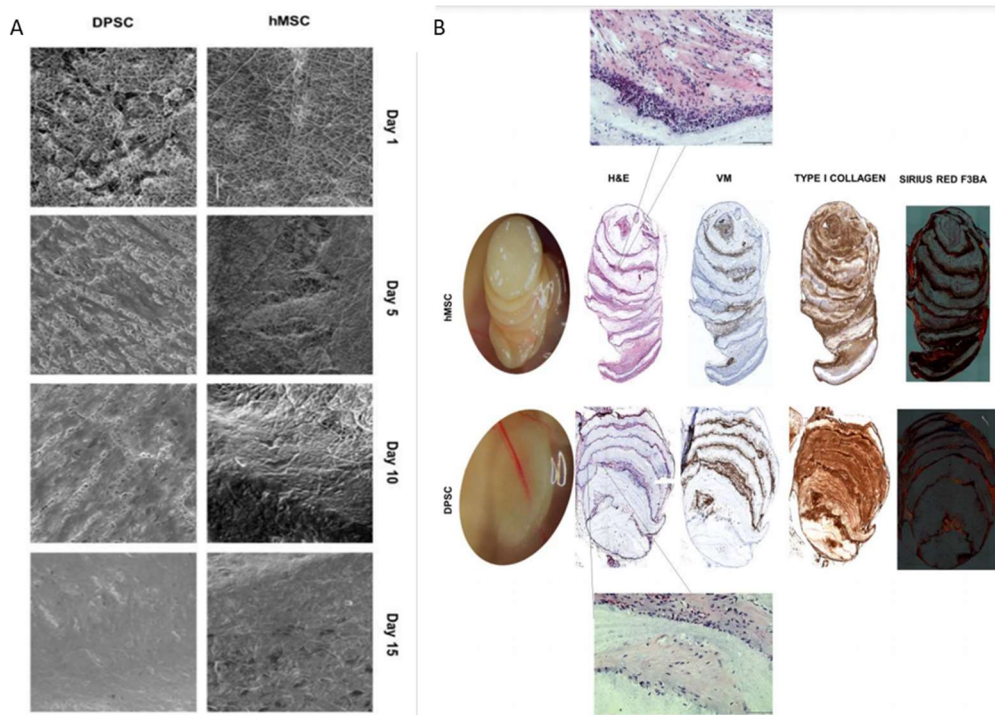


Figure 3 A) Cell proliferation and regeneration on PVA-PCL-HAB scaffolds for bone regeneration B) In vivo ectopic bone formation on subcutaneous implantation after eight weeks [25]

Fibrous scaffolds have been utilized to repair cardiovascular tissue as well. Some examples of scaffolds used in cardiovascular tissue include bioprosthetic valves such as aortic valve leaflets with three layers of fibers [29]. Cardiac patches are another example of fibrous scaffolds used in cardiovascular tissue. The patches allow grafts to mature *in vitro* to a sufficient functional level before being grafted into the body [30]. Scaffolds intended for cardiovascular tissue have been engineered to be seeded with stem cells to further improve their function and cardiac regeneration [31].

Fibrous scaffolds have found incredible success in dermal tissue engineering. Fibrous scaffolds are typically composites composed of different polymers to improve surface properties such as PLA and gelatin [32], PLLA/PAA/COLI&III [33], and PLLA with fibrin or collagen coatings [[32]- [34]]. Another interesting application for polymeric fibrous scaffolds that is gaining research popularity is periodontal disease. Periodontal disease affects the gums and can lead to tooth loss. Scaffolds have been used to improve periodontal tissue health through guided tissue regeneration [35]. Scaffolds have also been used to improve the tooth-ligament interface while treating supporting tissue around a damaged tooth [36]. The applications for fibrous scaffolds are varied and important; as medicine advances so to will the production techniques of these scaffolds. Figure 4 shows various scaffolds produced for these applications.

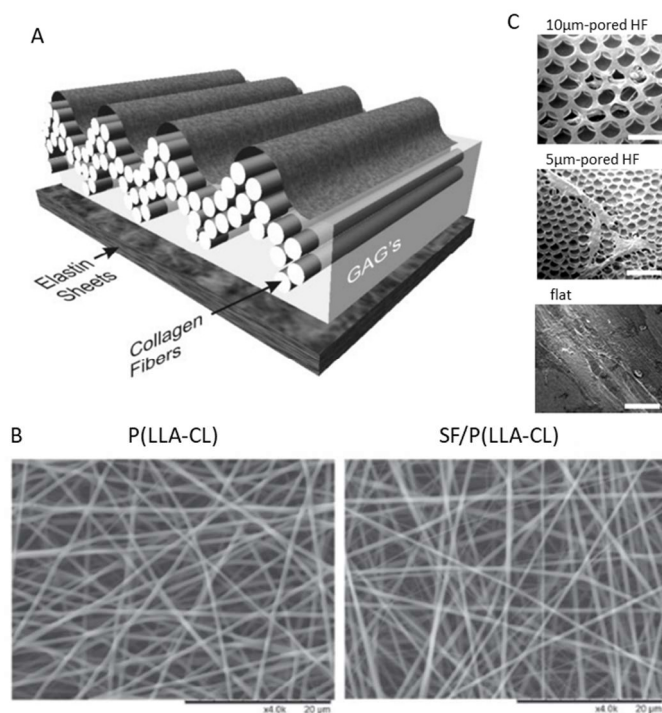


Figure 4 Images of scaffolds designed for various applications A) Diagram of multilayered aortic valve cusp using collagen fibers [29] B) SEM images of P(LLA-CL) and SF/P(LLA-CL) fibrous scaffolds for myocardial infarction [31] C) SEM images of PDL cells on honeycomb film (HF) for periodontal regeneration [35]

1.4 Techniques for fiber fabrication

Polymer fibers make up a considerable portion of current biomaterials research, and the fabrication techniques for these structures are in a constant state of improvement. While electrospinning is the most prevalent fabrication method, phase separation, self-assembly, and templating are also used to create polymeric materials [37]. The most common catalyst for phase separation is thermally induced. The phase separation process first requires the polymer be dissolved in a solvent that boils at a high temperature greater than the melting point of the chosen polymer. Once melted the molten polymer can be cast into the desired shape and must be left to cool. After cooling, the solvent is extracted such that only the polymer remains [38]. Self-assembly occurs when molecules organize themselves into structures determined by the molecules. Secondary bonds bind the molecules together, resulting in the final polymer structure [39]. Templating is a fiber fabrication process where fiber arrays are poured into molds with pore diameters ranging from 25 to 400 nm and depths from a few nanometers to micrometers; the resulting fiber arrays are released from the molds either by destroying the mold or mechanical detachment [40].

1.5 Introduction to electrospinning

Electrospinning is the prominent production method for fibrous scaffolds. In electrospinning, fibers are drawn from solution by a large electric force. There are many different techniques for electrospinning fibers of different diameters. All electrospinning techniques are reliant on the formation of a stable Taylor cone. A Taylor cone is a phenomenon that occurs when a droplet of a conductive liquid is introduced to an electric field with sufficiently high voltage. Provided the voltage is high enough, the droplet will invert and a jet

will form, emitting the liquid in a spray or stream-like fashion [41]. To electrospin polymers, the polymer must be either soluble or exhibit a melting or glass transition temperature. Figure 5 A shows the formation of a good Taylor cone and the effects of increasing voltage on the Taylor cone. Figure 5 B is a diagram of the two stages of flow in electrospinning after the Taylor cone has formed.

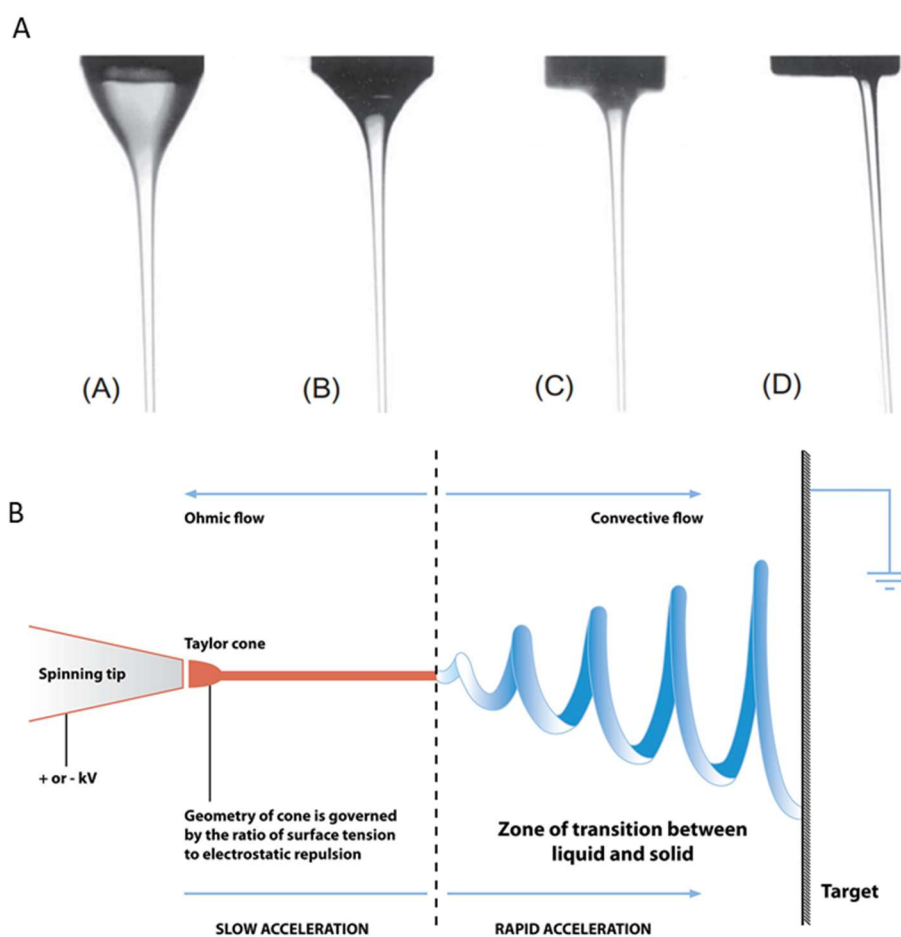


Figure 5 Taylor cone formation of electrospinning PEO/water at various voltages A A) 0.47 kV/cm B) 0.53 kV/cm C) 0.60 kV/cm D) 1kV/cm [42] B stages of flow in electrospinning [43]

Environmental factors including temperature, humidity, and air velocity can influence the formation of fibers when electrospinning. In conjunction with the environmental factors there are electrospinning parameters that are determined and controlled based on the fiber that is desired. The electrospinning parameters are polymer molecular weight, solution viscosity, solution conductivity, solution surface tension, flow rate, plate distance, needle gauge, and applied voltage [44]. The high voltage required when electrospinning has caused cell viability concerns when using proteins or DNA. Recent research suggests that these cells maintain their viability after being electrospun [45] and that using alternating current instead of direct current can carry less risk of damaging the cells [46]. The two major categories of electrospinning techniques are solution-based electrospinning and melt-based electrospinning, which are described in greater detail in the next sections.

1.6 Electrospinning techniques

1.6.1 Solution electrospinning

Solution electrospinning refers to all production techniques that require the polymer be dissolved in solution prior to electrospinning. When this solution is deposited on the tip of the needle or nozzle acting as an electrode, the process of forming a Taylor cone begins. Solution-based electrospinning produces fibers with small diameters and relies on the evaporation of the solvent during the electrospinning process for the solidification of the fibers. Solution electrospinning is the most common electrospinning technique in part due to the simpler equipment and higher productivity [47]. The concentration of polymer in solution can have a significant impact on the electrospinning process in solution electrospinning and must be carefully optimized to produce good fibers [48]. While this is the most common method, it is not

without its drawbacks, primarily the health and pollution risks associated with the solvents used in solution-based electrospinning. Figure 6 shows a standard electrospinning setup with proper jet formation with the fibers depositing onto a drum. The jet is divided into two segments, the streaming jet and the whipping jet. The streaming jet is the ejection of polymer solution from the buildup of material on the nozzle. The whipping jet occurs when the solution has traveled towards the collector and the "whipping" can be caused by the buildup of polymeric material on the collector causing slight changes in the localized strength of the magnetic field. The whipping jet is commonly observed in electrospinning and is a part of a stable Taylor cone.

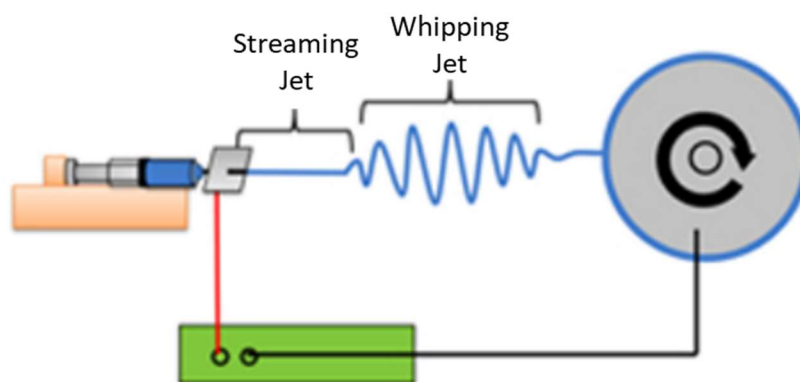


Figure 6 Diagram of a typical solution electrospinning setup, depositing onto a drum [48]

1.6.2 Melt electrospinning

Melt electrospinning is different from solution electrospinning in that rather than polymers being dissolved and loaded into syringes, they are melted. Only polymers that exhibit a melting point or glass transition temperature can be melt electrospun. This process requires a minimum temperature be maintained throughout the process, as the polymer must be kept in a molten state. Melt electrospinning can be favored over solution based in situations where the use

of solvents is not ideal or possible. Fibers produced by melt electrospinning are typically larger than a micron in diameter due to the high viscosity of the melt [49]. Melt electrospinning is not as common or as well researched as solution electrospinning because of the complex heating mechanisms needed to melt and maintain a pool of molten polymer. Using concentrated laser beams to heat and melt polymers for electrospinning has been investigated with some success [50]. By using a concentrated laser on only the segment of the polymer rod that was in position to be affected by the applied voltage, the average fiber diameter was reduced.

1.7 Fabrication techniques

1.7.1 Monoaxial electrospinning

Monoaxial electrospinning includes all electrospinning processes that dissolve the polymer in solution and eject the solution through a single nozzle to form a bead or droplet which is exposed to a set voltage. This is the most basic fabrication technique in electrospinning; the fibers collected should be solid and homogeneous throughout. Monoaxial fibers have been used in many applications as biomaterials in tissue engineering, including drug delivery [51]. Monoaxial fibers have found tremendous success in cell culture, such as integrating with smooth muscle cells and endothelial cells [52] as well as use in vascular grafts [53].

1.7.2 Collector selection

Electrospinning can utilize different collection devices, such as a flat plate, spinning drum, grid, or edge collector. The two most common collectors are a flat plate and a spinning drum. Any collector chosen should be electrically conductive and be grounded to create the electrical potential difference between the nozzle and the collector [54]. The flat plate is the

simpler of the two collectors. By electrospinning onto the plate, the scaffold will have a random alignment of fibers throughout. The rotating drum will partially align the fibers as they are being electrospun. This results in a scaffold that has a higher tensile strength in the drum's tangential direction, which is parallel to the orientation of the fibers [55]. Figure 7 further demonstrates the impact the collector can have on fiber morphology and scaffold strength. Figure 7 A shows the stress vs. strain graph for pure PHB and PHB-PANI blend polymers when collected on a rotating drum or a flat plate. For either solution, the rotating drum produced a scaffold with significantly higher tensile strength colinear to the orientation of the fibers. The random and aligned fibers are shown in Figure 7 B and the post-tensile test scaffolds are imaged in Figure 7 C.

1.8 Composite electrospinning techniques

A composite material is made by combining two or more materials, commonly those that have drastically different properties. The two materials work in conjunction with one another to give the composite unique properties [56]. With advances in manufacturing, composites are becoming more and more popular due to the increased control over mechanical and chemical properties making them tunable for different applications.

1.8.1 Blending

Blending is a process through which multiple polymers are combined into a single fiber. This process creates a blend that can result in a composite monoaxial fiber or a composite layer or section of a more diverse fiber. The two basic methods to create a polymer blend are either dissolving the polymers in the same solution together or dissolving them separately and combining those solutions after both polymers have been dissolved.

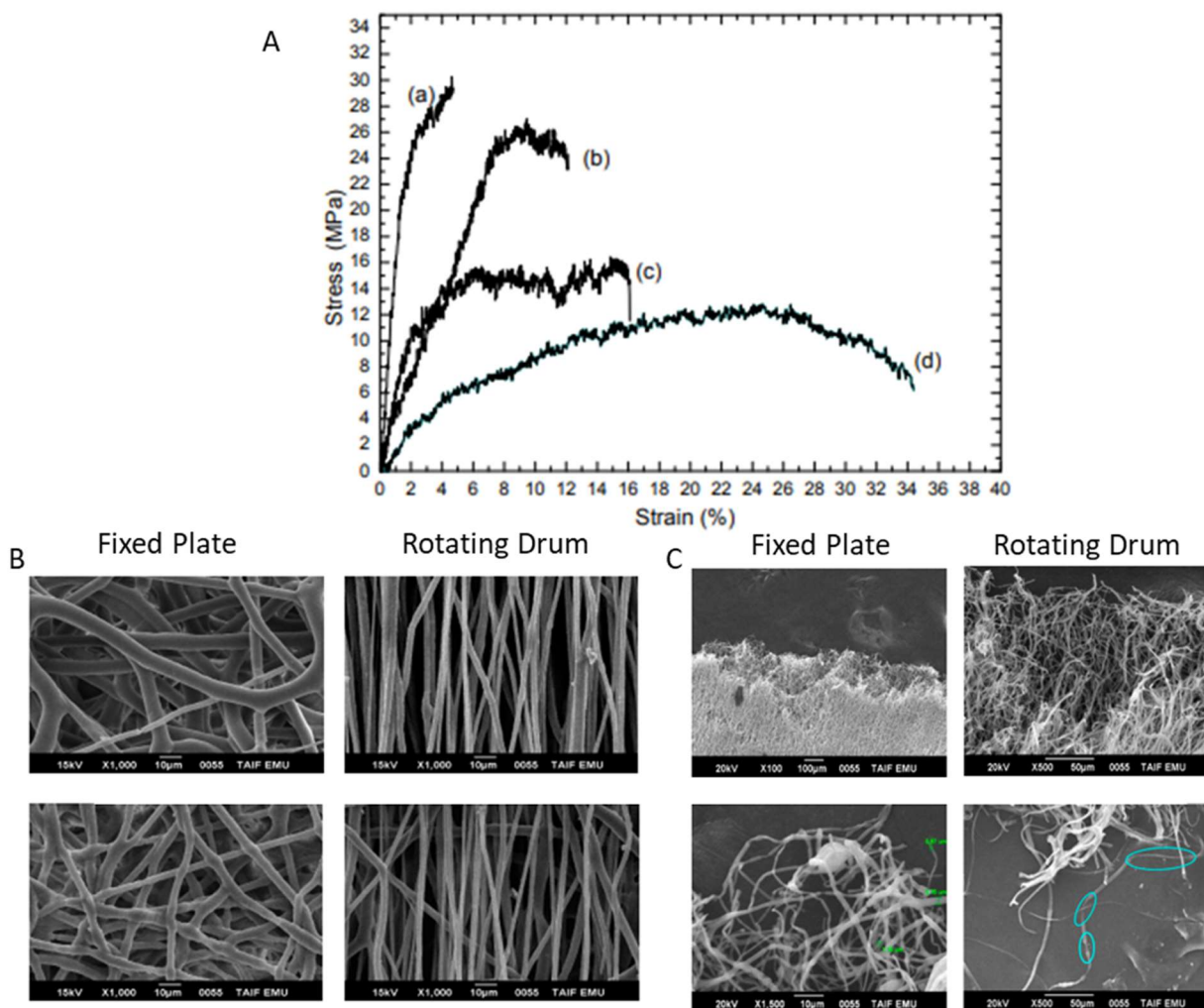


Figure 7 Effects of collector on pure PHB and PHB/plasticizer/PANI blended fibers A) stress-strain curves a) pure PHB 610rpm drum b) 79/20/1 blend 610rpm drum c) 79/20/1 blend plate d) 80/20 blend plate [55]

Generally, blended fibers consist of polymers that are dissolvable in the same solution, making their combination before the electrospinning process rather simple. It is possible to create polymer blends where the polymers are dissolved into different solutions but extra care must be taken to ensure there are no reactions between the solvents as the two will come into contact with each other in the spinneret and the syringe. Figure 8 A shows a conceptual image for the blended-fiber production process; Figure 8 B shows the improved mechanical properties blended fibers can have compared to pure fibers in PCL:PET blends.

Bi-component electrospinning can be considered a subset of the blending process. In bi-component electrospinning, two syringes are used, typically in a parallel or side-by-side fashion. The two syringes both feed into a single nozzle, creating a monoaxial fiber. The difference from other blending processes is that the blend is created in the nozzle after the solutions have exited the syringe [59]. Figure 9 shows how changing the concentration of a blend can impact fiber morphology. In Figure 9 the lower concentrations of propolis ethanolic extract (EEP) with respect to polyamide-6 (PA-6) in the electrospinning solution produced fibers with a cleaner morphology [60].

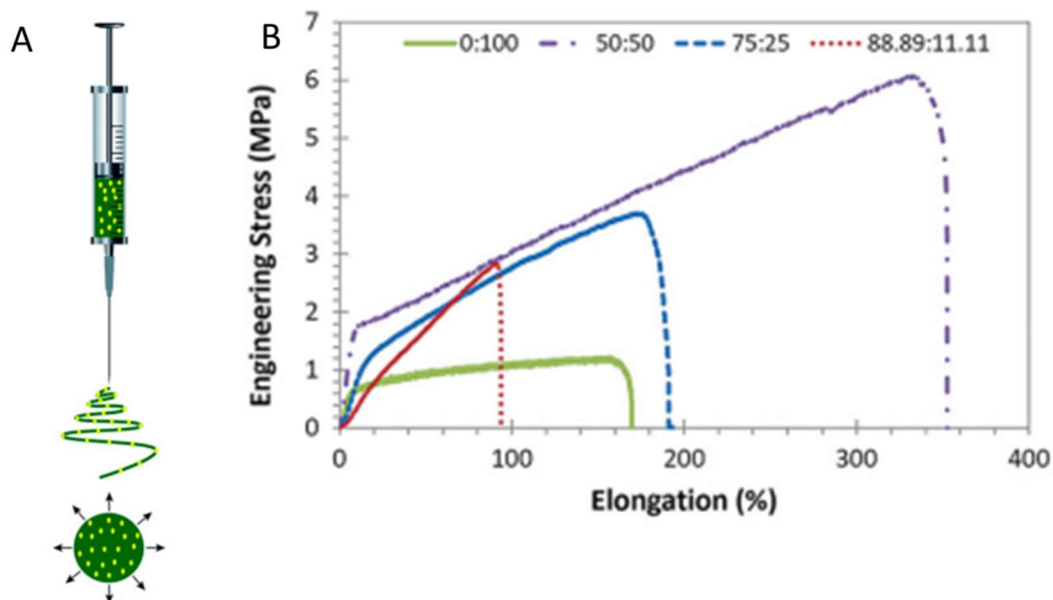


Figure 8 A) Conceptual image of the blended-fiber electrospinning process [57] B) Engineering stress vs. elongation curve for different blends of PCL:PET [58]

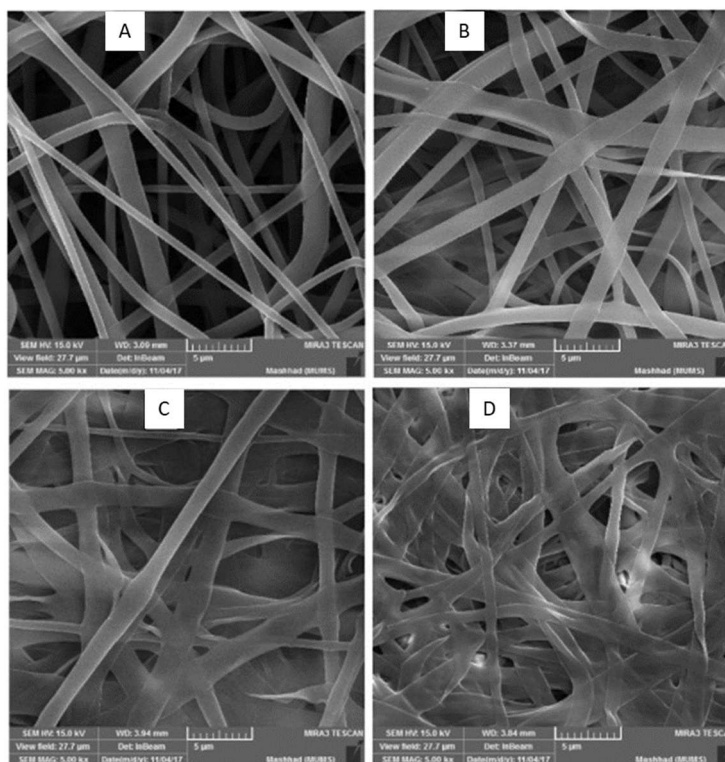


Figure 9 FESEM images of PA-6 (35% w/v), EEP blended fibers A) 20% (w/v) EEP B) 30% (w/v) EEP C) 40% (w/v) EEP D) 50% (w/v) EEP [60]

1.8.2 Layering

Layering is a composite scaffold production technique that creates a scaffold composed of different layers. This layer-by-layer method is seen with the electrospinning of alternating layers of PCL and F-127 [61]. Each layer can consist of a different polymer and be electrospun using different parameters as shown in Figure 10. The produced scaffold is not homogeneous as each layer will have different composition and thus different properties. The layering method allows the polymers to be dissolved in different solvents and because the electrospinning process is done separately for each layer, each solution can be optimized separately. When creating a layered scaffold, the thickness of each layer must be taken into consideration and controlled. This is another variable introduced to the production process that is unique to the layering technique. This is further illustrated when sintering is used to fuse the layers together, particularly when using PLGA electrospun fibers as they can retract and shrink, creating a variance in the topology of the layer [62]. A layering technique was utilized to create a large porous structure to promote tubular structure formation. By dividing the electrospinning process of PCL into steps, the layered scaffold was created. At the conclusion of each step a layer of aluminum foil was attached to the scaffold on the collector; this created a stacking mechanism that was repeated until the electrospinning process was complete [63]. Figure 10 B shows the results of this process; Figure 10 A shows a conceptual image of a layered composite scaffold.

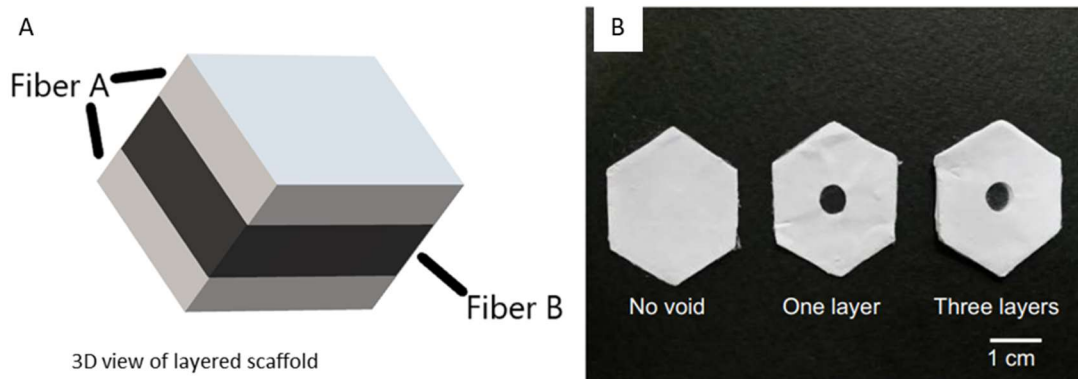


Figure 10 A) Conceptual image of a composite scaffold produced by layering B) Layered PCL scaffold for tubular structure formation [63]

1.8.3 Multiaxial electrospinning

Multiaxial electrospinning refers to any process that utilizes more than one nozzle. This can be further broken down based on the number of nozzles used and the application the nozzles are used in [64]. Although an experiment could be run with any number of nozzles, the two most common multiaxial electrospinning techniques are coaxial and triaxial.

Coaxial electrospinning is defined as electrospinning with two nozzles concentric to each other. This process creates a “fiber within a fiber,” commonly referred to as the core-shell method. The core-shell method has been experimented with for a variety of biological applications. Typically, core-shell fibers have a higher diameter than non-concentric fibers [65]. Silk fibroin and silk sericin core-shell fibers in the 1.6 μm diameter range have demonstrated superior mechanical properties compared to monoaxial fibers, such as improved breaking strength shown in Figure 11 [66]. Figure 11 A shows the tensile strength comparison between core-shell and monoaxial fibers and Figure 11 B shows the stress strain curve. These figures

further demonstrate the mechanical superiority of coaxial fibers over their monoaxial counterparts.

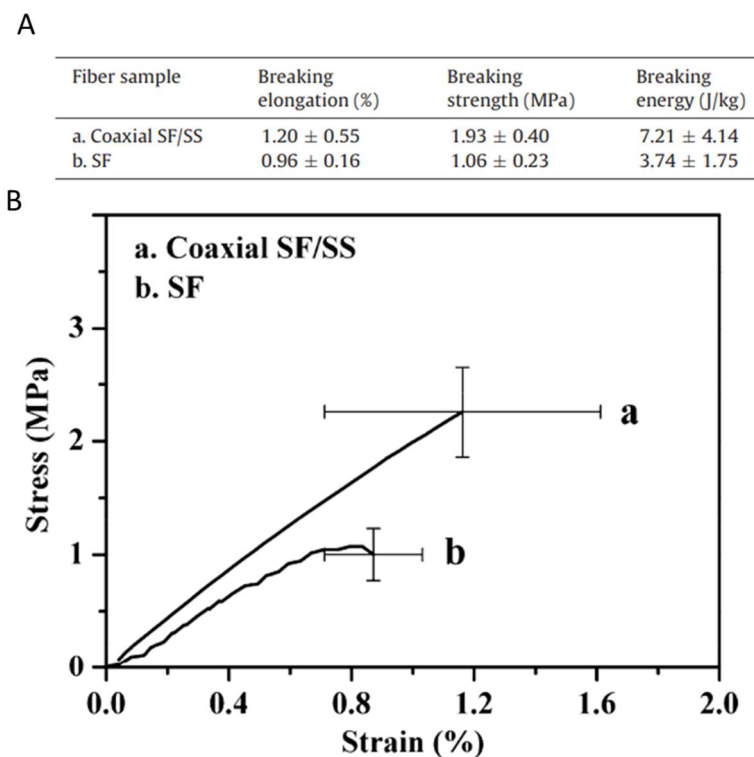


Figure 11 A) Mechanical strength of coaxial silk fibroin/silk sericin to monoaxial silk fibroin B) Stress strain curve of coaxial silk fibroin/silk sericin to monoaxial silk fibroin [66]

Concentric electrospinning has been used to create drug delivery mechanisms with tunable release rates for different applications and drugs [67]. Figure 12 shows the coaxial electrospinning setup as well as the Taylor cone composed of both solutions.

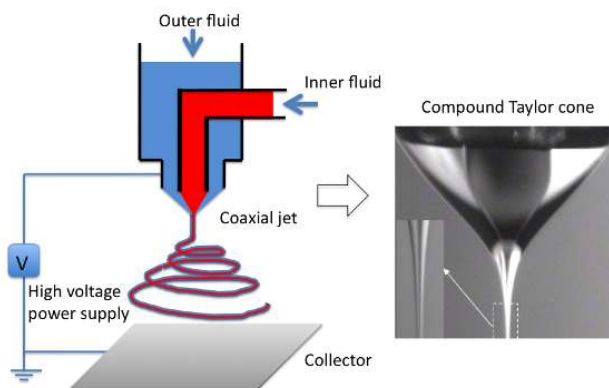


Figure 12 Diagram of standard coaxial electrospinning with Taylor cone [68]

Tri-axial electrospinning is similar to coaxial electrospinning; the difference is, in tri-axial, three total axes or nozzles are used. The nozzles are typically fed from three different syringes providing solution to the core, inner shell, and outer shell of the fiber. The resulting fibers are larger in diameter than monoaxial fibers but have added tunability compared to monoaxial and coaxial electrospinning techniques. Using PCL blends, monoaxial and coaxial fibers were electrospun by using water and ethanol as solvents. For both cases the coaxial fibers had a larger diameter than the monoaxial fibers [69]. In the case of a tri-axial core-intermediate-shell fiber consisting of PCL-gelatin-PLGA(50:50) with an average fiber diameter of 1.88 μm , the resulting scaffolds demonstrated a superior elastic modulus and because of the increased level of control over the fiber also exhibit improved biocompatibility [70]. Tri-axial electrospinning is not as common in part due to the added complexity of the equipment and the three-way solution interaction that must be accounted for while electrospinning.

1.9 Previous work

Composite fibers and scaffolds composed of polycaprolactone (PCL) and poly(lactic-co-glycolic acid) (PLGA) are relatively common as the mechanical properties of the two polymers make good scaffolds for a number of biological applications. PCL and PLGA have been used for prolonged drug release in three-layered scaffolds with a PCL outer layer and PLGA inner layer [71]. Using 40,000-75,000 g/mol PLGA (65:35) and 80,000 g/mol PCL, rhodamine B (RhB) was used to simulate drug loading to determine feasibility of prolonged drug release. Figure 13 shows the drug release vs. time for various parameters. Figure 13 A shows the drug release over time for the experiment and two finite element simulations of the model. Figure 13 B shows the drug release over time as a function of fiber diameter ranging from 80 to 280 μm . Figure 13 C shows the release of RhB over time as it pertains to the partitions of the simulated model. Fibers ranging from 2.50 to 1.53 μm were produced. The tri-layered scaffold successfully delayed the release of rhodamine B until 21 days after the scaffold was produced [71]. PCL and PLGA scaffolds have been created in conjunction with polyaniline to create fibrous scaffolds with electrical excitability for the treatment of spinal cord injuries [72]. Beyond electrospinning, work has been done on 3D printing PCL/PLGA scaffolds to further study production techniques and treat alveolar bone defects [73]. The combination of PCL and PLGA is becoming more popular among researchers due to the recent success of the polymers when used together as well as their complementary properties.

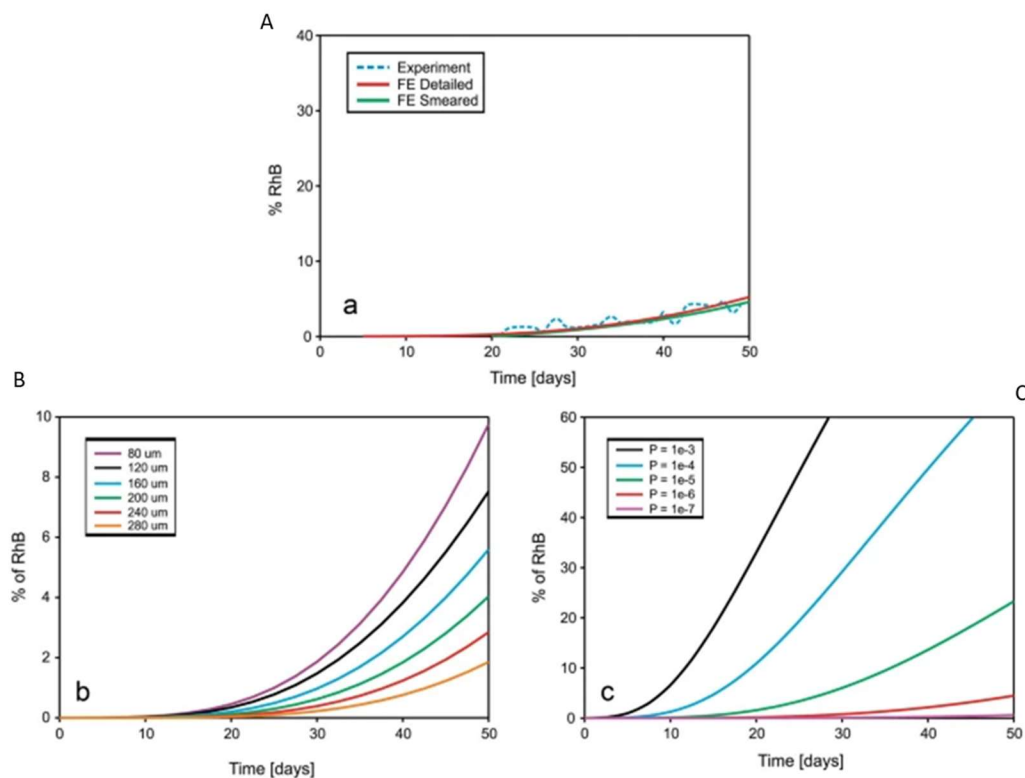
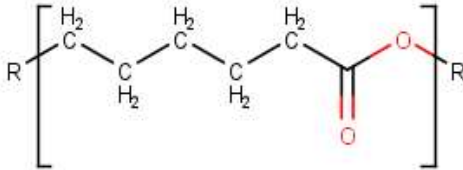
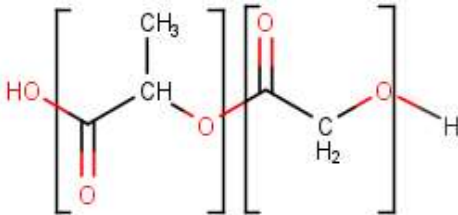
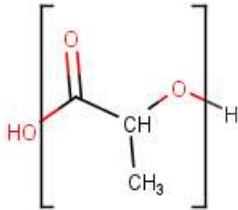

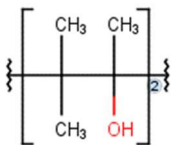
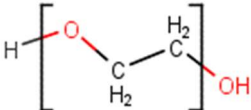


Figure 13 Rhodamine B release graphs A) Cumulative release vs. time lines are experiment vs simulation B) Release dependence on layer thickness lines are different thicknesses (um) C) Effect of hydrophobicity lines are different partitions [71]

PCL and PLGA were chosen for this research because of their electrospinnability and mechanical properties. PCL can overcome the brittle and low elongation properties of PLGA while PLGA has superior cell adhesion and proliferation [74]. Both polymers have been used as the foundation for scaffolds in tissue engineering applications. PLGA in particular is well regarded as a carrier for drugs and drug release [75]. PCL, while mechanically superior to PLGA, is not as efficient in drug loading, thus a combination of these materials creates a composite that is better suited for *in vivo* applications. Table 2 outlines the chemical structure and mechanical properties of different polymers that are used in similar applications.

Table 2 Polymer structure and properties

Polymer	Structure	Properties	Citation
PCL		Semicrystalline aliphatic polyester that is nontoxic. Bulk PCL has a tensile strength ranging from 10.5 to 16 MPa. melting point of 60°C and a glass transition temperature of -60°C. Easily degraded by lipases and esterases.	[76] [77]
PLGA		Co-polymer comprised of LA and GA, depending on the ratio the polymer can exhibit varying degrees of hydrophobicity and tensile strength. Physically strong and highly biocompatible. As PLA:PGA increases PLGA becomes more hydrophobic	[75]
PLA		Exists in two stereo forms L and D. The crystallinity of can be destroyed after D-Lactide is incorporated Thermoplastic polyester derived from corn starch. Poor toughness and slow degradation rate with low thermal stability. Hydrophobic melting temperature 180°C glass transition temperature 60°C	[76]
PGA		Simplest linear polyester, very crystalline with a high melting point and low solubility. A modulus of 7.0 GPa and a degradation time of 6-12 months	[78]
PVA		Semi-crystalline nontoxic with high dielectric strength, excellent thermal stability and high gas barrier. Water soluble can absorb protein molecules with minimal cell adhesion	[76] [79]
PEO		PEG class whose Mw is exceeding 100,000 g/mol. Excellent biodegradability, used in applications where materials such as chitosan or keratin would also be considered	[80]

1.9.1 Research goal and main tasks

The goal of this research is to produce composite fibrous scaffolds for potential use in tissue engineering with a special focus on periodontal disease. A research plan was created and divided the main tasks into three separate phases (Figure 14).

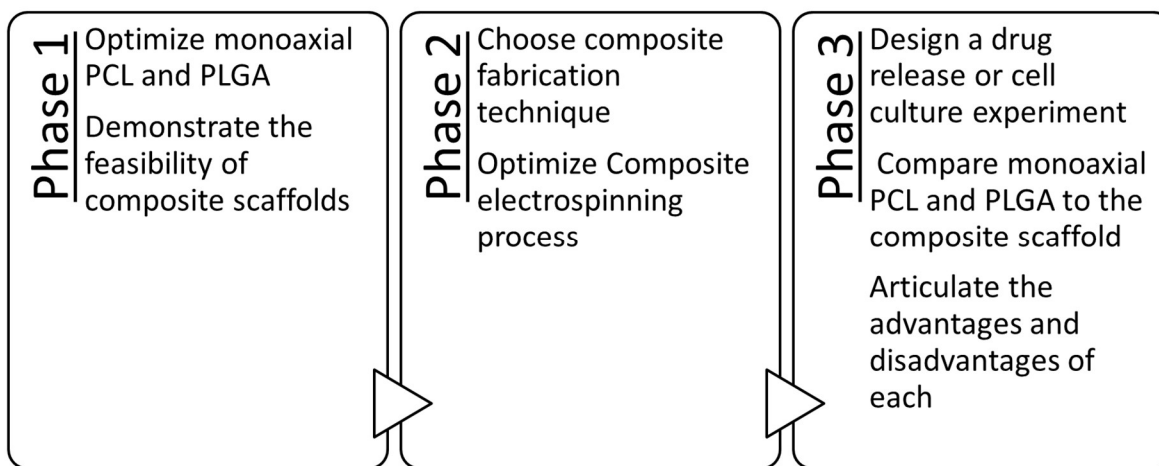


Figure 14 Phase diagram of research goals and tasks

Phase one consists of the initial and background research required to create a composite fiber. Starting with monoaxial electrospinning, each polymer must be separately optimized so the feasibility of a composite fiber can be demonstrated. Phase two includes choosing the composite fabrication technique and then optimizing the electrospinning process of the chosen technique. Phase three is the results phase where the produced composite is compared to the monoaxial fibers to determine the advantages and disadvantages of each. Theoretical drug or cell culture experiments will also be designed to inspire continued research. Beyond the

fabrication of a composite core-shell fiber, the impact and statistical significance of applied voltage, core feed rate, collector plate distance, and humidity will be determined.

CHAPTER 2

MATERIALS AND METHODS

A standard operating procedure (SOP) was created for future electrospinning experiments to follow and is included in its entirety in the Appendix.

2.1 Solution preparation

The solutions used in this research were prepared by first calculating the desired weight of solvent to volume of solution ratio (w/v). This ratio was calculated using Equation 2.2.1:

$$\frac{\textit{weight}}{\textit{volume}} \% = \frac{\textit{weight of solute}}{\textit{volume of solution}} \times 100 \quad (2.2.1)$$

The polymer particulate was massed using an electronic computing scale with a readability of 0.1 mg. A plastic weigh boat or weigh paper was used to prevent contact between the polymer and scale. The solvent used in this research is classified under NFPA 704 with a degree of hazard of 3 blue. Anytime the solvent needed to be removed from storage it was done in an open area on a lab bench inside a fume hood. The liquid solution was measured by pipetting the desired volume into a 10 mL glass graduated cylinder in 1 mL increments. If the desired volume could not be expressed as a whole number, then first the rounded-down integer value was added in 1 mL increments, and then the decimal value was added.

Once the solid polymer solute and liquid solvent were measured, both could be added to a 10 mL glass beaker for stirring. First, a 6.35 mm x 10.32 mm (1/4-inch by 13/32-inch) magnetic stir bar was added to a clean 10 mL glass beaker by gently placing the magnetic stir bar on the base of the beaker with a gloved hand. The polymer particulate was then carefully added by

tilting the weigh boat or weigh paper that the polymer was massed on and allowing the polymer to gently slide into the 10 mL glass beaker. After adding the polymer, the 10 mL glass beaker was inspected, and any polymer particulate found stuck on the sides of the 10 mL glass beaker was softly dislodged using a clean metal lab scoop such that the polymer would fall to the base of the 10 mL glass beaker. When all particulates stuck to the sides of the 10 mL glass beaker were removed, the liquid solvent was added by carefully pouring the measured quantity from the 10 mL graduated cylinder into the 10 mL glass beaker. After the liquid solvent was added to the 10 mL glass beaker, three sheets of parafilm cut into 100 mm x 100 mm squares were used to cover the open end of the 10 mL glass beaker. This covering process was done in three steps: 1) a sheet a parafilm is placed over the open end of the beaker such that the centroid of the face is coincident to the center of the open circular face on the beaker; 2) the parafilm is then pulled down, stretching over the lip on the 10 mL beaker such that it makes a seal covering the open end; 3) the parafilm is then stretched clockwise around the beaker until it tightly rests on the side of the 10 mL beaker. This process is repeated for each sheet of parafilm, alternating the direction the parafilm is stretched around the 10 mL beaker.

With three layers of parafilm covering the 10 mL beaker, the 10 mL beaker can be moved from the lab bench to the magnetic stir plate under the fume hood. Proper use of the Fisher magnetic stir plate used in this research requires the magnetic stir bar be placed as close to the center of the stir plate as possible. Once the 10 mL beaker was appropriately positioned on the stir plate, the stir level was gradually increased from 0 to 3. During the stirring process, the 10 mL beaker was frequently checked to ensure no polymer particulate had become stuck to the sides of the glassware. If such an event did occur, the stir level was gradually decreased from 3

to 0 and the 10 mL glass beaker was held with a gloved hand while the metal lab scoop was used to gently tap the outside of the beaker until the particulate became dislodged. Once any particulates stuck on the glassware were removed, the 10 mL glass beaker was placed back on the magnetic stir plate and the stir level was gradually increased from 0 to 3. The stirring process was run for a minimum of 30 minutes and continued until no visible polymer particulate remained in the 10 mL beaker. When no visible polymer particulate remained, the stirring process was continued for an additional 10 minutes to ensure the solution was homogenous. After the additional 10-minute stir period had elapsed, the stir plate was gradually decreased from level 3 to 0. Once the magnetic stir bar was no longer in motion, the three layers of parafilm were carefully removed from the 10 mL glass beaker one at a time. With the open end of the beaker now exposed, a 10 mL plastic syringe without a needle was used to collect the solution. At times, the 10 mL glass beaker was slightly tilted such that the solution accumulated on one side of the beaker to aid in the recovery process. The recovery rate was around 80% by volume.

2.2 Electrospinning Process

An Inovenso NS1 NanoSpinner electrospinning/electrospraying with an added plexiglass enclosure was used in this research. To safely operate the equipment a series of preparatory steps was followed. First the 10 mL plastic syringe containing the solution was placed in the appropriate loading zone in the NS1. The syringe was then held in place using the spring-loaded clamp. The plastic syringe hub to the tubing adapter was then fixed to the syringe and the necessary length of tubing to reach from the syringe to the nozzle was connected. For monoaxial electrospinning, the monoaxial nozzle with an inner diameter of 0.337 mm and an outer diameter

of 3.3 mm was used. For coaxial electrospinning, the coaxial nozzle with an inner diameter of 0.337 mm shell and 0.6414 mm core was used. Once the tubing was connected to the nozzle the electronic flow block was manually positioned such that it contacted the plunger but did not eject any solution.

With the block now in position and the syringe and nozzle connected with tubing, the collector plate could be positioned. The collector plate was positioned using a ruler that measured the distance from the tip of the nozzle to the desired placement location. The collector plate was then moved by sliding the plate on the mounting rail to the desired location within a 0.1 mm tolerance. The plexiglass enclosure was then closed, and the LCD screen was used to set the desired feed rate in mL/h, the applied voltage in kV, and to turn on the LED back light to improve visibility. The NS1 was kept under constant supervision throughout the electrospinning process. The creation of a Taylor cone was recorded and any imperfections with the electrospinning process or Taylor cone formation were noted. For a produced scaffold to be considered successful and undergo further analysis using a scanning electron microscope, the Taylor cone needed to remain consistent for five consecutive minutes. Depending on the severity of the flaws in the electrospinning process, an inferior Taylor cone may result in the experiment being terminated early. Examples of severe flaws in the Taylor cone include splitting, failure to form, consistent dripping, and the formation of fibers stretching from the collector plate to the nozzle.

2.3 Optimization process

To gather data on the impact of voltage, feed rate, plate distance, and concentration, the variables were varied. Voltage was changed in 0.5 kV increments, feed rate was changed in 0.2

mL/h increments, plate distance was changed in 5 cm increments, and concentration was changed in 2.5 % (w/v) for PCL and 10 % (w/v) for PLGA. The objective for this research was the successful fabrication of a core-shell fibrous structure using a PLGA core and a PCL shell. At the start of this research, electrospinning PLGA with a molecular weight of 30,000-60,000 had not been attempted due to the lack of electrospinning literature on PLGA, PCL was first optimized. The optimization process involved varying the electrospinning variables by the previously defined increments and observing the Taylor cone formation. With each experiment run the range of voltages and feed rates tested was decreased to help find what combination of voltage, feed rate, plate distance, and concentration produced the best results. Provided that the Taylor cone met the 5-minute standard used in this research, the fibers composing the scaffold were then observed under a SEM and characterized by their fiber diameter and standard deviation.

For the purposes of fabricating a core-shell structure, the consistency of the fibers was used as the primary metric to determine parameter viability. This was done because the added complexity of core-shell electrospinning would undoubtedly influence the electrospinnability of the solution. Therefore, it was theorized that the parameters that produced the more consistent scaffolds would provide a better probability for successful core-shell electrospinning. Once the PCL solution was optimized the parameters that produced consistent PCL fibers were then used to produce PLGA fiber. Producing PLGA fibers with the PCL parameters was considered a necessary and unavoidable step in the successful fabrication of a core-shell structure as the two polymer solutions would be electrospun simultaneously under the same parameters. When working with the PLGA solutions the voltage, feed rate, and plate distance could not be varied

beyond what had produced exceptional PCL scaffolds, and as such, polymer concentration in the solution was more heavily varied from 15% (w/v) to 35% (w/v).

In order to create a clear and reproducible path through the experimental process, a decision tree was created to guide all experiments for optimizing the electrospinning of the solution. The decision tree shown in Figure 15 was used to guide the optimization process in this research. This decision tree can also be used to guide future research on the effect of electrospinning parameters on Taylor cone formation.

2.4 Characterization process

The electrospinning process was first characterized by its ability to form a stable Taylor cone. If the parameters of the electrospinner could not induce a stable Taylor cone, they would be retried again, and if jet formation remained an issue, the combination of solution and parameters was recorded as unsuccessful. Provided that a stable Taylor cone and jet did form, the resulting fibers were characterized first by their surface morphology and outer diameter by using scanning electron microscopy (SEM); a Hitachi S4500 or the Hitachi TM-1000 tabletop SEM was used depending on availability. The Hitachi S4500 offers greater magnification and image resolution; however, for the purposes of determining fiber diameter and morphology, the TM-1000 tabletop SEM was sufficient. Two samples were taken from each produced scaffold and imaged at two different, randomly chosen locations at 0.5k and 2k magnification, resulting in a total of two images at each of the four locations. At 2k magnification, a random selection of fibers had their dimensions measured to give a distribution of diameters found in the selection. The dimensions were measured using the built-in measurement software for the SEM. The measurements were then averaged with the three other locations imaged from the same scaffold

to create an average fiber diameter and standard deviation for the whole scaffold. The produced fibers were also characterized for the chemical bonds that exist by using attenuated total reflectance Fourier transform infrared spectroscopy analysis (ATR-FTIR). ATR-FTIR was conducted on two samples from a scaffold to ensure the properties were consistent throughout.

2.5 Statistical analysis

Statistical analysis was conducted on the resulting fiber diameters in the form of an unsigned t test to infer the significance of the impact changing electrospinning parameters has on fiber diameter. For the unsigned t test a p -value $< .05$ is considered significant and a p -value $< .01$ is considered very significant

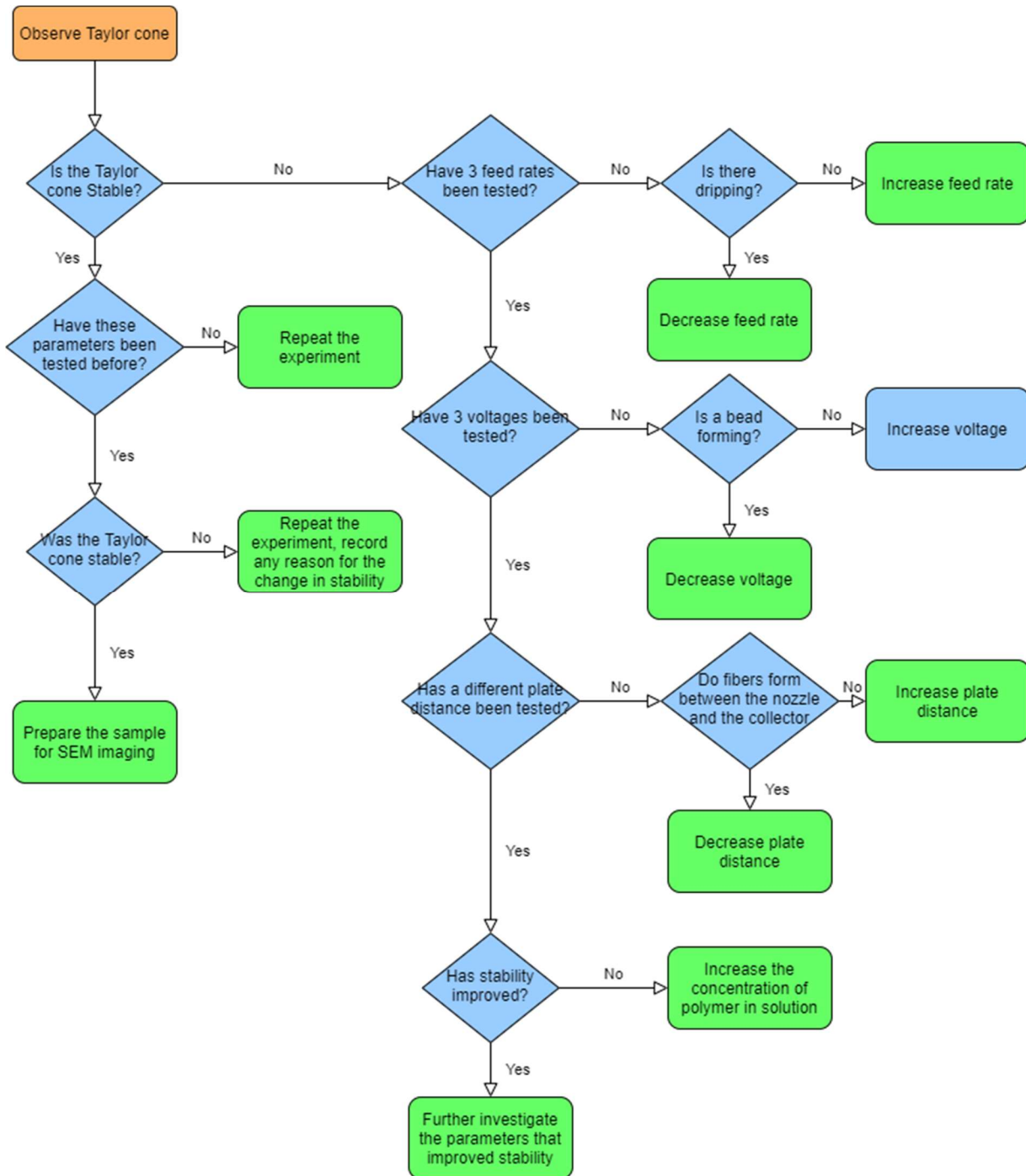


Figure 15 Electrospinning decision tree

CHAPTER 3

MONOAXIAL POLY(CAPROLACTONE)

3.1 Introduction

Polycaprolactone (PCL) is a synthetic hydrophobic polymer that is commonly used in biomaterials and tissue engineering. PCL is chosen for tissue engineering applications due to its biocompatibility and slow biodegradation rate [74] [81]. The *in vivo* degradation of PCL can be split into two stages. The first stage results in a decrease in molecular weight (MW) with no fiber deformation, the second stage began when the MW dropped to 5000 where the polymer began to break apart [82]. The body's inflammatory response to foreign objects is an important factor to consider. *In vivo* experiments on mice have found that the degradation of PCL scaffolds induced successful accumulation of CD11b+ and CD68+ cells around the implant [83]. The accumulation of CD11b+ and CD68+ shows that the body's immune response was preparing the initial steps for tissue regeneration. PCL has also been used as a medium for drug release, such as with dexamethasone for intravitreal implants, which allows for controlled and prolonged delivery of the drug throughout the therapeutic time frame of at least 55 weeks [84].

PCL is a good choice for electrospinning because a plethora of solvents can be used. Many of these solvents have already been researched and the resulting solutions have been found to be electrospinnable. The goal of monoaxial electrospinning polycaprolactone was to optimize the electrospinning process of PCL in hexafluoro-2-propanol (HFIP) solution for eventual core-shell electrospinning experiments. This was accomplished by following the electrospinning decision tree created for this research, starting with a 5% w/v solution of PCL in HFIP and

increasing the concentration to 7.5% w/v to determine what concentration produced more consistent results. The concentration was not further increased to limit the total amount of material needed to produce the scaffolds with the ambition of minimizing construction costs should the scaffolds see use in a clinical setting. Provided that the electrospinning process met the 5-minute requirement set to ensure a stable Taylor cone, further analysis was done to determine the morphology and fiber diameter.

3.2 Results

3.2.1 Fiber optimization

To optimize fiber production, a litany of parameters were tested during a 5-minute time frame to ensure the results were the product of a stable process. The ideal concentration of the polymeric solution was determined first. For 5% (w/v) PCL/HFIP, the observations on the Taylor cones were inconsistent despite changing the electrospinning parameters plate distance, voltage, and feed rate. The 1.5 mL/h feed rate produced the best results while adequately feeding the solution through the nozzle and was kept consistent in later experiments. A smaller than standard nozzle with a diameter of 0.337 mm was used to further assist with the formation of a stable Taylor cone. The electrospinning decision tree was followed to achieve a consistent Taylor cone. Increasing the concentration of PCL in HFIP to 7.5% (w/v) improved the stability of the Taylor cone. To determine what parameters could be optimized further, the voltage was varied each trial until the range of 7kV to 8kV was found to produce the most stable cone and fibers. Further experiments were done with 7.5% (w/v) PCL/HFIP at 1.5mL/h at 8kV, 7.5kV, and 7kV that all produced good fibers and consistent Taylor cones.

3.2.2 SEM

Once a stable Taylor cone was shown throughout the electrospinning process, the resulting scaffolds could be further analyzed for their morphology and diameter. The existence of a stable Taylor cone is not an indication of good fibers, as beading, branching, or other inconsistencies can form in the scaffold.

Figure 16 shows the SEM images of scaffolds formed from the most consistent Taylor cone using 5% PCL (w/v). Figure 16 A shows a wide area of the scaffold; at both the top right and the bottom left of Figure 16 A significant beading can be seen. The beads formed are more clearly shown in Figure 16 C. Figure 16 B shows the scaffold at 0.5k magnification. Here the fibers formed do not appear to have any defects and are consistent throughout the image. Figure 16 D shows the same location of the scaffold at 2k magnification so the consistency and properties of individual fibers can be observed. In Figure 16 D the diameters of the fibers appear similar; however, there are multiple areas where branching of the fibers has occurred. No other electrospinning parameters using 5% w/v PCL in HFIP solution produced a stable Taylor cone for the 5-minute time frame, so the concentration was increased as outlined by the electrospinning decision tree.

The instability of the Taylor cone at other parameters and the beading and branching shown in Figure 16 A and D resulted in the concentration of PCL in solution being increased from 5% w/v to 7.5% w/v. The concentration was not increased further to preserve as much material as possible. This increase in polymer resulted in the solution having greater viscosity which resulted in the feed rate being increased from 1.2 mL/h to 1.5 mL/h to ensure the nozzle was sufficiently saturated. Figure 17 shows SEM images taken of scaffolds produced with the 7.5%

w/v solution at a 15 cm plate distance. Figure 17 A and B show the consistency of the scaffold through a large area while Figure 17 C and D show the range of fiber diameters that compose the scaffold. Some of the fibers in Figure 17 C have a wave like shape, this by itself is not a defect but was noted due to the strange morphology. Both Figure 17 C and D show a wide range of fiber diameters with larger diameter fibers in the background, meaning they were formed earlier in the 5-minute experiment and deposited closer to the collector.

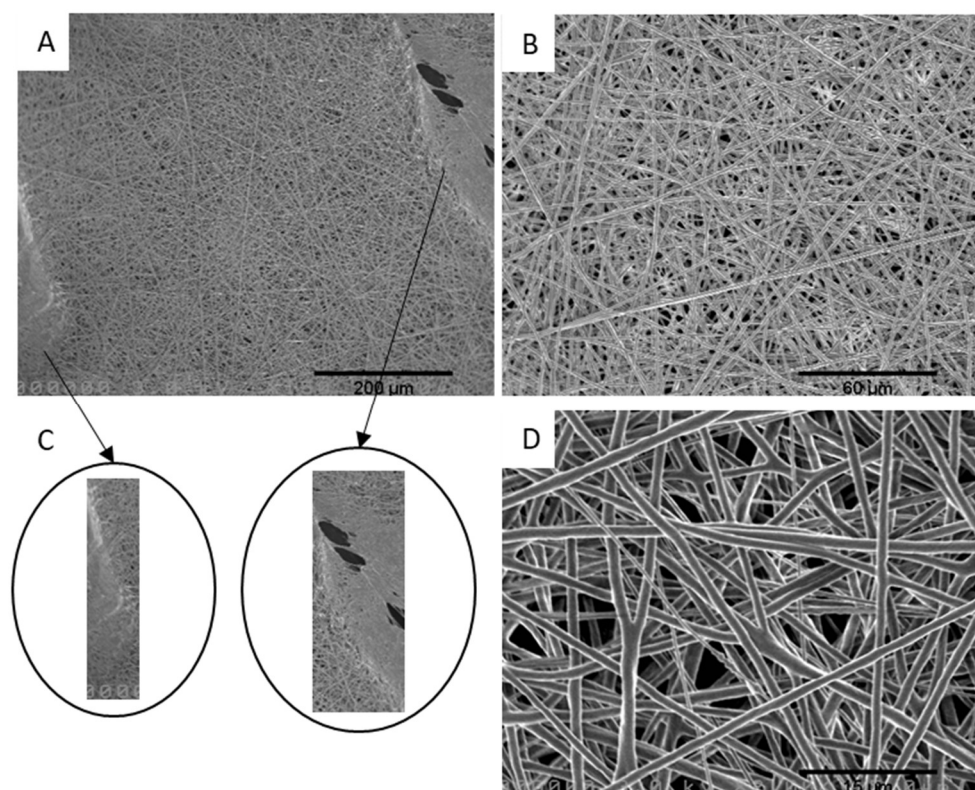


Figure 16 SEM images of 5% (w/v) PCL/HFIP electrospun at 1.2 mL/h 15cm 12kV A) 0.15k magnification, B) 0.5k magnification, C) Cutaway images of beading found in A D) 2k magnification

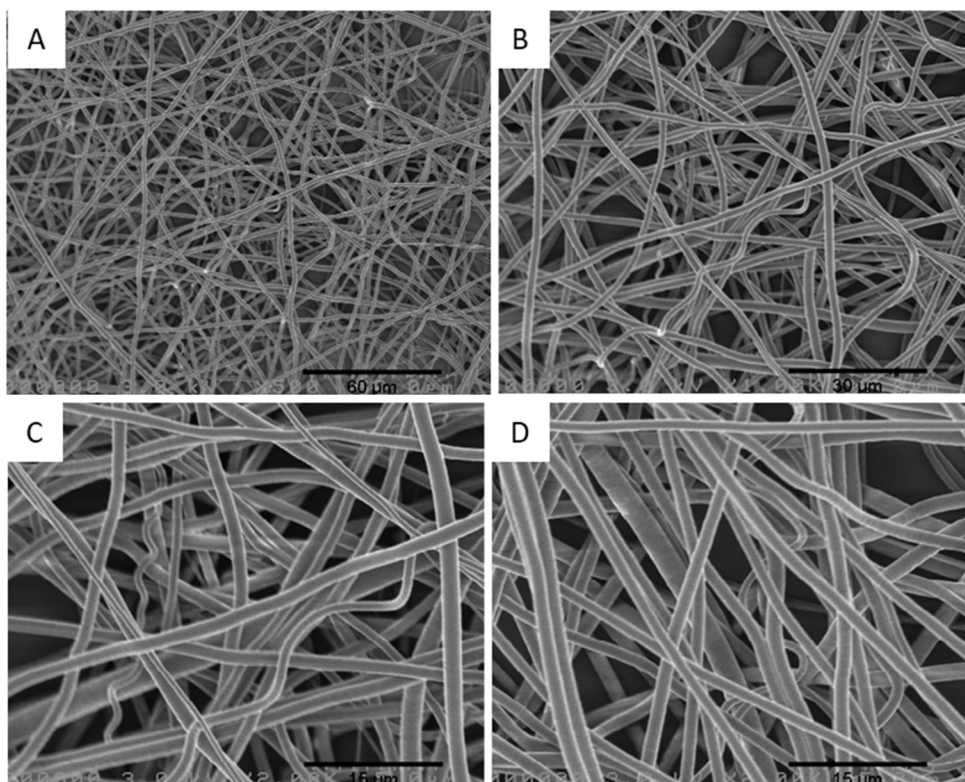


Figure 17 7.5% (w/v) PCL/HFIP electrospun at 1.5mL/h 15cm 7kV A) 0.5k magnification B) 1k magnification C) 2k magnification, C) 2k magnification

The next step for Taylor cone optimization is to adjust the plate distance. The plate distance was decreased because, when testing voltages beyond 7 kV, fibrous structures formed between the collector and the nozzle. Figure 18 shows images taken of scaffolds produced with a 10 cm plate distance. Figure 18 A and B show the fibrous structure formed at 0.5k and 1k magnification. Figure 18 C and D show clear images of the fibers that make up the scaffold. Compared to the fibers shown in Figure 17 C and D, the diameters are more consistent and the wave-like structure is no longer apparent. Future experiments were run using the 10 cm plate distance due to the improved consistency of the fiber diameters and stability of the Taylor cone.

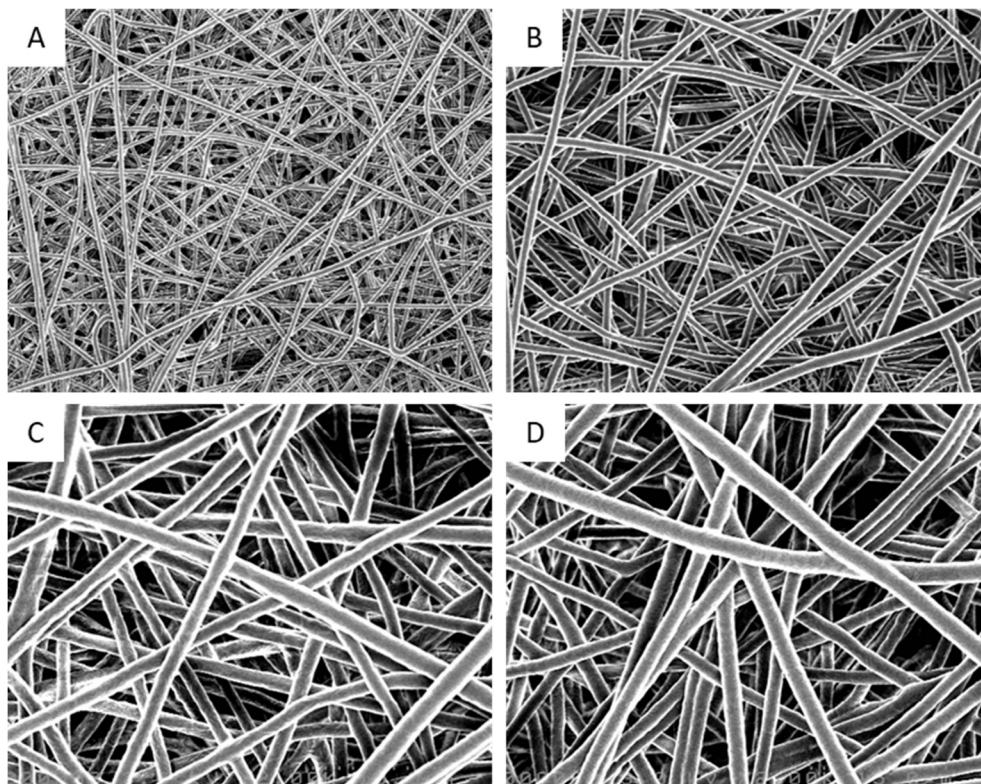


Figure 18 7.5% (w/v) PCL/HFIP electrospun at 1.5mL/h 10cm 7kV A) 0.5k magnification B) 1k magnification C) 2k magnification D) 2k magnification

The 10 cm plate distance allowed the electrospinning process to create stable Taylor cones at 7 kV, 7.5 kV, and 8 kV. Scaffolds produced at each of these applied voltages are shown in Figure 19 A, B, and C respectively. Each of the scaffolds shown in Figure 19 has a clear fibrous structure without beading or branching. The consistency of the fiber diameters all appear similar. To further quantify the characteristics of each scaffold, the average fiber diameter and standard deviation were calculated and are recorded in Table 3. A trend of decreasing average fiber diameter with increasing applied voltage was found. Figure 19 D shows a scaffold imaged at 11k. In the image the surface properties of a fiber produced using an 8 kV applied voltage can be seen. The relatively smooth surface does not show any signs of stress or fracture.

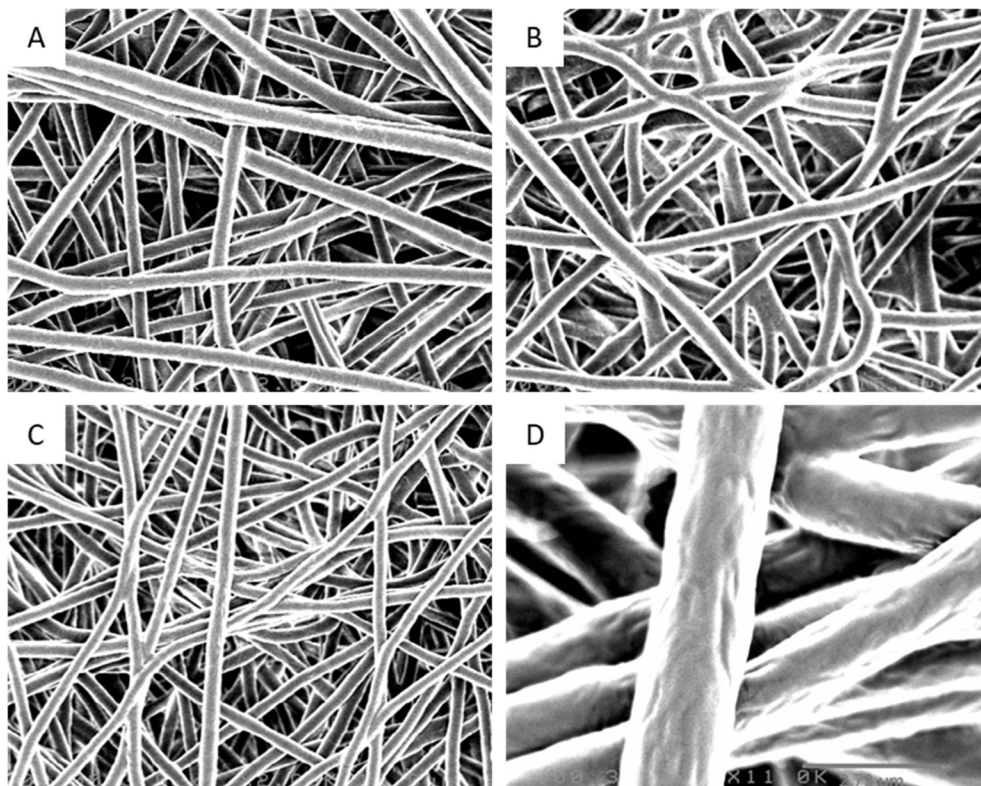


Figure 19 SEM images of PCL electrospun fibers 10cm 1.5mL/h A) 7kV 2k B) 7.5kV 2k, C) 8kV 2k D) 8kV 11k

Table 3 Impact of voltage on monoaxial PCL fiber diameter at 1.5 mL/h and 10 cm

Voltage Applied (kV)	Fiber Diameter (diameter (um) + STDev)	P-value
7	1.8738 + 0.3433	-
7.5	1.7108 + 0.3517	0.0393
8	1.3611 + 0.1566	0.0001

To understand the impact of applied voltage on fiber diameter and standard deviation, the statistical significance of the changes found were calculated. This was achieved by using the scaffolds produced under a 7 kV applied voltage as the reference. Increasing the voltage to 7.5 kV resulted in a statistically significant decrease in fiber diameter and standard deviation. The

increase in applied voltage to 8 kV resulted in a very statistically significant decrease in fiber diameter and standard deviation. The P-values of both cases are shown in Table 3.

To further contextualize the impact of changing electrospinning parameters on fiber diameter and standard deviation, a phase diagram was created using the average fiber diameter and standard deviation calculated for parameters that induced a stable Taylor cone. Figure 20 shows the phase diagram created. From Figure 20, voltage had the greatest impact on reducing standard deviation; this is clearly shown in the side view of the 3D plot where both 7 kV and 7.5 kV show a range of standard deviations from 0.35 to 0.15 while 8 kV has a range of 0.2 to 0.1. The impact of feed rate on standard deviation cannot be discerned from the data due to the significant impact voltage has on the fibers produced.

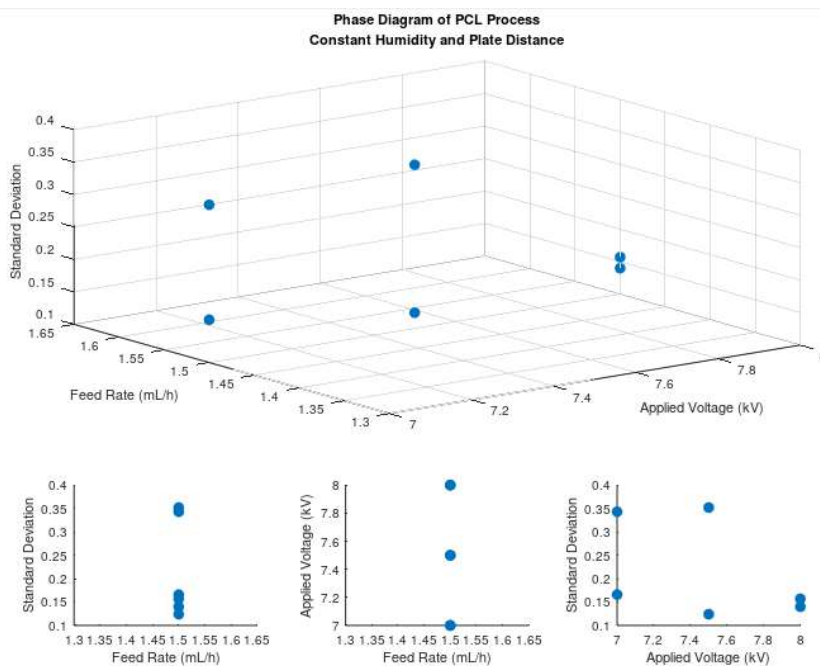


Figure 20 Phase diagram of PCL process

3.2 ATR-FTIR bond analysis

ATR-FTIR was conducted to determine the bonds present in the scaffold to ensure the scaffold was in no way tainted and had not reacted with the environment. Figure 21 shows the resulting plot from FTIR analysis on the electrospun PCL scaffold. The spikes near 1200 and 1700 are indicative of PCL. The initial spike near 2900 also matches established literature for FTIR of PCL [85], confirming the integrity of the scaffold and the absence of foreign materials.

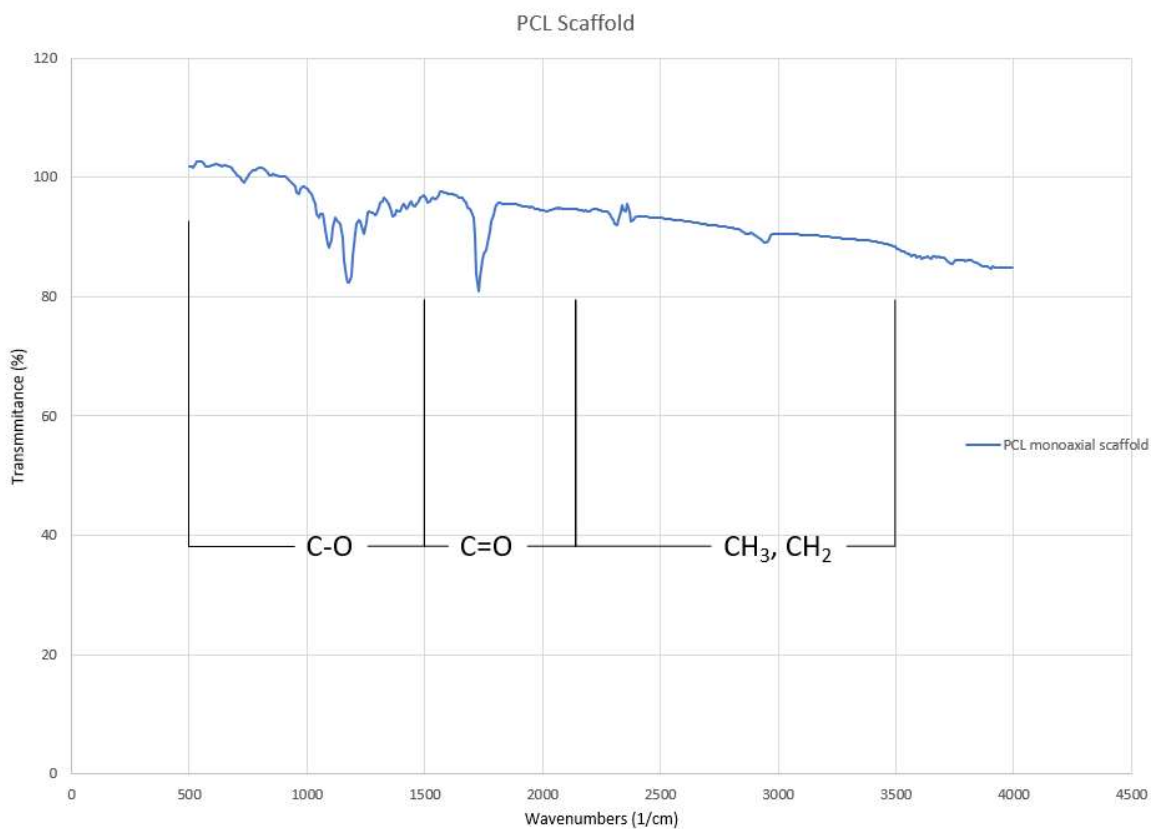


Figure 21 ATR-FTIR analysis of a pure PCL scaffold

3.3 Discussion

3.3.1 Fiber diameter

Table 3 shows the resulting fiber diameters and standard deviations for electrospun PCL scaffolds at 7.5% (w/v) in HFIP, a 1.5 mL/h feed rate, and 10 cm plate distance. The fiber diameters found fall near the wide range of 94 to 1548 nm for randomly aligned PCL fibers [86]. While the fibers produced at 7.0 and 7.5kV fall out of this range, this difference can be explained by the voltage, concentration, and solvent differences. The range created in literature was done using 14% - 28% (w/v) PCL in a mixture of acetic and formic acid 1:9 (v/v). Electrospinning was conducted at 32kV and flow rates between 0.5 and 0.7 mL/h with a plate distance of 10-20cm. The higher concentration of PCL in solution led to a more viscous solution that could produce cone stability at 32kV. Given the lower feed rate used also decreased fiber diameter, compared to the 1.5mL/h that PCL was fed at, it is apparent that the differences in electrospinning parameters account for the discrepancies in fiber diameters. The diameters fall into a narrower range than that found with 8%-12% wt PCL in PEO and PAN [87]. Comparing the diameter range of 1.50-6.65 μm (12% wt) and 1.77-4.04 μm (8% wt) found in this literature to the diameters produced with 7.5% PCL in HFIP (w/v) (46.875% wt) of 1.5305-2.2171 μm at 7.0kV, 1.3597-2.0625 μm at 7.5kV, and 1.2044-1.5177 μm at 8.0kV, the smaller range of diameters produced allows the scaffold properties to be more confidently predicted. The likely cause for the larger range found in literature can be attributed to solution concentration and solution feed rate. The feed rate used in the literature ranges from .3 mL/h to 1.8 mL/h when compared to the 1.5 mL/h feed rate used for 7.5% (w/v) PCL in HFIP. With the established direct relationship of feed rate on fiber diameter, the largest third of fiber diameters recorded to

encompass the feed rates most similar to the 1.5mL/h used in this experiment. The largest third being 4.43-6.65 and 2.69-4.04 μm compared to the ranges found in the research conducted in this paper (1.5305-2.2171, 1.3591-2.0625, and 1.2044-1.5177 μm) shows that this research has produced fibers with lower average diameters while using more PCL per solution at approximately the same feed rate in HFIP opposed to PEO [87]. The fiber morphology is smooth, and the standard deviation of the fiber diameter fall within the expected values outlined by literature [86].

The fiber diameters and morphology depicted are consistent with literature using PCL dissolved in HFIP at 7% w/v electrospun with 15kV. The mode of fiber radii recorded is approximately 0.65 μm or 1.30 μm in diameter; 1.30 μm compared to the average fiber diameters of 1.8738, 1.7108, and 1.3611 μm shows that, regardless of the difference in voltage, fibers with similar diameters can be produced [88]. The potential branching of fibers produced at 7.5kV when compared to research done on branching in electrospon fibers the area appears at worst to be a very minor and contained case [89]. Branching shown in established literature is frequent and can be observed throughout the scaffold, this is represented quantitatively as a large standard deviation. The results in Table 3 results for 7.5kV show a standard deviation of .3517 μm is not significant compared to the range of diameters found for branching in polymer fibers. The FITR results for PCL depicted in Figure 21 are consistent with FTIR of PCL fibers showing spikes at 2940, 1724, and 1540; this is very similar to the spikes found in this research [85].

3.3.2 Tensile strength

The mechanical properties of the PCL scaffolds were not directly tested in this experiment but can be inferred from established literature. 120,000-300,000 Mw PCL dissolved

in HFIP at 10% w/v were electrospun at 20 kV, 0.8 mL/h, and a 15 cm plate distance produced fiber diameters in the range of 0.440-1.040 μm . Individual fibers produced were found to have a strain of 98 +/- 30% at an average stress of 12 +/- 7 MPa. This was found by electrospinning the solution onto a substrate where individual fibers could be anchored to ridges with glue and pulled at a continuous rate of 300 nm/s [90]. Comparing the electrospinning process to the one used here, the molecular weight of 120,000-300,000 is 40,000-220,000 da higher than the 80,000 used in this experiment. In polymer science, the molecular weight has an indirect impact on yield strength; low MW components tend to depress the yield point of whole polymers [91]. Looking at PE, yield strength is a function of density and, to a first approximation, independent of MW. The yield strength of low-density material has been found to increase with MW in the range of 1.6×10^4 to 2.9×10^4 . Given the information on MW and the impact it can have on yield strength as well as the increased concentration of polymer in solution, it is reasonable to project the yield point of the fibers produced in this experiment to be lower than the 12 MPa found.

The tensile modulus was also determined for the 120,000-300,000 MW PCL. The fiber was stretched to a fixed strain and then held for a 50-second interval to allow for stress relaxation and then stretched again. For fibers less than one month old it was found that tensile modulus was 62 +/- 26 MPa. The impact of PCL fiber diameter on tensile strength has been examined by cutting specimens of electrsun PCL at different dimensions for bulk tensile testing. Using samples cut at $3.15 \times 63.15 \times 0.5$ and $3.17 \times 63.17 \times 0.5 \text{ mm}^3$, the resulting tensile test found over a 300% increase in tensile strength using the larger sample. A similar tensile test was set up to measure the impact of individual fiber diameter of tensile strength, the resulting test found that tensile strength increases with decreasing fiber diameter. This was attributed to improved

molecular orientation in the smaller diameter fibers found using wide-angle X-ray diffraction [92]. Using this information, it can be concluded that the fiber produced in the research conducted would have a lower tensile strength than that produced using 120,000-300,000 MW PCL due to the larger fiber diameters found in this research.

3.3.3 Degradation rate

The degradation of polymer scaffolds is key in determine their usefulness and applications. Other literature has quantified the degradation rate of fibers produced from the electrospinning of PCL in HFIP mixed at 10% w/v and electrospun at 1 mL/h, a plate distance of 20 cm and a voltage of 20 kV. A drum collector was used as the electrospinning target and was rotated at 600 rpm. A degradation study of these fibers was done over 180 days in a temperature-controlled environment set to 37 °C. Using fiber diameter as the metric to determine changes in fiber morphology caused by degradation, the initial average fiber diameter was found to be 0.219 μm . Measurements were taken at intervals and the following average fiber diameters were observed: Day 30 fiber diameters within the range of the initial reading. Day 90 15.5% increase to fiber diameter (this was not considered significant). Day 180 average fiber diameter 0.214 μm [93]. The key differences between this research and the research conducted in this paper is the concentration of polymer in solution at 10% vs 7.5% w/v and the electrospinning parameters. The higher voltage and the use of a spinning drum collector to create aligned scaffold would have significant effects on fiber diameter, as shown comparing the initial (Day 0) measurement of 0.219 μm to the macroscale fiber created in this paper.

The impact of fiber diameter on degradation rate has been studied for chitosan fiber-mesh scaffolds. The scaffolds were created using chitosan with a degree of deacetylation of 89% and a

MW of 366 kDa and spinning a 3% chitosan solution in 2% acetic acid into a sodium hydroxide and sodium sulphate solution using a wet spinning technique. Different fiber diameters were created by using needles with 800 and 450 μm diameters. Four samples were produced, two with 1 mL of chitosan with different needle diameters and two with 0.5 mL of chitosan and different needle diameters. Results of the degradation study were gathered after 35 days and found that, in terms of degradation rate (average diameter, volume of chitosan), $63\ \mu\text{m}\ 0.5\ \text{mL} > 102\ \mu\text{m}\ 0.5\ \text{mL} > 63\ \mu\text{m}\ 1\ \text{mL} > 102\ \mu\text{m}\ 1\ \text{mL}$ [94]. The research goes on to state that scaffolds with higher porosity degraded faster; looking between structures, those composed of thinner fibers had a slightly higher degradation rate, but it was not considered statistically significant. The significant impact of porosity on degradation rate adds to the difficulty of comparing the literature on PCL degradation and the fibers created in this research. The fibers in literature were aligned by being deposited onto a rotating drum; it is likely that those scaffolds have lower porosity than the scaffolds produced in this paper. As such it can be concluded that the fibers produced would have a faster degradation rate.

3.3.4 Drug release

PCL fibers have been loaded with doxorubicin hydrochloride (DOXO) for drug release applications, dissolving 15% wt PCL in a DMF:DCM 30:70 v/v ratio solvent and electrospun at 15 kV, 20 cm plate distance, and 2 l/min air flow. The resulting PCL/DOXO fibers were studied for nine days in incubation. The HeLa-WT cells showed a distinct drop in viability from Day 1 to 9 when treated with PCL/DOXO fibers. The drug was successfully encapsulated and released over the nine-day period, but even when cell viability was tested using the more resistant MCF-7 cells, a reduction in viability was found [95]. Gauifenesin-loaded PCL fibers and timolol-loaded

PCL fibers have been experimented with to further analyze the drug release properties of PCL scaffolds. Gua+PCL reached 100% drug release in 10 hours while Tim+PCL reached 89% drug release in 8 hours. The release of Gua and Tim was determined to be diffusion based and the release rates from being encapsulated in PCL versus encapsulation in PLC-O a PCL-based esteramide was reported. FITC-dextran-loaded PCL and PCL-O release was studied over an 18 day period, PCL released just over 10% over the period while PCL-O released over 40% [96]. The difference in total release over the 18-day period shows the importance of blended polymers for drug release applications. Comparing both drug release experiments to the fibers fabricated in this paper, the PCL fibers will be capable of carrying any of the drugs described above. DOXO, Gua, and Tim could all be loaded and released using the PCL scaffolds produced; the release rates would likely be more favored toward a burst release due to the increased degradation rate discussed previously.

3.4 Summary

The electrospinning of PCL was a success. Scaffolds with consistent fiber morphology were produced and optimized. Increasing the concentration of PLC from 5% (w/v) to 7.5% (w/v) resulted in more consistent scaffolds as noted by the calculated standard deviation for 7.5% (w/v) fibers being less than 0.40. The electrospinning of 7.5% (w/v) PCL at a 7.0-8.0 kV applied voltage, a 1.5 mL/h feed rate, and a 10 cm plate distance resulted in fibrous scaffolds that have the potential for coaxial electrospinning. An 8.0 kV applied voltage with these parameters produced the smallest diameter fibers, making it the most optimized for monoaxial PCL. With the success of this experiment in producing consistent PCL scaffolds, properties such as

mechanical strength, scaffold degradation rate, and drug loading and release can be investigated in future research.

CHAPTER 4

MONOAXIAL POLY(LACTIC-CO-GLYCOLIC) ACID

4.1 Introduction

Poly(lactic-co-glycolic) acid (PLGA) is a synthetic co-polymer frequently used in biomaterials and electrospinning in drug release applications. As a co-polymer, the mechanical and chemical properties are in part determined by the ratio of the biopolymers. Polyglycolic acid (PGA) is a hydrophilic crystalline polymer that degrades rapidly [97]. Polylactic acid (PLA) is a hydrophobic polymer divided into two enantiomers D-lactic acid and L-lactic acid. The difference between the enantiomers is the location of a hydroxide/hydrogen group on the mer structure. L-lactic acid is naturally found in the body while D-lactic can be fatal to humans in large quantities [98]. Poly(L-lactide) has a less crystalline structure than PGA and poly(D-lactide) has an amorphous structure. This is important to consider when working with PLGA or PGA in general, as the mechanical properties of the two enantiomers are different. L-lactide was used in this research because of its natural occurrence in the body. The ratio used in this research is (50:50) LA:GA. This ratio of LA:GA possesses an amorphous structure [97]. The ability to electrospin PLGA has been extensively researched and high-molecular-weight PLGA of various ratios ranging from (50:50) to (85:15) has been found to produce consistent fibers with diameters ranging from 750 nm to 1500 nm [99] - [101]. The range of diameters

produced in literature demonstrates the adaptability of PLGA-based electrospun scaffolds.

The degradation rate makes PLGA particularly well suited for *in vivo* applications. Using PLGA stents coated with amorphous calcium phosphate (ACP), the *in vivo* degradation of PLGA in rats was characterized as having less than 25% weight loss over the first week after implanting and only 40% weight loss after three weeks [102]. *In vitro* degradation was also examined using different ratios of PLGA from (50:50) to (100:0) LA:GA. After 45 days, (65:35) PLGA had lost the most weight at approximately 30%, while (50:50) and (75:25) had only lost 20% [102]. This degradation rate allows PLGA to be used as a biodegradable material, eliminating the need for removal surgery's. Such as in the case of creating a biodegradable orthopedic screw to eliminate the need for future removal surgery in pelvic osteotomies in children [103]. This shows the degradation rate of PLGA is tunable by changing the ratio of lactic to glycolic acid.

The goal of monoaxial electrospinning of poly(lactic-co-glycolic) acid was to optimize the electrospinning process around the viscosity and conductivity of PCL in hexafluoro-2-propanol (HFIP) solution. Once optimized, the solution would be electrospinnable with PCL for composite PCL/PLGA scaffold fabrication research. This was accomplished by attempting to electrospin different concentrations of PLGA in HFIP. The solution viscosity and conductivity can have a great impact on the electrospinning process and resulting fibers. Both the Taylor cone and the prevalence of fiber defects are dependent in part on the solution viscosity and conductivity. Starting with a 15% w/v solution of PLGA in HFIP and increasing the concentration in 10% w/v increments to 35% w/v, we can determine the impact of concentration on the process and the best concentration for PLGA. The resulting fibrous scaffolds from each

concentration were compared by using scanning electron microscopy (SEM) to take diameter measurements.

4.2 Results

4.2.1 SEM

4.2.1.1 PLGA (50:50 LA:GA ratio) in HFIP at 15% (w/v)

Using a voltage of 8 kV, a plate distance of 10 cm, and a feed rate for 1.5 mL/h on the electrospinning machine, a 15% (w/v) of PLGA (50:50) in HFIP was tested. The electrospinning process for this experiment was not stable. The Taylor cone was not consistent and at times would fail to form entirely. Because the Taylor cone was so unstable, the experiment was deemed unsuccessful. Additional experiments were run on varying voltages, plate distances and feed rates.

The most consistent Taylor cones were found when using a voltage of 8 kV, a 15 cm plate distance, and a 1.2 mL/h feed rate. The resulting SEM scaffold from this experiment is depicted in Figure 22. In Figure 22 A it is difficult to discern whether a fibrous structure has formed as the morphology of the scaffold resembles balls or clumps of polymer with random dimensions. Figure 22 B shows a few fibers that have formed; however, because they are not indicative of the scaffold's morphological makeup, diameter measurements were not taken.

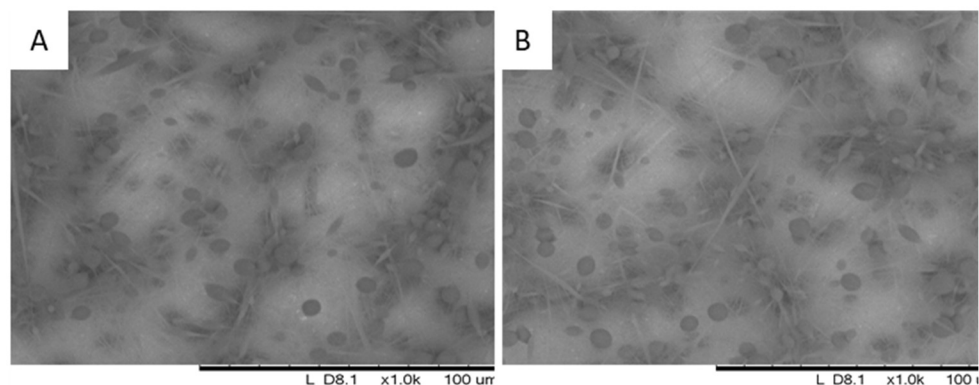


Figure 22 SEM images of (50:50) PLGA electrospun at 8.0 kV, 15% w/v, 1.2 mL/h, and 15 cm plate distance imaged at 1k magnification A) Spot A B) Spot B

4.2.1.2 PLGA (50:50 LA:GA ratio) in HFIP at 25% (w/v)

With the lack of success using a 15% (w/v) concentration of PLGA in HFIP and with no improvement found by changing voltage or feed rate, the concentration was increased. The experiments were re-run using a 25% (w/v) concentration of PLGA in HFIP. Using a concentration of 25% (w/v) the Taylor cone became most stable when using a voltage of 7.5 kV and a plate distance of 10 cm. Figure 23 shows the results of varying feed rate to further optimize fiber production. Those results are discussed below.

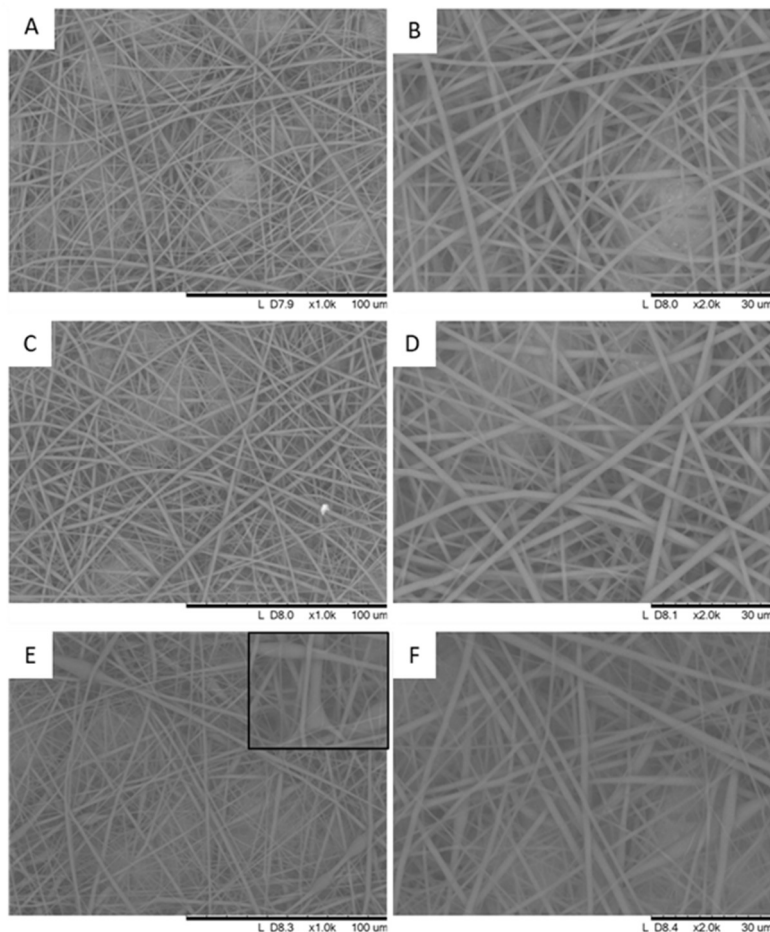


Figure 23 SEM images of (50:50) PLGA electrospun at 7.5 kV, 25% w/v, and 10 cm plate distance A) 0.9 mL/h 1k B) 0.9 mL/h 2k C) 1.1 mL/h 1k D) 1.1 mL/h 2k E) 1.3 mL/h 1k f) 1.3 mL/h 2k

Figure 23 A and B show different magnifications of a scaffold produced by electrospinning with a 0.9 mL/h feed rate. At this feed rate, the scaffold has a fibrous morphology and Figure 23 A shows that the morphology is consistent throughout the scaffold. This scaffold at greater magnification, as shown in Figure 23 B, however, exposes some inconsistencies in fiber diameter that resulted in an approximate standard deviation of 0.4 recorded in Table 4.

Table 4 Impact of feed rate on monoaxial PLGA (50:50) fiber diameter at 25% w/v 7.5 kV and 10 cm

Feed rate (mL/h)	Fiber Diameter (diameter (um) + STDev)	P-value
0.9	1.6224 +/- 0.4055	-
1.1	1.964 +/- 0.4266	0.0134
1.3	1.6004 +/- 0.5227	0.8826
1.5	1.6296 +/- 0.4218	0.9567
1.7	2.0665 +/- 0.5596	0.0066

Figure 23 C and D show magnifications of the scaffold created using a 1.1 mL/h feed rate. Figure 23 C shows a consistent fibrous structure throughout the scaffold. The fiber diameters and morphology shown in Figure 23 C appear very similar to those in Figure 23 A. At greater magnification, the fibers in Figure 23 D again show inconsistent fiber diameters. Comparing the scaffolds in Figure 23 B (0.9 mL/h feed rate) to Figure 23 D (1.1 mL/h feed rate), the differences are very subtle. Both scaffolds are shown to have smooth fibrous morphology with wide ranging diameters. The difference is the scaffold created using the 0.9 mL/h feed rate (Figure 23 B) has fibers that skew more towards a smaller diameter than those created with the 1.1 mL/h feed rate (Figure 23 D). This difference in fiber diameters is confirmed by the average fiber diameters in the 0.9 mL/h scaffold being smaller than the average fiber diameters for the 1.1 mL/h scaffold shown in Table 4. This increase in fiber diameter observed when changing the feed rate from 0.9 to 1.1 mL/h has been determined to be statistically significant.

The feed rate was again increased to 1.3 mL/h; SEM images of these scaffolds are shown in Figure 23 E and F. Figure 23 E shows some bead formation in the scaffold that immediately shows electrospinning at this feed rate is not optimized. Figure 23 F does not show the clear beading found in Figure 23 E but does have fibers with drastically different diameters and this

could be attributed to beading. While fiber defects such as beading are not measured when calculating the average fiber diameter, fibers with beads typically have smaller diameters. The average fiber diameter recorded in Table 4 for a scaffold created with a feed rate of 1.3 mL/h is very similar to that recorded for 0.9 mL/h. However, due to the prevalent beading in this scaffold, the results are not considered to be as good as those produced at 0.9 or 1.1 mL/h feed rates.

Feed rates of 1.5 mL/h and 1.7 mL/h were also tested but resulted in fibrous scaffolds with worse morphology than the 1.3 mL/h scaffold shown in Figure 23 E and F. While the standard deviation calculated for the 1.5 mL/h scaffold recorded in Table 4 is less than the standard deviation recorded for the 1.3 mL/h scaffold, the beading was more consistent throughout the scaffold.

To characterize the impact of feed rate on fiber formation and consistency, statistical analysis was conducted. The *p*-values resulting from the confidence interval using the 0.9 mL/h feed rate scaffold as the constant are shown in Table 4. From the analysis it was found that the 1.1 mL/h feed rate resulted in a statistically significant increase in fiber diameter and the 1.7 mL/h feed rate caused a very statistically significant increase in fiber diameter.

After changing the feed rate under a 7.5 kV applied voltage, the continuation of the electrospinning decision tree suggests a new voltage be tested. To complete the electrospinning process, the voltage was increased to 8 kV. SEM images taken are shown in Figure 24. Images taken of scaffolds produced from 0.7 mL/h, 0.9 mL/h, and 1.7 mL/h feed rates are omitted from the figure because each scaffold showed similar inconsistencies and defects that are better observed in the images taken for the 1.1 mL/h and 1.3 mL/h scaffolds.

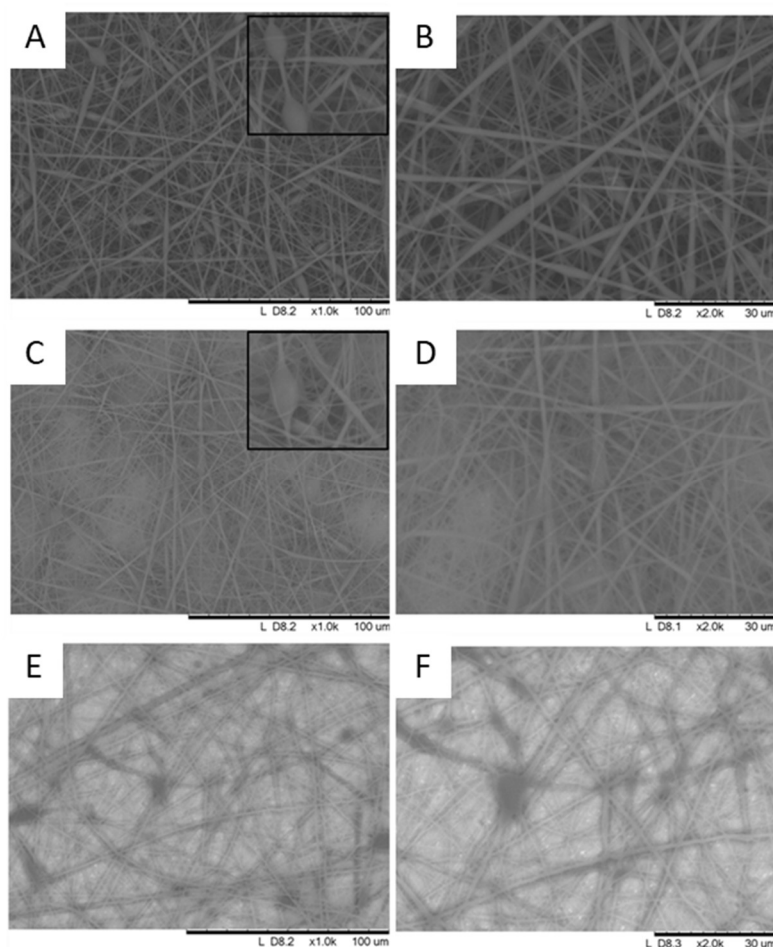


Figure 24 SEM images of (50:50) PLGA electrospun at 8.0 kV, 25% w/v, and 10 cm plate distance A) 1.1 mL/h 1k B) 1.1 mL/h 2k C) 1.3 mL/h 1k D) 1.3 mL/h 2k E) 1.5 mL/h 1k F) 1.5 mL/h 2k

Figure 24 A shows SEM imagery of a scaffold produced with a 1.1 mL/h feed rate. Figure 24 A shows a fibrous morphology with some bead formation throughout; Figure 24 B increases the magnification, and the beading and inconsistent fiber diameters can be more clearly observed. The inset in Figure 24 A shows more bead formation in a different section of the scaffold, illustrating that the beading was consistent throughout the scaffold.

Scaffolds produced with a 1.3 mL/h feed rate shown in Figure 24 C and D. The fiber formation and consistency appears to have improved; however, shown in the Figure 24 C inset, there were instances of beading in other areas of the scaffold. Figure 24 D shows some of the inconsistencies in fiber diameter from scaffolds produced at the 1.3 mL/h feed rate, as well as some possible bead formation in the scaffold. Table 5 shows the scaffold has a smaller average fiber diameter than the 1.1 mL/h scaffold. The standard deviation again decreases when compared to the 1.1 mL/h feed rate scaffold, showing that the changes in conditions from a 0.7 mL/h feed rate to a 1.3 mL/h feed rate are producing more consistent scaffolds.

Table 5 Impact of feed rate on monoaxial PLGA (50:50) fiber diameter at 25% w/v 8 kV and 10 cm

Feed rate (mL/h)	Fiber Diameter (diameter (um) + STDev)	P-value
0.7	1.1694 +/- 0.7459	-
0.9	1.313 +/- 0.8055	0.5045
1.1	1.4836 +/- 0.4715	0.0438
1.3	1.208 +/- 0.3102	0.0001
1.5	1.0616 +/- 0.3825	0.0001
1.7	1.1721 +/- 0.5727	0.0006

Figure 24 E shows SEM image taken of a scaffold produced at a 1.5 mL/h feed rate. Figure 24 I has an interesting fiber morphology as it appears branching has started to occur within the scaffold. Figure 24 F is the same location at a greater magnification. Here at least one branching zone is shown where three or four fibers come together at a single point. Table 5 shows that the average fiber diameter is the smallest in this scaffold compared to the other feed rates tested with these parameters. The standard deviation for this scaffold is within the range of standard deviations calculated for the other feed rates tested. The P-values calculated from the statistical

analysis are shown in Table 5. All of the produced scaffolds are compared to the 0.7 mL/h feed rate scaffold.

The increase in average fiber diameter and standard deviation found in the 0.9 mL/h feed rate scaffold was determined to not be statistically significant. Table 5 shows the average fiber diameter of the 1.1 mL/h feed rate scaffold has significantly increased compared to the 0.7 mL/h scaffolds and the standard deviation decreased. The change in fiber diameter from a 0.7 mL/h feed rate to 1.3 mL/h feed rate is statistically very significant. The statistical significance is illustrated in Table 5. Comparing the calculated average fiber diameter and standard deviation of the 1.5 mL/h feed rate scaffolds to the 0.7 mL/h feed rate scaffolds, a statistically very significant decrease in average diameter and standard deviation was found. Assessing the average fiber diameter and standard deviation of the 1.7 mL/h feed rate scaffolds to the 0.7 mL/h feed rate scaffolds, and a statistically very significant increase in fiber diameter and decrease in standard deviation was found.

To further show the impact of electrospinning parameters on fiber production, a phase diagram was created and is shown in Figure 25. From the first subplot in the figure, the impact of feed rate on standard deviation is shown. A trend of increasing standard deviation as the feed rate diverges from 1.3 mL/h is found. Comparing the range of standard deviations at all feed rates tested, the spread is very similar regardless of the applied voltage, as shown in the last subplot.

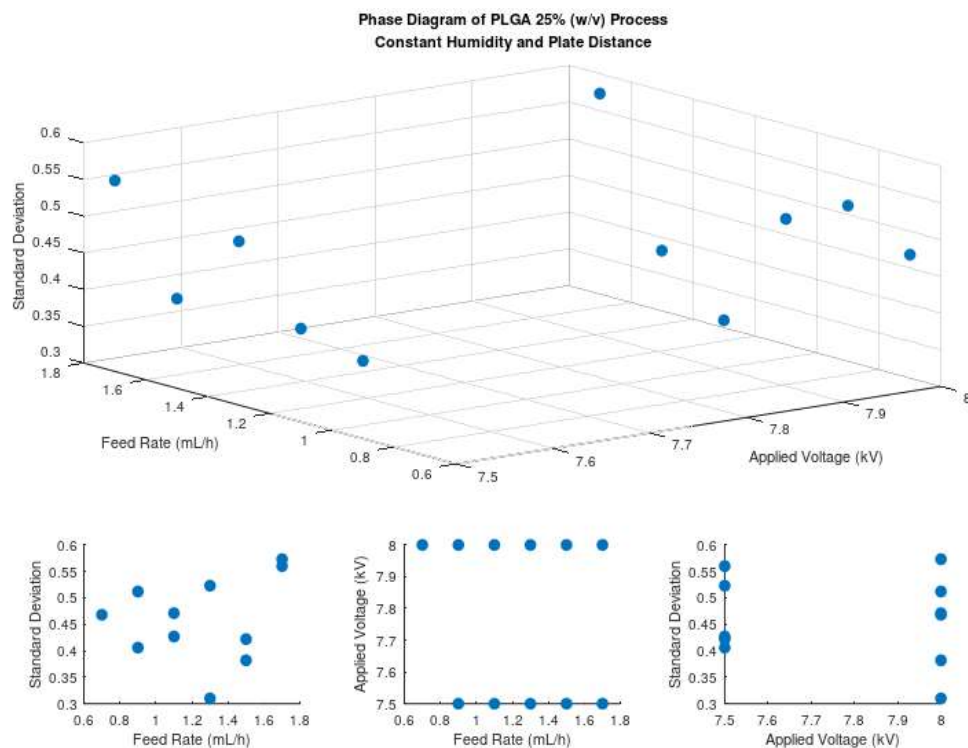


Figure 25 Phase diagram of the 25% (w/v) process

3.3.1.3 PLGA (50:50 LA:GA ratio) in HFIP at 35% (w/v)

With the improvement in scaffold morphology observed when increasing the concentration of PLGA in HFIP from 15% (w/v) to 25% (w/v), and after exhausting all other options in the electrospinning decision tree, the concentration was increased further. By increasing the PLGA content to 35% (w/v), the experiment could determine whether a higher concentration would produce a further optimized scaffold. From the 25% (w/v) experiment, the 1.7 mL/h feed rate produced significant fiber defects and was removed from the 35% (w/v) experiment. While increasing the voltage from 7.5 kV to 8 kV, the lower feed rates struggled to keep the nozzle saturated with solution. This could explain why the 0.7 mL/h and 0.9 mL/h 25%

(w/v) scaffolds have high standard deviations. These lower feed rates were also removed from the 35% (w/v) experiment. The first feed rate tested was 1.1 mL/h at 7 kV, and the electrospinning decision tree was followed after gathering data from these parameters.

Figure 26 provides the SEM images taken of scaffolds produced from 35% (w/v) PLGA in HFIP under all three of the applied voltages tested and a 10 cm plate distance at feed rates ranging from a 1.1 mL/h feed rate to a 1.3 mL/h feed rate. A 1.5 mL/h feed rate was also tested but is not imaged in the figure due to the significantly higher fiber diameter and standard deviation.

Figure 26 A shows a scaffold produced from a 1.1 mL/h feed rate. The scaffold shows a fibrous structure with no morphological defects. Figure 26 B shows the same location imaged at greater magnification. Here, the differences in fiber diameters can be observed. The average fiber diameter was calculated to be smaller than the scaffolds produced at both 7.5 and 8 kV for 1.1 mL/h feed rate 25% (w/v) PLGA and is recorded in .

Figure 26 C shows a scaffold produced with a 1.3 mL/h feed rate. This scaffold has clear fibrous morphology with no signs of fiber defects. Figure 26 D shows that the fiber diameters appear relatively consistent. The standard deviation is smaller than that calculated for a 1.1 mL/h feed rate scaffold shown in Figure 26 A and B, (see in).

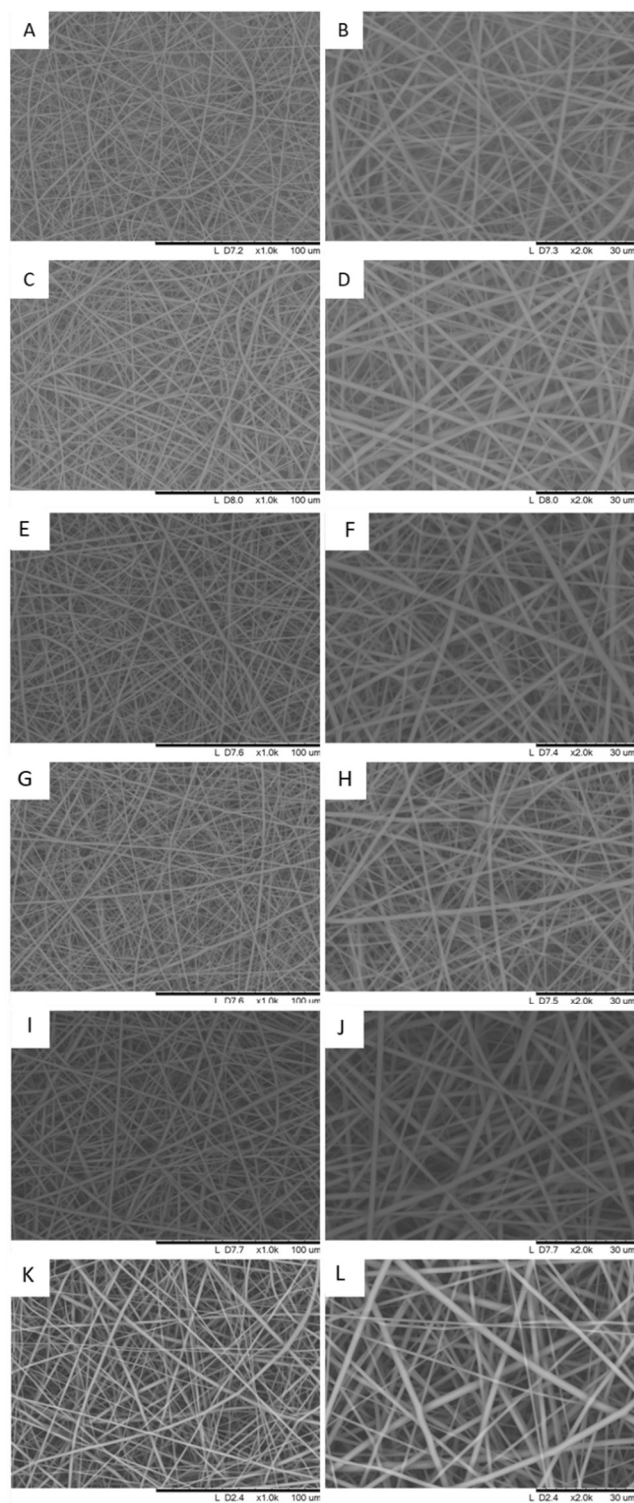


Figure 26 SEM imagery of electrospun (50:50) PLGA at 35% w/v 10 cm A) 7 kV 1.1 mL/h 1k B) 7 kV 1.1 mL/h 2k C) 7 kV 1.3 mL/h 1k D) 7 kV 1.3 mL/h 2k E) 7.5 kV 1.1 mL/h 1k F) 7.5 kV 1.1 mL/h 2k G) 7.5 kV 1.3 mL/h 1k H) 7.5 kV 1.3 mL/h 2k I) 8 kV 1.1 mL/h 1k J) 8 kV 1.1 mL/h 2k K) 8 kV 1.3 mL/h 1k L) 8 kV 1.3 mL/h 2k

Table 6 Impact of feed rate on monoaxial electrospun (50:50) PLGA at 35% w/v 7 kV and 10 cm

Feed rate (mL/h)	Fiber Diameter (diameter (um) + STDev)	P-value
1.1	1.4034 +/- 0.4397	-
1.3	1.7485 +/- 0.4019	0.0135
1.5	3.0465 +/- 0.5112	0.0001

The average fiber diameter is larger than the average fiber diameter for the 1.1 mL/h feed rate scaffold. It was also found that the diameter calculated is similar to the average diameter recorded in Table 4 for the 1.1 mL/h feed rate scaffold, which was produced from 25% (w/v) PLGA electrospun at 7 kV.

Comparing the scaffolds depicted in Figure 26 A-D to those shown in Figure 23, only Figure 23 C and D scaffolds produced with 25% (w/v) and 1.1 mL/h feed rate at 7.5 kV are as consistent. For the parameters tested, the 35% (w/v) scaffolds are more consistent and possess better fiber formation than any scaffold resulting from 15% (w/v) or 25% (w/v).

Figure 26 E shows a scaffold produced from a 1.1 mL/h feed rate. The scaffold has a clear fibrous morphology without any fiber defects. Figure 26 F shows the same location at greater magnification. Here the slight differences in fiber diameter can be observed. The average fiber diameter and standard deviation are recorded in Table 7. Comparing this scaffold to the scaffold produced from 35% (w/v) PLGA in HFIP with a 7 kV applied voltage and a 1.1 mL/h feed rate shown in Figure 26 D, the average fiber diameter slightly increased while the standard deviation decreased. This suggests a more consistent scaffold was produced at 7.5 kV for a 35% (w/v) PLGA in HFIP solution with a 1.1 mL/h feed rate and a 10 cm plate distance.

Table 7 Impact of feed rate on monoaxial PLGA (50:50) fiber diameter at 35% w/v 7.5 kV and 10 cm

Feed rate (mL/h)	Fiber Diameter (diameter (um) + STDev)	P-value
1.1	1.4738 +/- 0.4239	-
1.3	1.2882 +/- 0.3577	0.1427
1.5	2.1115 +/- 0.4367	0.0001

Figure 26 G depicts a scaffold produced with a 1.3 mL/h feed rate. The figure shows a clear fibrous morphology with consistent diameters and no defects. Increasing the magnification in Figure 26 H confirms the morphology; however, there is some variance in fiber diameter throughout the scaffold. The average fiber diameter and standard deviation recorded in Table 7 suggest the parameters are more optimized for this feed rate, as both average fiber diameter and standard deviation decrease compared to the 1.1 mL/h feed rate. Comparing this scaffold to scaffolds produced with a 1.3 mL/h feed rate at 7.5 kV (Figure 23 E) and 8 kV (Figure 23 K) both with 25% (w/v) PLGA in HFIP, the scaffold has a smaller average fiber diameter than the 7.5 kV scaffold and has no fiber defects, unlike the 8 kV scaffold.

Figure 26 I shows a scaffold produced from a 1.1 mL/h feed rate. Figure 26 J shows the same location at greater magnification. Here the inconsistencies in fiber diameter can be observed. The average fiber diameter and standard deviation calculated are recorded in Table 8. From Table 8 the standard deviation is higher than any standard deviation calculated for 35% (w/v) PLGA solution electrospun at 7.5 kV. The average fiber diameter is also larger than what was calculated for 35% (w/v) PLGA solution electrospun at 7.5 kV at a 1.1 mL/h feed rate. This could indicate that the electrospinning process is not as optimized at 1.1 mL/h under an 8 kV voltage compared to a 7.5 kV voltage.

Table 8 Impact of feed rate on monoaxial PLGA (50:50) fiber diameter at 35% w/v 8 kV and 10 cm

Feed rate (mL/h)	Fiber Diameter (diameter (um) + STDev)	P-value
1.1	1.6071 +/- 0.5169	-
1.3	1.7377 +/- 0.4732	0.4098
1.5	2.062 +/- 0.5919	0.0136

Figure 26 K shows a scaffold produced at a 1.3 mL/h feed rate. Increasing the magnification, some variance in fiber diameter is observed in Figure 26 L. The decrease in standard deviation suggested that at 8 kV, the faster feed rate of 1.3 mL/h is more optimized than the 1.1 mL/h feed rate.

To conduct statistical analysis, the data gathered from the 1.1 mL/h scaffolds at each tested voltage was used as a comparator; 7 kV, 7.5 kV, and 8 kV experiments have their calculated average fiber diameters, standard deviations, and *p*-values shown in , Table 7, and Table 8 respectively.

Under an applied voltage of 7 kV *p*-values were calculated for statistical analysis and are shown in . The increase in average fiber diameter found when increasing the feed rate to 1.3 mL/h was determined to be statistically significant. Increasing the feed rate further to 1.5 mL/h resulted in a very significant increase in average fiber diameter.

The impact of feed rate on fiber production was determined and is illustrated in Table 7. In Table 7, the increase from a 1.1 mL/h feed rate to a 1.3 mL/h feed rate did not have a significant impact on fiber diameter under these parameters. The increase from a 1.1 mL/h feed rate to a 1.5 mL/h feed rate was found to have a very significant impact on the resulting fiber diameter.

The increase in average fiber diameter, recorded in Table 8, compared to the 1.1 mL/h feed rate at the same electrospinning parameters was not found to be statistically significant. As with both the 7 kV and 7.5 kV experiments with 35% (w/v) PLGA in HFIP, further increasing the feed rate to 1.5 mL/h results in a very significant increase in average fiber diameter.

Analysis was conducted on the statistical significance of voltage on the resulting fiber diameters shown in Figure 27. Focusing first on the 1.1 mL/h feed rate, the impact of voltage on fiber diameter was found to be insignificant. The 1.3 mL/h feed rate comparison found that increasing the voltage from 7 kV to 7.5 kV resulted in a very significant decrease in fiber diameter while the larger increase in voltage from 7 kV to 8 kV had an insignificant effect. Comparing the 1.5 mL/h feed rates, a very significant decrease in fiber diameter was found when increasing the voltage from 7 kV to 7.5 kV and when increasing the voltage from 7 kV to 8 kV.

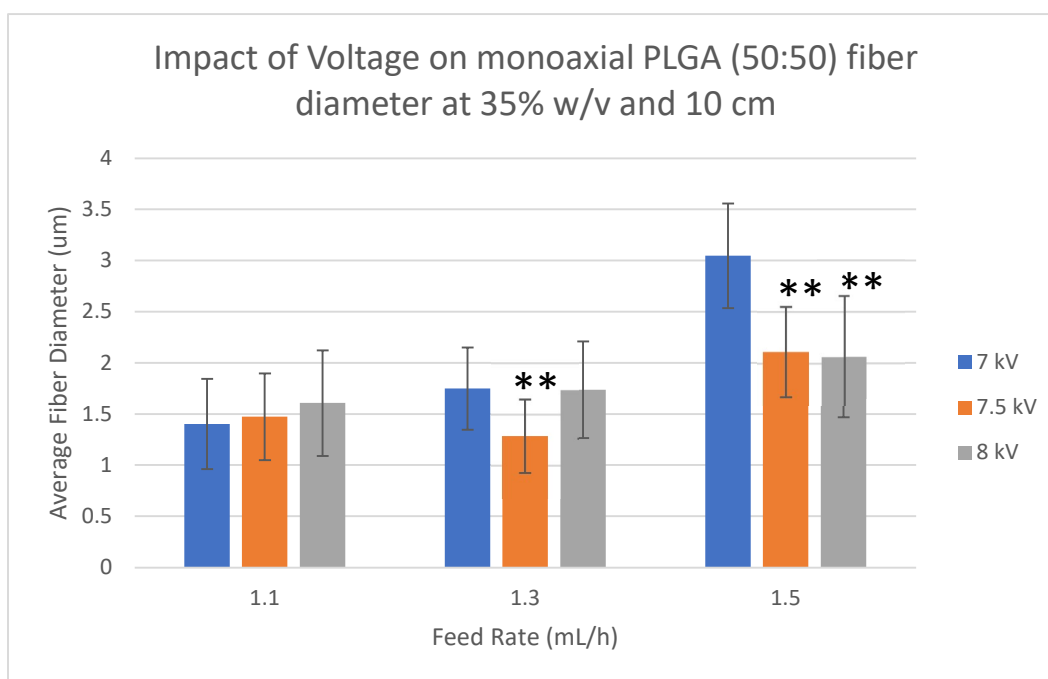


Figure 27 Impact of voltage on monoaxial PLGA (50:50) fiber diameter at 35% w/v and 10 cm (*) $p < .05$ (**) $p < .01$

Further analysis on the impact of concentration was conducted to determine whether the trend of a direct relationship between increasing feed rate and fiber diameter was influenced by the other electrospinning parameters. Figure 28 shows the comparisons made between the 25% (w/v) PLGA solution and the 35% (w/v) PLGA solution electrospun at 1.1, 1.3, and 1.5 mL/h feed rates. At every condition aside from 1.1 mL/h feed rate at 8 kV, the change in concentration was found to have at least a significant impact on fiber diameter. In only two instances did the increased concentration of PLGA solution result in a smaller average fiber diameter. Those are both at 7.5 kV with 1.1 and 1.3 mL/h feed rates.

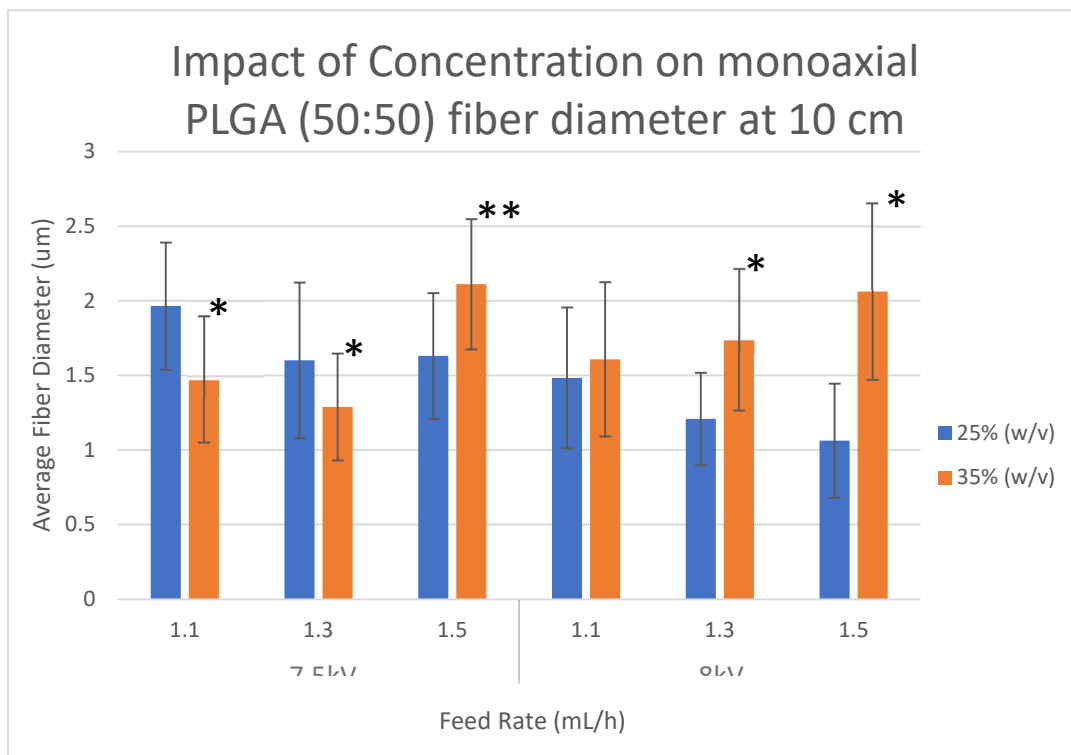


Figure 28 Impact of concentration on monoaxial PLGA (50:50) fiber diameter at 10 cm

A phase diagram was created to further illustrate the impact of the electrospinning parameters on the resulting fibers and is shown in Figure 29. From Figure 29 the total impact of each parameter can be analyzed. A general trend of decreasing standard deviation with increasing humidity is shown. This trend is confirmed when isolating applied voltage as a variable shown in the last subimage in Figure 29.

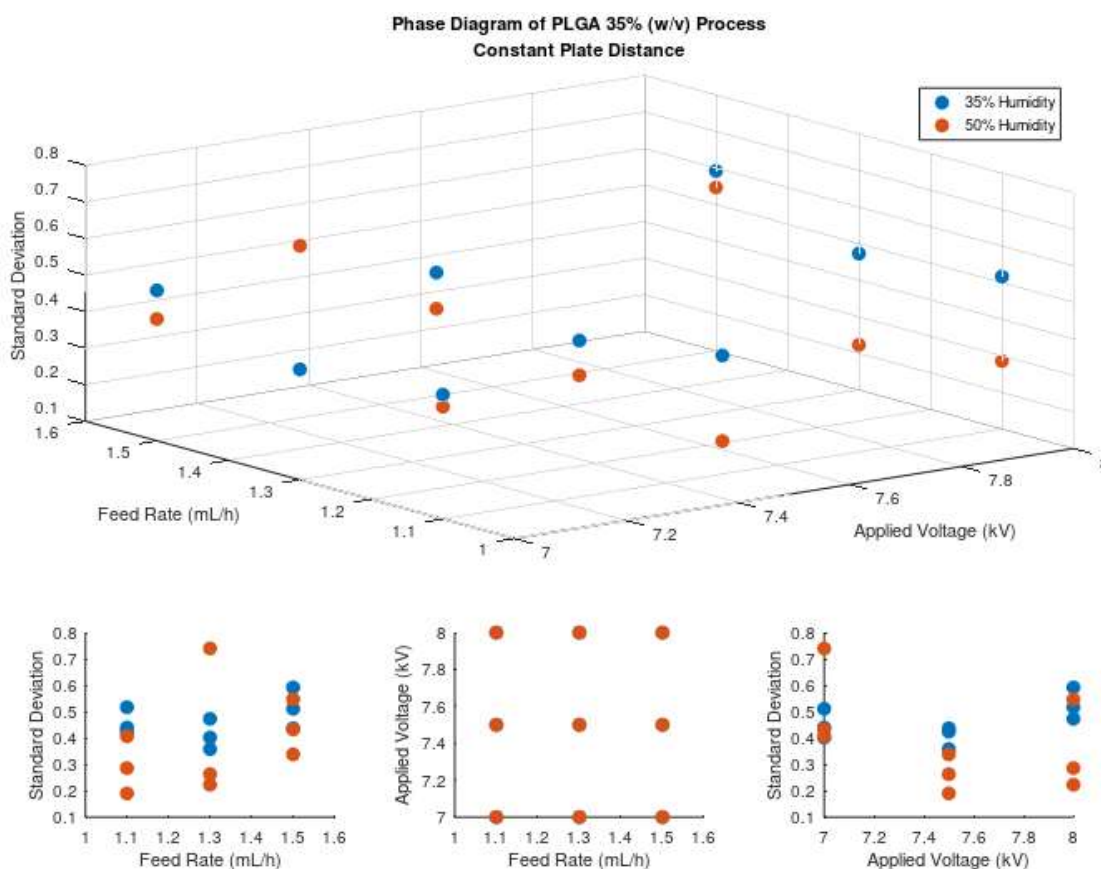


Figure 29 Phase diagram of the 35% (w/v) process

4.2.2 ATR-FTIR bond analysis

ATR-FTIR was conducted on two samples of (50:50) PLGA scaffold to determine the chemical bonds in the structure. ATR-FTIR is an important analysis for characterization. If the

results fall outside of what is expected from (50:50) PLGA, some chemical contamination has occurred in the scaffold changing the bonds. An electrospun (50:50) PLGA scaffold was cut to a 2 mm x 1 mm rectangle and then analyzed. The spikes near 1300 and 1700 are indicative of PLGA; the initial spike around 2400 also matches established literature for FTIR of PLGA [104], confirming the integrity of the scaffold and the absence of foreign materials.

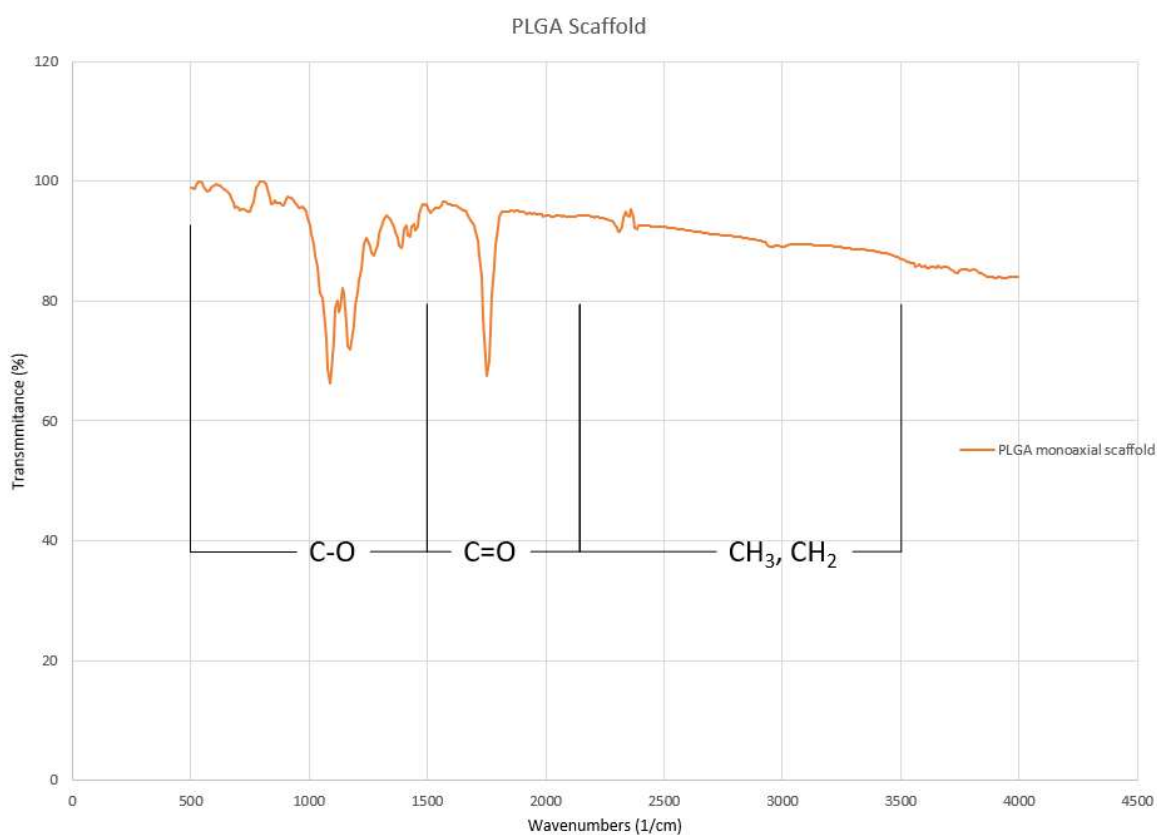


Figure 30 ATR-FTIR analysis of (50:50) PLGA scaffolds

4.3 Discussion

4.3.1 Impact of feed rate

At each voltage tested for the electrospinning of PLGA, multiple feed rates were used to determine the impact of feed rate on the electrospinning process and whether changes in feed rate would produce better scaffolds. The feed rate was always increased in increments of 0.2 mL/h.

In the case of 35% (w/v) PLGA (50:50) in HFIP, a correlation between increasing feed rate and increasing fiber diameter appears in all three of the voltages tested. Under a 7 kV applied voltage increasing the feed rate from 1.1 mL/h to 1.3 mL/h resulted in a statistically significant increase in average fiber diameter shown in .

Further increasing the feed rate from 1.1 mL/h to 1.5 mL/h, at this voltage the increase in fiber diameter was determined to be very statistically significant. This shows a clear connection between the feed rate and the scaffold fiber diameter, as all other electrospinning parameters were kept the same. A similar conclusion can be reached using the 7.5 kV applied voltage results. While the increase in feed rate from 1.1 mL/h to 1.3 mL/h resulted in a slight decrease in average fiber diameter, with a similar standard deviation, this decrease was not found to be statistically significant (shown in Table 7). When comparing the changes in scaffold fiber diameters from a 1.1 mL/h feed rate to a 1.3 mL/h feed rate, a very statistically significant increase in average fiber diameter was found; the standard deviation calculated for the 1.5 mL/h feed rate scaffold was similar to the 1.1 mL/h feed rate scaffold. The last voltage tested in this research was 8 kV. At 8 kV the increase in feed rate from 1.1 mL/h to 1.3 mL/h resulted in a slight increase in average fiber diameter that was not found to be statistically significant.

Comparing the 1.1 mL/h feed rate scaffold to the 1.5 mL/h feed rate scaffold, a statistically significant increase in average fiber diameter was found.

From the data collected in this research, the scaffolds produced show a direct relationship between fiber diameter and feed rate. This relationship has been examined in literature with conflicting conclusions. Research on the effects of feed rate on fiber diameter in the electrospinning of 10 wt% polyacrylonitrile (PAN) solutions found there was no significant impact on fiber diameter when increasing feed rate from 1.50 $\mu\text{L/h}$ to 350 $\mu\text{L/h}$ [105]. This increase of 200 $\mu\text{L/h}$ is the same as the incremental increase of 0.2 mL/h used in this research. Both the 7.5 kV and 8 kV applied voltages for 35% (w/v) PLGA (50:50) in HFIP found a statistically insignificant change in average fiber diameter from 1.1 mL/h to 1.3 mL/h, agreeing with the data collected using PAN. Research conducted on the effect of feed rate on the production of polyurethane (PU) nanofibers found feed rate had a significant influence on the resulting fiber diameters. The research done on PU increased the feed rate by 0.25 mL/h in each trial, ranging from a 1.0 mL/h to a 1.5 mL/h feed rate [106]. With a larger increase in feed rate the significant influence of feed rate over fiber diameter was found. This agrees with the statistically very significant increase in average fiber diameter found when increasing the feed rate from 1.1 mL/h to 1.5 mL/h at both 7 kV and 7.5 kV, as well as the statistically significant increase in average fiber diameter found at 8 kV.

4.3.2 Impact of voltage

To determine the best parameters to electrospin PLGA, multiple voltages were tested. Voltage was increased by 0.5 kV in each trial to determine the impact of voltage on the resulting scaffold.

In the case of 35% (w/v) PLGA (50:50) in HFIP, some observations between increasing voltage and changes in fiber diameter can be made. In each experiment, 7, 7.5, and 8 kV were tested. Under a 1.1 mL/h feed rate, an increase in average fiber diameter was found when increasing the applied voltage. This increase in average fiber diameter was found to not be statistically significant, but the trend is clearly shown in Figure 27. Electrospinning with a 1.3 mL/h feed rate, the change in voltage from 7 kV to 7.5 kV resulted in a very statistically significant decrease in average fiber diameter. This decrease in average fiber diameter was not found when further increasing the voltage to 8 kV; compared to the 7 kV scaffold, the increase in average fiber diameter was not found to be statistically significant. At a 1.5 mL/h feed rate, increasing the voltage from 7 kV to 7.5 kV or 8 kV resulted in a very statistically significant decrease in average fiber diameter.

Established literature has worked to define the relationship between the applied voltage and the resulting fibers when electrospinning. Research using polyvinyl alcohol (PVA) and sodium alginate (SA) found that increasing the voltage when electrospinning these solutions improved the scaffold's morphology but did not result in a clear correlation with changing fiber diameter [107]. The effects of voltage on fiber diameter were further studied on the electrospinning of polyvinylidene fluoride (PVDF). The results from this literature found that the average fiber diameter increased when a voltage over 60 kV was applied. The literature also found that fiber diameter would slightly increase with increases in voltage; however, this was determined to not be statistically significant [108]. The reported increases in fiber diameter agree with the average fiber diameters recorded for 7 kV, 7.5 kV, and 8 kV electrospun at 1.1 mL/h shown in Figure 27. In needle electrospinning, the impact of voltage on fiber diameter was

found to be significant when electrospinning polycaprolactone (PCL) at 10 kV, 15 kV, and 20 kV [109]. The reported significant decrease in fiber diameter matches the results found comparing 7 kV to 7.5 kV at a 1.3 mL/h feed rate and comparing 7 kV to 7.5 kV and 8 kV at a 1.5 mL/h feed rate shown in Figure 27. Literature published on the electrospinning of polystyrene (PS) at 10 kV, 15 kV, and 20 kV found that as the applied voltage was increased the resulting fiber diameters increased [110]. The reasoning given that at 20 kV the voltage made the polymer solution eject in a more fluid jet. The literature also found a decrease in the range of fiber diameters at 15 kV compared to 10 kV and 20 kV. This matches the data recorded for 1.3 mL/h feed rate scaffolds at 7.5 kV compared to 7 kV and 8 kV in Figure 27. Here the average fiber diameter increases from 7.5 kV to 8 kV and the standard deviation calculated at 7.5 kV is smaller than that calculated for 7 kV and 8 kV. The disagreements in literature on the impact of voltage on fiber diameter could explain the lack of a consistent trend between the three feed rates tested at 7 kV, 7.5 kV, and 8 kV.

4.3.3 Impact of concentration

Two concentrations of PLGA (50:50) produced fibrous scaffolds. Both 25% (w/v) and 35% (w/v) PLGA (50:50) in HFIP were electrospun at 7.5 kV and 8 kV with a 1.1, 1.3, and 1.5 mL/h feed rate to determine the impact of polymer concentration on electrospun scaffolds.

Figure 28 shows the data collected in this research on the impact of concentration. Under a 7.5 kV applied voltage a very statistically significant and a statistically significant decrease in fiber diameter occurred for scaffolds produced with a 1.1 mL/h and 1.3 mL/h feed rate respectively. With a 1.5 mL/h feed rate at 7.5 kV, the average fiber diameter had a very statistically significant increase with increasing concentration. Under an 8 kV applied voltage,

the increase in average fiber diameter with increasing PLGA concentration was found to be statistically insignificant for scaffolds produced with a 1.1 mL/h feed rate and statistically very significant for scaffolds produced with 1.3 mL/h or 1.5 mL/h feed rates.

Published research has investigated the effects of polymer concentration on electrospun fiber diameter. The electrospinning of polystyrene (PS) found that the resulting fiber diameters increased with increasing polymer concentration [110]. This agrees with the observed trend found when electrospinning 25% (w/v) and 35% (w/v) PLGA (50:50) at 8 kV shown in Figure 28. Research conducted on the electrospinning of PCL found the same trend; as the concentration of PCL in solution increased, the average fiber diameters also increased [109]. The electrospinning of PVDF found that the beading defects in fibers produced with 8 wt% were not presented when electrospinning 10 wt% PVDF solutions. It was also observed that increasing the concentration of polymer in solution significantly increased the fiber diameters produced [108]. From established literature there is a significant relationship between increasing polymer concentration and increasing fiber diameter that was observed in this research when electrospinning 25% (w/v) and 35% (w/v) PLGA (50:50) at 8 kV. The same observation was made when electrospinning these concentrations of PLGA at 7.5 kV with a 1.5 mL/h feed rate. The discrepancy found when electrospinning PLGA at 7.5 kV with a 1.1 mL/h and 1.3 mL/h feed rate could suggest the influence of other environmental factors.

4.3.4 Fiber diameter

The fiber diameters recorded for (50:50) PLGA fall into a range of 1.20 – 1.60 μm and with a standard deviation less than 1.0. Research has been conducted using (50:50) PLGA with carboxyl end groups dissolved in HFIP at a 1:9 w/v ratio. The solution was electrospun at 15 kV

and a collection distance of 15 cm was found to have an average fiber diameter of $700 + 62.9$ nm with a feed rate of 0.1-0.5 mL/h [111]. The electrospinning of (75:25) PLGA with a molecular weight of 66-107 kDa dissolved in dichloromethane at 22% w/v resulted in fiber diameters of $1.37+0.52$ μ m [112]. This diameter is significantly lower than the $1.6071+/-0.5169 - 2.062+/-0.5919$ μ m range from 1.1-1.5 mL/h found when electrospinning (50:50) PLGA at 35% w/v in 8 kV and 10 cm plate distance. The likely causes for the smaller fiber diameter are the lower concentration of polymer in solution, the higher voltage compared to the 8 kV (50:50) PLGA was electrospun at, and the lower feed rate of 0.1-0.5 mL/h compared to 1.1-1.5 for (50:50) PLGA [111].

Electrospinning (75:25) PLGA with multiwalled carbon nanotubes (MWNT) with 25 wt% PLGA with 0.25% w/v MWNT at 20 kV, a 13 cm plate distance, and a 0.2 mL/min feed rate was done to determine the impact of polymer concentration and applied voltage on average fiber diameter. The results found that average fiber diameter increased with increasing concentration from 327 nm at 17 wt% to 2253 nm at 28 wt% [113]. This trend was not clearly observed when increasing (50:50) PLGA from 25% w/v to 35% w/v at 7.5 kV and 10 cm plate distance. It is probable that this is due to the 12, 14, 20 wt% PLGA solution not producing good Taylor cones. Comparing the 25 wt% fibers, which are described as uniform and continuous, the recorded average fiber diameter was 1257 nm. The increase from 25 to 28 wt % is only 996 nm, considerably less drastic than the change found from 17 to 28 wt% [113]. The concentration used in this research was 35% w/v for (50:50) PLGA. The average fiber diameter of 2253 nm for 28 wt% PLGA exceeds the average fiber diameter found for (50:50) PLGA that produced scaffolds without beading in this research.

The impact of voltage was examined by using a 15-25 kV range; it was found that voltages below 20 kV did not produce fibers with smooth morphologies. The average fiber diameter increased from approximately 1260 nm at 20 kV to approximately 1400 nm at 22.5 kV and decreased from 1400 nm at 22.5 kV to approximately 1100 nm at 25 kV [113]. The indirect and direct relationship between voltage and average fiber diameter was also observed in this research with 0.5 kV increments. Due to the considerably smaller voltage changes done when electrospinning (50:50) PLGA, the impact of voltage was often determined to not have a significant impact on fiber diameter compared to feed rate.

4.3.5 Mechanical strength

The tensile strength of electrospun fibers is one of the most common mechanical strength tests used to characterize a scaffold. In literature mechanical strength testing was done by using 10x60x0.2 mm cut samples of scaffold produced at 25 wt% in dimethylformamide and under an applied voltage of 0.56 kV (50:50) and (75:25) PLGA, scaffolds were tested. With a deforming speed of 0.05 cm/s (75:25) PLGA had a tensile modulus of 110.78 MPa while (50:50) PLGA was recorded as 65.68 MPa. The impact of LA:GA ratio also created a change in the resulting ultimate tensile stress and ultimate tensile strain, which was found to be 4.67 MPa and 145.50 % for (75:25) and only 1.78 MPa and 112.50 % for (50:50) [114].

The effects of the concentration of polymer in solution were also studied and it was determined that a 30 wt% solution possessed significantly higher tensile modulus, ultimate tensile strength, and ultimate tensile strain than a 25 wt% solution 110.78 and 95.53 MPa, 4.67 and 3.10 MPa, and 145.50 and 78.95 % respectively [114]. Comparing this to the research done in this paper, the higher concentration of lactic acid in the polymer chain would result in better

mechanical properties. A higher concentration of polymer in solution would also improve the mechanical properties of the scaffold.

Experiments done of (75:25) PLGA with a fiber diameter of 1.130 μm were found to have an ultimate tensile stress of 1.22 MPa and a percent elongation at break of 112.53 %, with a Young's modulus of 33.17 MPa [115]. The fiber diameter is in a similar range to that found for (50:50) PLGA. The impact of fiber diameter on ultimate tensile strength and Young's modulus has been studied using (85:15) PLGA. This PLGA was electrospun at 8 and 12 %wt in HFIP, resulting in two scaffolds with 1.27 and 2.5 μm average fiber diameters respectively [116]. From the research, both scaffolds showed an insignificant change in maximum load 1.90 N and 1.71 N and ultimate tensile strength 15.52 MPa and 14.73 MPa. There was a significant increase in Young's modulus for the smaller fiber diameter scaffolds 350.3 MPa and 117.7 MPa. The opposite trend was found for fracture strain resulting in a very significant improvement for the larger diameter scaffolds 122.4 % and 365.5 % [116]. From available research it can be concluded that for the impact of the larger fiber diameters, some of the (50:50) PLGA scaffolds possess will be negligible for ultimate tensile strength and maximum load.

With present literature, it can be confidently stated that a larger ratio of LA PLGA will have a higher tensile strength due to the higher lactic acid ratio in the co-polymer than the (50:50) PLGA. Both scaffolds will possess mechanical properties similar to those described in research; a likely range for ultimate tensile strength would be between 1.0 and 5.0 MPa as found with (75:25) PLGA and (50:50) PLGA [114] [115].

4.3.6 Degradation

The degradation of PLGA both *in vitro* and *in vivo* is an important component of the polymer as, like all co-polymers, it must be determined for each ratio. Research done on the factors influencing the hydrolytic degradation of (50:50), (75:25), and (100:0) PLGA found that while all ratios of PLGA degraded over time, in 70 °C water the degradation was more rapid with decreasing LA:GA ratio. Within 5 hours the (50:50) and (75:25) PLGA had been nearly completely hydrolyzed [117]. This is explained by increasing GA ratio in the co-polymer increases the hydrophilicity of the polymer, leading to increased water content. The ratio of LA:GA was found to be significant; when determining the degradation rate of PLGA co-polymers in water, it can be confidently stated that the (50:50) PLGA scaffolds would degrade faster than higher LA content PLGA scaffolds due to the difference in LA content in the polymer chain. Further research was conducted on the degradation of PLGA scaffolds using (70:30), (75:25), and (80:20) PLGA ratios dissolved in HFIP and created using a salt fusion technique. In vitro degradation was tested by immersion method over a 21-day period. Weight loss over this period was used to determine the percent of the total scaffold that had degraded. The (70:30) PLGA scaffold suffered the greatest weight loss across all samples tested; the loss was between 11% to 22%. This was attributed to the higher GA content in the co-polymer. The (75:25) and (80:20) PLGA scaffolds suffered a weight loss of 9% to 12% and 4% to 8% respectively [118]. This again confirms the positive impact of LA on degradation rate in PLGA co-polymers.

Based on established literature and the characterization of the scaffolds from this research. The (50:50) PLGA scaffolds can be assumed to lose more than 11% of their weight

after 21 days in simulated body fluids due to the LA content being lower than the (70:30) worked with in literature.

4.3.7 Drug release

The drug release of PLGA is also dependent on the LA:GA ratio of the co-polymer. Research was conducted on (50:50) PLGA with a 100 kDa molecular weight and its ability to deliver nerve growth factor and glial cell-line-derived neurotrophic factor (GDNF) intended for peripheral nerve repair. The PLGA was electrospun at 16 kV with an 8 cm plate distance and a 2 mL/h feed rate; both 12% and 15% w/v were tested [119]. The resulting scaffolds had an average fiber diameter of approximately 310 nm and 500 nm respectively. The encapsulation efficiency of GDNF/PLGA fibers was found to be about 86%. The GDNF-loaded PLGA achieved a sustained *in vitro* release over 42 days. The 12% w/v PLGA reached 70.1% cumulative release while the 15% w/v reached 62.5% over the 42-day period. It is stated in the research that a larger fiber diameter may further curb the burst release of loaded fibers.

The fibers produced from (50:50) PLGA are of significantly larger average diameter, which would likely further reduce the burst release noticed from literature. The 50:50 LA:GA ratio would make the encapsulation of hydrophilic drugs relatively easy as the scaffold would have hydrophilic properties.

4.4 Summary

The research conducted successfully produced PLGA scaffolds with a (50:50) LA:GA ratio. The scaffolds were optimized for 35% in HFIP for an electrospinning process of 7-8 kV with a feed rate of 1.1mL/h and a plate distance of 10 cm. The resulting fibers were found to

have average diameters consistent with available literature. The (50:50) PLGA was found to be slightly smaller in average diameter than in the literature.

For 35% w/v (50:50) PLGA the range of parameters that produced scaffolds with consistent fiber diameters and good morphologies were 7-8 kV, 1.1-1.3 mL/h, and 10 cm plate distance. The best scaffolds produced for core-shell electrospinning was with 7.5 kV, a 1.1 mL/h feed rate, and a 10 cm plate distance.

For (50:50) PLGA it was found feed rate did not have a consistent impact on the resulting fiber diameters. While increases in feed rate did result in increases in fiber diameter, the impact was not always found to be statistically significant.

4.5 Future work

With the successful electrospinning of PLGA, future work could focus on further characterization and analysis of electrospun scaffolds. The properties of mechanical strength, degradation, and drug release can be tested and confirmed in future experiments on the electrospinning of (50:50) PLGA. Mechanical strength can be examined by using a 10 mm by 2.5 mm testing strip for tensile testing. Degradation can be tested using lab rats for *in vivo* degradation or simulated body fluids for *in vitro* degradation. Drug release has been studied in previous literature and the use of doxycycline is common, where the drug is added to the polymer solution prior to electrospinning. The impact of feed rate on fiber diameters can be explored by controlling the environmental factors such as temperature and humidity to further isolate the influence of feed rate on the electrospinning process. The impact of voltage should be investigated as there is no clear consensus in published literature. To fully understand how voltage can change the resulting scaffold, the range of voltages tested should be increased from

7-8 kV to 6-10 kV. The impact of concentration is well established, but the results gathered from 25% (w/v) PLGA (50:50) electrospun at 7.5 kV with a 1.1 mL/h or 1.3 mL/h feed rate do not agree with the published trends. To continue investigating, two more concentrations of 30% (w/v) and 40% (w/v) should be analyzed along with the 25% (w/v) and 35% (w/v).

CHAPTER 5

COAXIAL CORE-SHELL

5.1 Introduction

Core-shell electrospinning is a composite fiber fabrication technique that creates a “fiber within a fiber.” Core-shell scaffolds are commonly used for drug release applications because drug loading and release are better controlled in core-shell fibers than in monoaxial fibers [120]. The improved control of drug release is derived from the bi-layer system that core-shell fibers exhibit. By changing the thickness of the shell layer, the drug must permeate through a larger or smaller barrier before being released [121]. Core-shell fibers are also used to carry growth factors and release them in the body to improve tissue regeneration [122]. Core-shell fibers have demonstrated improved thermal properties over monoaxial fibers. In the core-shell electrospinning of polyvinyl alcohol and polycaprolactone PVA-PCL, it was found that the moisture loss in the fibers was significantly lower before 100 °C compared to moisture loss of monoaxial PLA fibers [123]. Core-shell poly(vinyl pyrrolidone) and poly(L-lactide-co-caprolactone) PVP-PLCL fibers have been experimented with for applications in tissue engineering. The PVP-PLCL fibers demonstrated superior cell viability measured by MTT assay of human embryo skin fibroblasts (hESFs) than monoaxial PLCL fibers [124].

PCL was chosen as the shell material as its hydrophobic properties would act as a barrier, prolonging drug release and reducing the initial burst. PLGA was used as the core material

because its more hydrophilic nature gives it better drug encapsulation efficiency. A degradation study of 10% w/v PCL in HFIP conducted over a 180-day period showed a 15.5% increase in fiber diameter after 90 days and that was not determined to be statistically significant [93]. An *in vitro* degradation analysis on (70:30), (75:25), and (80:20) PLGA using the immersion method found that the higher the GA content, the greater the weight loss over the 21-day period. The (70:30) PLGA, which is most similar to the (50:50) PLGA used in this research, suffered the greater weight loss across all samples tested from 11% to 22% [118]. PCL is a crystalline polymer with a slow degradation rate compared to (50:50) PLGA, which has an amorphous structure [125].

It is believed that a composite fibrous scaffold can be created using PCL and PLGA as component polymers with the coaxial electrospinning technique. The goal of this research is to create a core-shell composite coaxially electrospun fibrous scaffold. The hypothesis of this research will be tested with creation of a core-shell composite using the optimized monoaxial electrospinning parameters of 7-8 kV applied voltage, a 1.5 mL/h PCL feed rate and a 1.1-1.3 mL/h PLGA feed rate with a 10 cm plate distance. It is further hypothesized that for this coaxial core-shell electrospinning experiment, the resulting core-shell structure will have a larger fiber diameter than either of the monoaxial fibers it is made from.

5.2 Results

5.2.1 SEM

Figure 31 shows SEM images taken of scaffolds produced at 7.5 kV and a 10 cm plate distance with a 1.5 mL/h shell feed rate and different core feed rates. All of the scaffolds

produced in this experiment resulted in the formation of a fibrous scaffold without beading or branching.

Figure 31 A and B show a scaffold produced using a 0.5 mL/h core feed rate. The consistency of the scaffold can be observed in Figure 31 A. Figure 31 B shows the same location at greater magnification, where some inconsistencies in fiber diameters can be seen. In Figure 31 B the existence of very small-diameter fibers that could not be observed in Figure 31 A show that there is some variance in diameter.

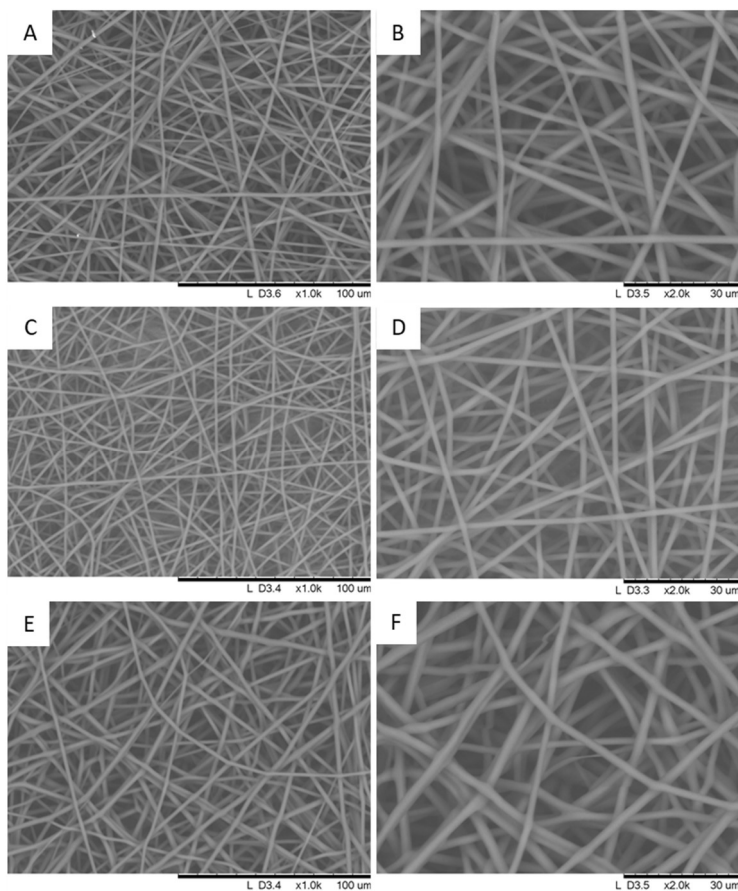


Figure 31 SEM imagery of 35% w/v PLGA (50:50) – 7.5% w/v PCL core-shell fibers electrospun at a plate distance of 10 cm with a 7.5 kV applied voltage A) 0.5-1.5 mL/h feed rate (core-shell) 1k B) 0.5-1.5 mL/h feed rate (core-shell) 2k C) 0.9-1.5 mL/h feed rate (core-shell) 1k D) 0.9-1.5 mL/h feed rate (core-shell) 2k E) 1.1-1.5 mL/h feed rate (core-shell) 1k 1.1-1.5 mL/h feed rate (core-shell) 2k

Figure 31 C and D show a scaffold produced with a higher core feed rate of 0.9 mL/h. The scaffold shown in Figure 31 C has a very similar structure to the scaffold produced with a 0.5 mL/h core feed rate shown in Figure 31 A. At greater magnification, Figure 31 D shows there is some variance in fiber diameter; however, the fibers appear much more consistent than those shown in Figure 31 B. Table 9 shows the average fiber diameters and standard deviations calculated for each scaffold shown in Figure 31. From , the increase in core feed rate from 0.5 mL/h to 0.9 mL/h resulted in a smaller average fiber diameter and standard deviation. This decrease in average fiber diameter was determined to be very statistically significant, as shown in .

Table 9 Impact of feed rate on coaxial fiber diameter at 7.5 kV and a 10 cm plate distance

Core-Shell Feed Rate (Core feed rate (mL/h) - Shell feed rate (mL/h))	Fiber Diameter (diameter (um) +/- STDev)	P-value
1.1-1.5	2.064 +/- 0.4225	0.0038
0.9-1.5	1.412 +/- 0.1883	0.0002
0.5-1.5	1.718 +/- 0.2711	-

Figure 31 E and F show a scaffold produced with a core feed rate of 1.1 mL/h. Comparing the fibers from Figure 31 E to Figure 31 C, the 1.1 mL/h core feed rate fibers appear to have larger diameters. At higher magnification, small-diameter fibers can be seen, showing some inconsistencies in fiber diameter in Figure 31 F. These small fibers were present throughout the scaffold. The small-diameter fibers appear similar to those found in the 0.5 mL/h core feed rate scaffold shown in Figure 31 B. The average fiber diameter and standard deviation calculated in show that the 1.1 mL/h core feed rate scaffold had the largest average fiber diameter and standard deviation out of all of the scaffolds produced under 7.5 kV and a 10 cm

plate distance. The increase in average fiber diameter compared to the 0.5 mL/h core feed rate scaffold was found to be very statistically significant in .

To determine the impact the applied voltage has on the coaxial electrospinning process the voltage was increased by 0.5 kV to 8 kV. This applied voltage was found in Chapter 2 to produce consistent PCL scaffolds and was found in Chapter 3 to produce consistent PLGA (50:50) scaffolds. SEM images of scaffolds produced under an 8 kV applied voltage and a 10 cm plate distance with a 1.5 mL/h shell feed rate are shown in Figure 32. All of the scaffolds produced with these parameters showed good fiber formation without any defects.

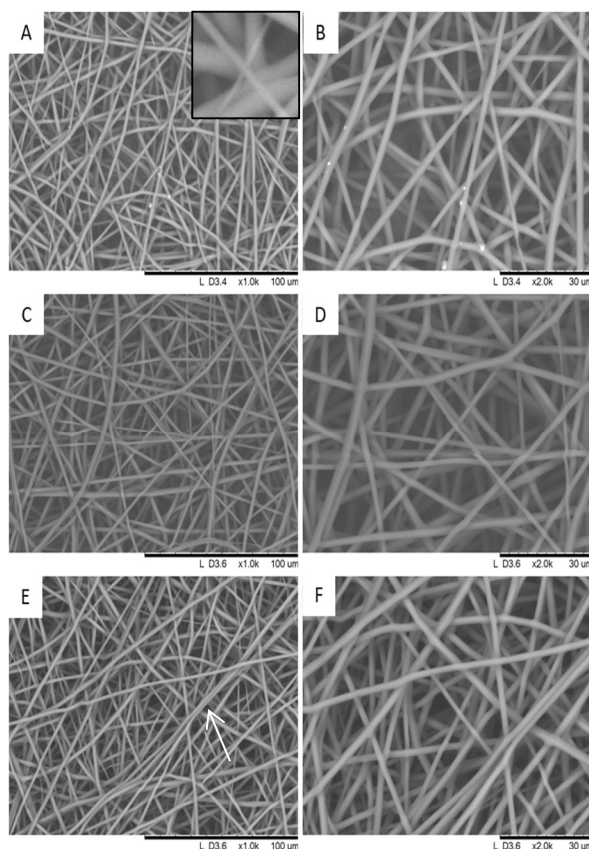


Figure 32 SEM imagery of 35% w/v PLGA (50:50) – 7.5% w/v PCL core-shell fibers electrospun at a plate distance of 10 cm with an 8 kV applied voltage A) 0.9-1.5 mL/h feed rate (core-shell) 1k B) 0.9-1.5 mL/h feed rate (core-shell) 2k C) 1.1-1.5 mL/h feed rate (core-shell) 1k D) 1.1-1.5 mL/h feed rate (core-shell) 2k E) 1.3-1.5 mL/h feed rate (core-shell) 1k F) 1.3-1.5 mL/h feed rate (core-shell) 2k

Figure 32 A and B show a scaffold produced from a 0.9 mL/h core feed rate. Figure 32 A shows good fiber formation throughout the scaffold, the random orientation of fibers has led some to bend or twist in the fiber, but no breaks are observed. Figure 32 B shows some variance in fiber diameter with small-diameter fibers shown that could not be observed in Figure 32 A. The average fiber diameter and standard deviation shown in Table 10 are both larger than the calculated values for a 0.9 mL/h core feed rate electrospun at 7.5 kV shown in , imaged in Figure 31 C and D.

Table 10 Impact of Feed Rate on Coaxial Fiber Diameter at 8 kV and a 10 cm plate distance

Core-Shell Feed Rate (Core feed rate (mL/h) - Shell feed rate (mL/h))	Fiber Diameter (diameter (um) +/- STDev)	P-value
1.3-1.5	1.883 +/- 0.2809	0.7990
1.1-1.5	1.885 +/- 0.3168	0.7935
0.9-1.5	1.8497 +/- 0.5083	-

Figure 32 C and D show the resulting fibers from a 1.1 mL/h core feed rate. The fibers shown in Figure 32 C appear to have diameters and morphologies similar to those imaged at a 0.9 mL/h core feed rate in Figure 32 A. Figure 32 D shows a similar variance in fiber diameter compared to Figure 32 B with the existence of small-diameter fibers that could not be easily observed in Figure 32 C. The average fiber diameter and standard deviation are calculated in Table 10. Comparing the 1.1 mL/h core feed rate scaffold to the 0.9 mL/h core feed rate scaffold, average fiber diameter increased while standard deviation decreased. The change in average fiber diameter was found to not be statistically significant, shown in Table 10.

Figure 32 E and F depict scaffolds produced from a 1.3 mL/h core feed rate. The fibers shown in Figure 32 E look very similar to those produced from a 1.1 mL/h core feed rate shown

in Figure 32 C. Figure 32 E does show an entanglement of fibers moving from the top left to the bottom right of the image. Observing this location under greater magnification in Figure 32 F depicts the random orientation of fibers led to some being deposited on top of each other. The average fiber diameter and standard deviation calculated in Table 10 are very similar to that calculated for the 1.1 core feed rate scaffolds. Compared to the 0.9 mL/h core feed rate scaffold, the average fiber diameter increased and standard deviation decreased. This change in average fiber diameter was determined to be statistically insignificant shown in Table 10.

To determine the impact of plate distance on the coaxial electrospinning process, the plate was moved 5 cm farther away from the nozzle. Fibers were then electrospun at 7.5 kV and a 15 cm plate distance with a 1.5 mL/h shell feed rate and various core feed rates as shown in Figure 33. All of the fibers produced with these parameters had good fibrous morphologies and fibers without any defects.

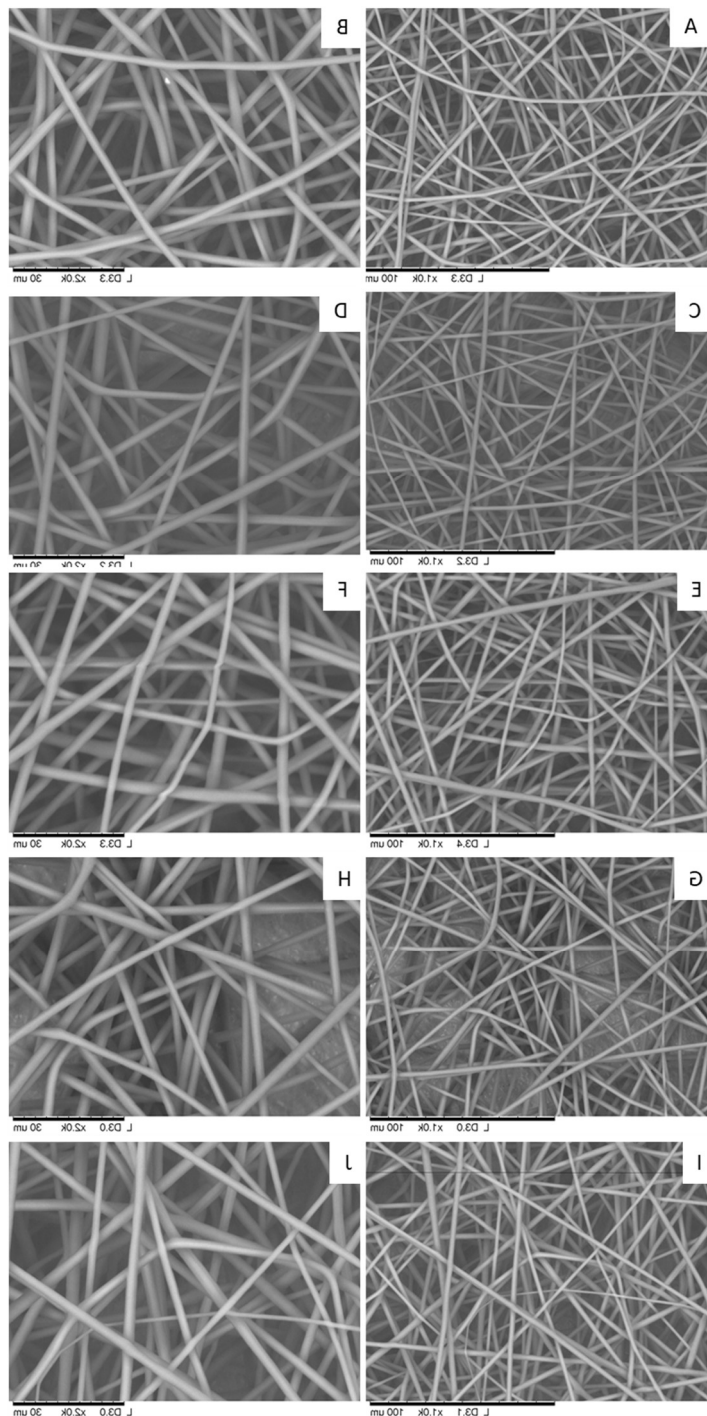


Figure 33 SEM imagery of 35% w/v PLGA (50:50) – 7.5% w/v PCL core-shell fibers electrospun at a plate distance of 15 cm with a 7.5 kV applied voltage A) 0.5-1.5 mL/h feed rate (core-shell) 1k B) 0.5-1.5 mL/h feed rate (core-shell) 2k C) 0.7-1.5 mL/h feed rate (core-shell) 1k D) 0.7-1.5 mL/h feed rate (core-shell) 2k E) 0.9-1.5 mL/h feed rate (core-shell) 1k F) 0.9-1.5 mL/h feed rate (core-shell) 2k G) 1.1-1.5 mL/h feed rate (core-shell) 1k H) 1.1-1.5 mL/h feed rate (core-shell) 2k I) 1.3-1.5 mL/h feed rate (core-shell) 1k J) 1.3-1.5 mL/h feed rate (core-shell) 2k

Figure 33 A and B show a scaffold produced from a 0.5 mL/h core feed rate.

Figure 33 A shows the consistency of the scaffold with fibers that look similar to those produced under a 7.5 kV voltage and 10 cm plate distance with a 1.1 mL/h feed rate shown in Figure 31 A. Under greater magnification some variance in fiber diameter can be observed in

Figure 33 B similar to the differences in fiber diameters found in scaffolds produced at 8 kV and a 10 cm plate distance with a 1.1 mL/h feed rate shown in Figure 32 D. The average fiber diameter and standard deviation calculated for this scaffold are recorded in . Comparing the average fiber diameter and standard deviation of this scaffold to the scaffold produced with 7.5 kV and a 10 cm plate distance with a 0.5 mL/h feed rate, shown in Figure 31 A and B, both average fiber diameter and standard deviation increased with the larger plate distance.

Table 11 Impact of feed rate on coaxial fiber diameter at 7.5 kV and a 15 cm plate distance

Core-Shell Feed Rate (Core feed rate (mL/h) - Shell feed rate (mL/h))	Fiber Diameter (diameter (um) +/- STDev)	P-value
1.3-1.5	2.5765 +/- 0.7026	0.0164
1.1-1.5	2.0805 +/- 0.5323	0.6711
0.9-1.5	2.426 +/- 0.4574	0.0296
0.7-1.5	2.268 +/- 0.3834	0.2675
0.5-1.5	2.1405 +/- 0.3313	-

Figure 33 C and D show the resulting scaffolds from a 0.7 mL/h core feed rate. The fibers shown in

Figure 33 C appear to have a structure and diameter similar to those produced with a 0.5 mL/h core feed rate in

Figure 33 A. At greater magnification, some variance in fiber diameter can be observed that appears to be slightly more rampant than what was observed in

Figure 33 B. The average fiber diameter and standard deviation calculated in show both increased with the increase in core feed rate compared to the 0.5 mL/h core feed. This increase was found to not be statistically significant as shown in .

Figure 33 E and F show scaffolds produced with a 0.9 mL/h core feed rate.

Figure 33 E shows the random orientation of fibers caused some to bend at various points; however, no break in the fiber is observed. Some inconsistencies in fiber diameter can be seen. At greater magnification, the variance in fiber diameters is easier to observe. One of the bent fibers can also be more clearly analyzed, where again no breaking is shown. The average fiber diameter and standard deviation recorded in are both larger than the 0.7 mL/h core feed rate scaffolds and the 0.5 mL/h feed rate scaffolds shown in

Figure 33 C-D and A-B respectively. The increase in average fiber diameter compared to the 0.5 mL/h core feed rate scaffold was determined to be statistically significant in .

Figure 33 G and H show SEM images of a scaffold produced from a 1.1 mL/h core feed rate. The fibers shown in

Figure 33 G appear very similar to those produced with 7.5 kV and a 10 cm plate distance with a 1.1 mL/h core feed rate shown in Figure 31 A.

Figure 33 H shows a much greater variance in fiber diameter than any of the scaffolds produced at 7.5 kV with a 15 cm plate distance determined by the standard deviation calculated in . The average fiber diameter and standard deviation recorded in for this scaffold are the smallest and second largest calculated for all scaffolds produced under these parameters. The decrease in fiber diameter compared to the 0.5 mL/h core feed rate scaffold was not found to be statistically significant (). This shows that despite the increase in standard deviation, the changes in average fiber diameter were minimal. The Taylor cone under these parameters created a very large jet that created a scaffold across a larger area than other parameters. This large area resulted in poor fiber coverage as shown in

Figure 33 G and H, where the aluminum foil the scaffold was deposited on is partially visible.

Figure 33 I and J show images of scaffolds produced from a 1.3 mL/h core feed rate.

Figure 33 I shows some bending in the fibers as well as some variance in fiber diameter. At greater magnification,

Figure 33 J shows the highest variance in fiber diameter shown in any of the scaffolds depicted in

Figure 33.

Figure 33 J also shows that despite the nearly 90 degree bending in the fibers there were no breaks or tears. The average fiber diameter and standard deviation recorded in are the largest calculated for any of the scaffolds in the 7.5 kV 15 cm plate distance experiment. The increase in average fiber diameter compared to the 0.5 mL/h core feed rate scaffold was found to be statistically significant .

To determine the impact of voltage on the coaxial electrospinning process with a 15 cm feed rate, the voltage was increased by 0.5 kV to 8 kV. Fibers were then electrospun at 8 kV and a 15 cm plate distance with a 1.5 mL/h shell feed rate and various core feed rates shown in Figure 34. All of the fibers produced with these parameters had good fibrous morphologies without any defects. With the increase in applied voltage, core feed rates below 0.9 mL/h were unable to sustain a stable Taylor cone and as such were not imaged with scanning electron microscopy.

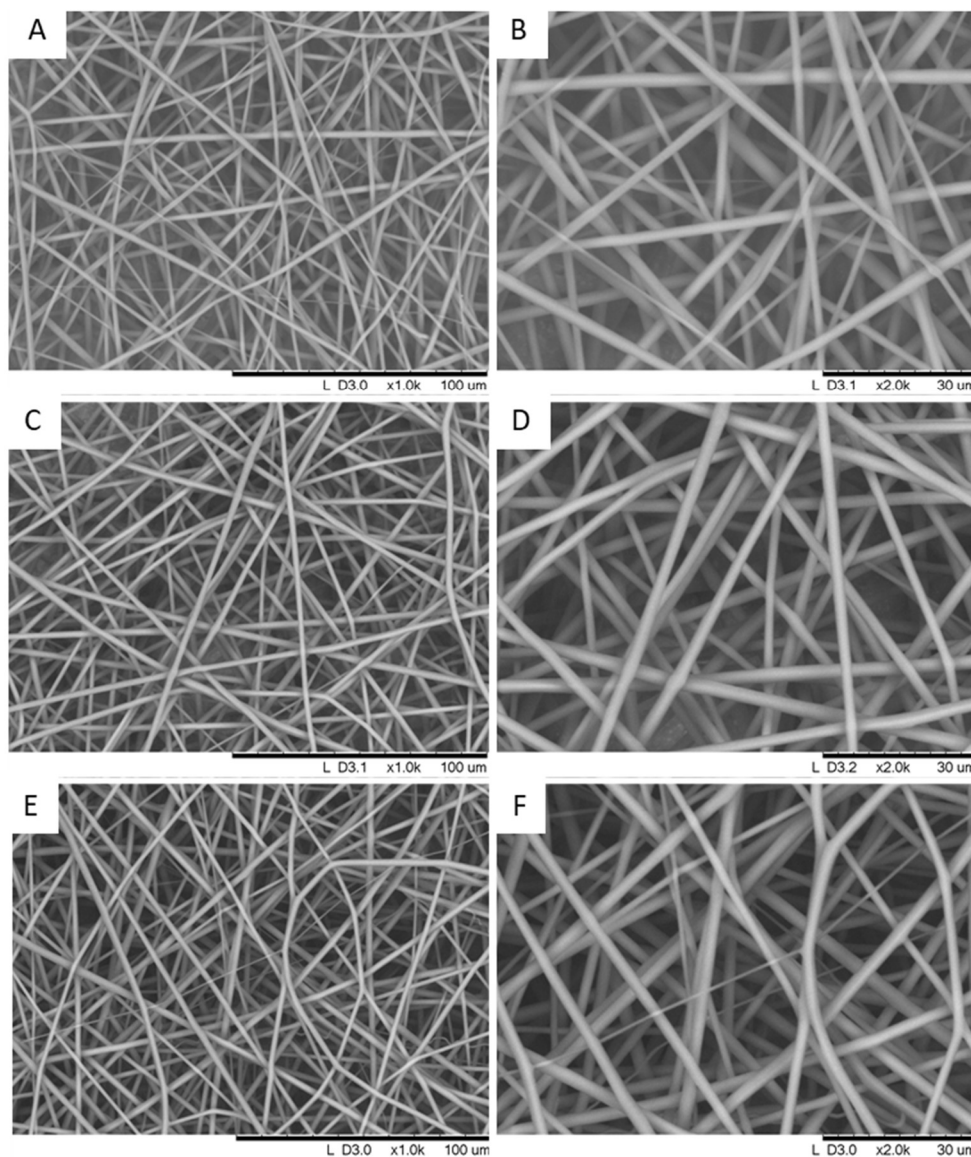


Figure 34 SEM imagery of 35% w/v PLGA (50:50) – 7.5% w/v PCL core-shell fibers electrospun at a plate distance of 15 cm with an 8 kV applied voltage A) 0.9-1.5 mL/h feed rate (core-shell) 1k B) 0.9-1.5 mL/h feed rate (core-shell) 2k C) 1.1-1.5 mL/h feed rate (core-shell) 1k D) 1.1-1.5 mL/h feed rate (core-shell) 2k E) 1.3-1.5 mL/h feed rate (core-shell) 1k F) 1.3-1.5 mL/h feed rate (core-shell) 2k

Figure 34 A and B show scaffolds produced with a 0.9 mL/h core feed rate. Figure 34 A shows the fibers produced appear smaller than the 0.9 mL/h core feed rate fibers produced at 7.5 kV with a 15 cm plate distance shown in

Figure 33 E. At greater magnification, the existence of small diameter fibers can be observed in Figure 34 B. The average fiber diameter and standard deviation are recorded in . The average fiber diameter for this scaffold is smaller than all the average fiber diameters found for any scaffold produced with 7.5 kV and a 15 cm plate distance recorded in . The standard deviation for the 0.9 mL/h core feed rate scaffold produced at 8 kV with a 15 cm plate distance is similar to the standard deviation found for the 1.1 mL/h core feed rate scaffold produced at 7.5 kV with a 15 cm plate distance shown in .

Table 12 Impact of feed rate on coaxial fiber diameter at 8 kV and a 15 cm plate distance

Core-Shell Feed Rate (Core feed rate (mL/h) - Shell feed rate (mL/h))	Fiber Diameter (diameter (um) +/- STDev)	P-value
1.3-1.5	2.0535 +/- 0.5101	0.9390
1.1-1.5	2.2465 +/- 0.3711	0.2312
0.9-1.5	2.0664 +/- 0.5481	-

Figure 34 C and D show scaffolds produced from a 1.1 mL/h core feed rate. Figure 34 C shows fibers that look similar to those produced from 7.5 kV and a 15 cm plate distance with a 0.7 mL/h feed rate shown in

Figure 33 G. At greater magnification, some variance in fiber diameter can be seen in Figure 34 D. The average fiber diameter and standard deviation are recorded in . The average fiber diameter of the 1.1 mL/h core feed rate scaffold is larger than the average fiber diameter found for the 0.9 mL/h core feed rate scaffold while the standard deviation for the 1.1 mL/h core feed rate scaffold is smaller than the 0.9 mL/h core feed rate scaffold. The change in average fiber diameter compared to the 0.9 mL/h core feed rate scaffold was found to not be statistically significant in .

Figure 34 E and F show scaffolds produced from a 1.3 mL/h core feed rate. Figure 34 E shows fibers that have some bending as a result of the random orientation. The fibers appear to have a diameter and surface morphology similar to those produced from the 0.9 mL/h core feed rate shown in Figure 34 A. At greater magnification in Figure 34 B, there are some very small fibers that were formed in the scaffold that could not be seen in Figure 34 A. The average fiber diameter recorded in is the smallest out of any scaffold produced with a 15 cm plate distance at either 7.5 kV or 8 kV. The standard deviation calculated for this scaffold was similar to the standard deviation calculated for the 0.9 mL/h core feed rate scaffold shown in Figure 34 A. The slight decrease in average fiber diameter compared to the 0.9 mL/h core feed rate scaffold was determined to not be statistically significant, as shown in .

With the success of the 8 kV electrospinning process, the voltage was increased further by 0.5 kV to 8.5 kV. Fibers were then electrospun at 8.5 kV and a 15 cm plate distance with a 1.5 mL/h shell feed rate and various core feed rates shown in Figure 35. All of the fibers produced with these parameters had good fibrous morphologies without any defects. With the

increase in applied voltage, core feed rates below 0.9 mL/h were unable to sustain a stable Taylor cone and as such were not imaged with scanning electron microscopy.

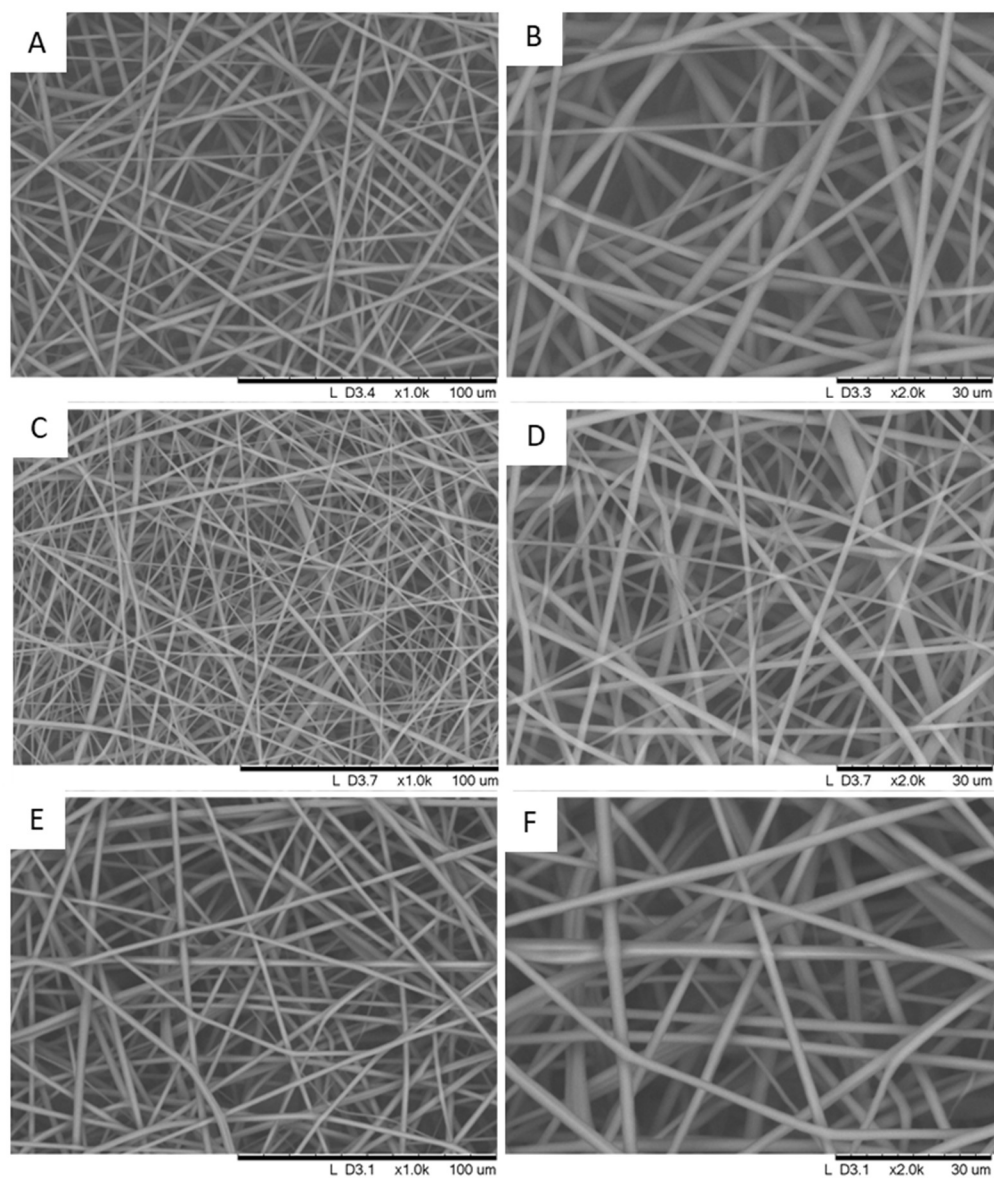


Figure 35 SEM imagery of 35% w/v PLGA (50:50) – 7.5% w/v PCL core-shell fibers electrospun at a plate distance of 15 cm with an 8.5 kV applied voltage A) 0.9-1.5 mL/h feed rate (core-shell) 1k B) 0.9-1.5 mL/h feed rate (core-shell) 2k C) 1.1-1.5 mL/h feed rate (core-shell) 1k D) 1.1-1.5 mL/h feed rate (core-shell) 2k E) 1.3-1.5 mL/h feed rate (core-shell) 1k F) 1.3-1.5 mL/h feed rate (core-shell) 2k

Figure 35 A and B show scaffolds produced with a 0.9 mL/h core feed rate. Figure 35 A shows the fibers produced are similar to those produced under 7.5 kV and a 10 cm plate distance with a 1.1 mL/h core feed rate shown in Figure 31 E. Imagery done at greater magnification in Figure 35 B shows some variance in fiber diameter with the formation of very small-diameter fibers within the scaffold. These small-diameter fibers are similar to those that were found in Figure 34 F from 8 kV and 15 cm with a 1.3 mL/h core feed rate scaffolds.

Figure 35 C and D show scaffolds produced from a 1.1 mL/h core feed rate. Figure 35 C shows some variance in fiber diameter. The scaffold appears to have the smallest diameter fibers out of any fibers produced. The scaffold also has some large-diameter fibers that formed behind the small-diameter fibers. Increasing the magnification reveals more small-diameter fibers that formed in the scaffold shown in Figure 35 D. The variance in fiber diameter observed is similar to the variance shown in Figure 35 B for a scaffold produced with the same parameters and a 0.9 mL/h core feed rate. The average fiber diameter and standard deviation recorded in show that this scaffold has the smallest average fiber diameter produced out of any core-shell experiment conducted in this research. The standard deviation calculated for this scaffold is the second largest recorded, only smaller than the standard deviation calculated for scaffolds produced with a 1.3 mL/h core feed rate under 7.5 kV and a 10 cm plate distance recorded in . The decrease in average fiber diameter compared to the 0.9 mL/h core feed rate scaffold was not found to be statistically significant.

Table 13 Impact of feed rate on coaxial fiber diameter at 8.5 kV and a 15 cm plate distance

Core-Shell Feed Rate (Core feed rate (mL/h) - Shell feed rate (mL/h))	Fiber Diameter (diameter (um) +/- STDev)	P-value
1.3-1.5	2.164 +/- 0.3802	0.2596
1.1-1.5	1.6898 +/- 0.6172	0.1787
0.9-1.5	1.9679 +/- 0.6656	-

Figure 35 E and F show a scaffold produced from a 1.3 mL/h core feed rate. Figure 35 E shows fibers similar to those produced with a 1.1 mL/h core feed rate under 8 kV and a 15 cm plate distance shown in Figure 34 C. Figure 35 F shows some variance in fiber diameter; the range of fibers shown closely resembles those depicted in Figure 34 C and

Figure 33 D. The average fiber diameter and standard deviation are recorded in . The average fiber diameter is larger than what was recorded for the 0.9 mL/h core feed rate scaffold produced under the same conditions. The standard deviation is similar to what was found for the 1.1 mL/h core feed rate scaffold produced with a 8 kV applied voltage and a 15 cm plate distance recorded in . The slight increase in fiber diameter compared to the 0.9 mL/h core feed rate scaffold was determined to be statistically insignificant .

The impact of humidity on coaxially electrospun scaffolds was examined by running the same experiment under 25% and 65% relative humidity. Figure 36 shows SEM imagery taken of scaffolds produced with a 7.5% (w/v) PCL shell and a 35% (w/v) PLGA (50:50) core, electrospun with a plate distance of 10 cm at the two humidity levels.

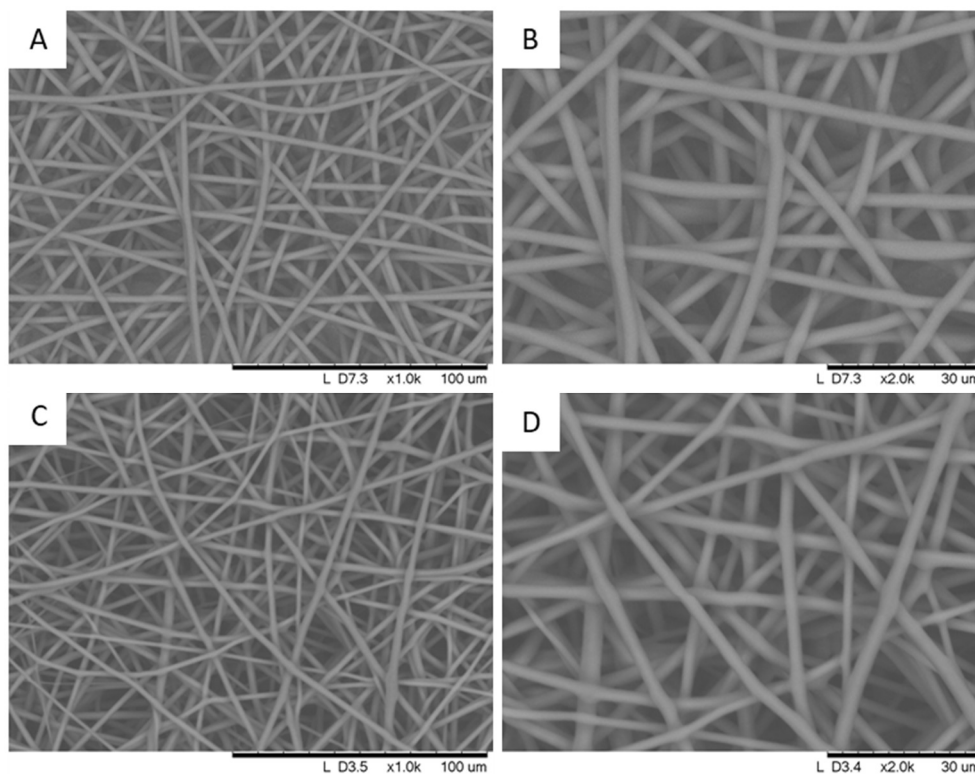


Figure 36 SEM imagery of 35% w/v PLGA (50:50) – 7.5% w/v PCL core-shell fibers electrospun at a plate distance of 10 cm with a 1.1-1.5 mL/h feed rate (core-shell) A) 1k magnification 7.5kV 65% rel. humidity B) 2k magnification of A C) 1k magnification 7.5kV 25% rel. humidity D) 2k magnification of C

Figure 36 A and B show scaffolds produced by electrospinning this solution under a 7.5 kV voltage with a 1.1-1.5 mL/h (core-shell) feed rate in a 65% relative humidity environment. Figure 36 A shows no defects in the scaffold and Figure 1 B shows the fibers have consistent diameters.

Figure 36 C and D show scaffolds produced when electrospinning a core-shell structure under a 7.5 kV voltage with a 1.1-1.5 (core-shell) feed rate in a 25% relative humidity environment. The fibrous structure shown in Figure 36 C is similar to the structure shown in Figure 36 A. Figure 36 D shows some inconsistencies in the fiber diameters that make up the

scaffold with noticeably smaller fibers stretching throughout the scaffold. Figure 37 gives the calculated average fiber diameter and standard deviation for both scaffolds. From Figure 37 the increase in humidity resulted in a larger average fiber diameter but a smaller standard deviation. The statistical significance of the increase in fiber diameter from 25% relative humidity to 65% relative humidity was found to be very significant and is shown in Figure 37.

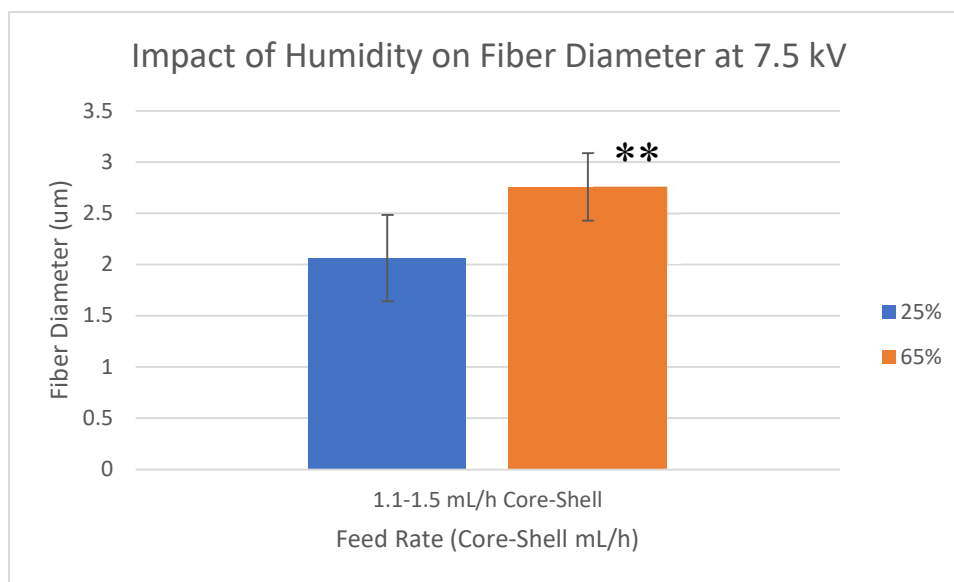


Figure 37 Impact of humidity on fiber diameter at 7.5 kV (*) $p < .05$ (**) $p < .01$

The impact of voltage on fiber diameter was determined using the scaffolds produced at 7.5 kV, 8 kV, and 8.5 kV with a 1.3 mL/h, 1.1 mL/h, and 0.9 mL/h core feed rate at a 15 cm plate distance shown in Figure 38.

Looking at the 1.3 mL/h core feed rate, increasing voltage was found to have a statistically significant impact on decreasing the fiber diameter. Both the 8 kV and 8.5 kV

scaffolds under these conditions had an average fiber diameter smaller than the average fiber diameter calculated for the 7.5 kV scaffold.

With a 1.1 mL/h core feed rate, increasing the voltage by 0.5 kV to 8 kV from 7.5 kV was found to have no statistically significant impact on fiber diameter. Shown in Figure 38, the average fiber diameter increased with increasing the voltage from 7.5 kV to 8 kV. When the voltage was further increased to 8.5 kV, the decrease in average fiber diameter compared to the 7.5 kV scaffold was determined to be statistically significant.

Using a 0.9 mL/h core feed rate, the increase in voltage resulted in a decrease in fiber diameter shown in Figure 38. Comparing the 7.5 kV scaffold to the 8 kV scaffold, a statistically significant decrease in average fiber diameter was found. Further increasing the voltage to 8.5 kV resulted in a slight decrease in average fiber diameter compared to the 8 kV scaffold. This further decrease was also considered to be statistically significant compared to the 7.5 kV scaffold. The impact of plate distance on fibrous scaffold production was also determined using the scaffolds produced at 7.5 kV with both 1.1 mL/h and 0.9 mL/h core feed rates at 10 cm and 15 cm shown in.

Comparing the 10 cm and 15 cm scaffolds produced from the 1.1 mL/h core feed rate, no statistically significant change in average fiber diameter was found. shows almost no change in average fiber diameter between the 1.1 mL/h core feed rate scaffolds at different plate distances. There is a slight increase in standard deviation observed in when increasing the plate distance from 10 cm to 15 cm.

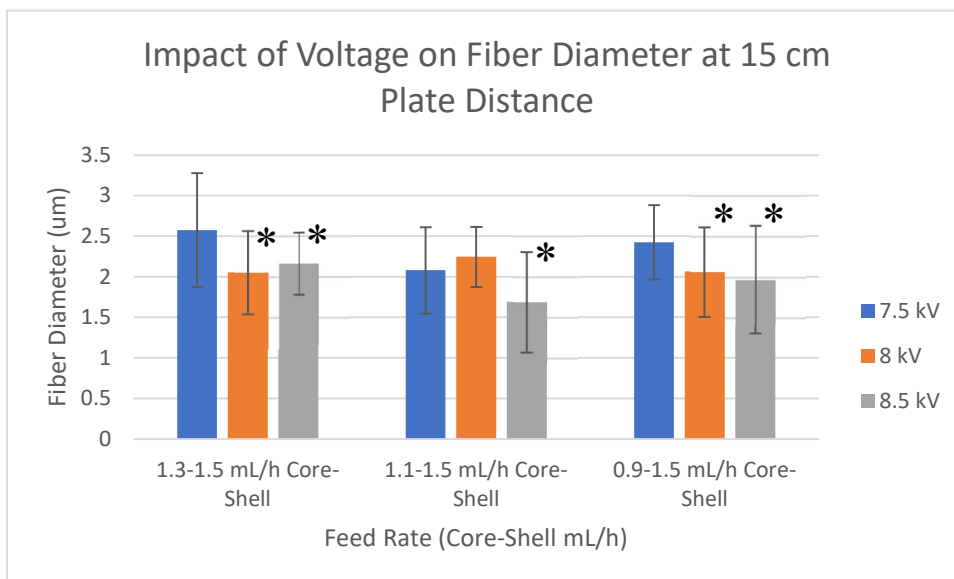


Figure 38 Impact of voltage on fiber diameter at 15 cm plate distance (*) $p < .05$ (**) $p < .01$

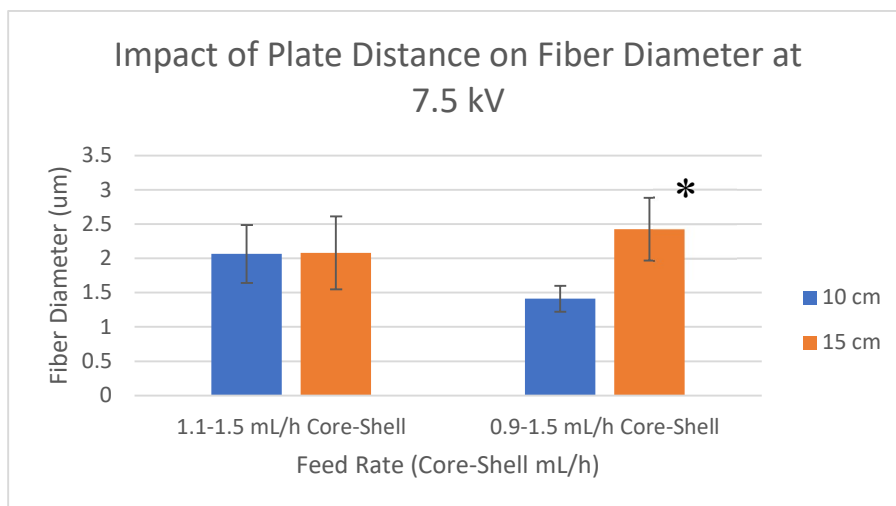


Figure 39 Impact of plate distance on fiber diameter at 7.5 kV (*) $p < .05$ (**) $p < .01$

The 0.9 mL/h core feed rate scaffolds showed a very statistically significant increase in average fiber diameter when the plate distance was increased from 10 cm to 15 cm. An increase in standard deviation was also observed when increasing the plate distance shown in .

Figure 40 is a phase diagram created to further analyze the impact of each parameter on Taylor cone formation. In the core-shell experiments four parameters changed: voltage, core feed rate, humidity, and plate distance. The data collected in Figure 40 represents all experiments, run with a 10 cm plate distance that produced stable Taylor cones and a fibrous morphology. Based on the phase diagram, increasing humidity had the greatest impact on Taylor cone formation and fiber morphology. When all other variables were kept constant, the increase in humidity resulted in large changes in standard deviation. From the subplots below the 3D phase diagram, it was found that as feed rate increased, the range of standard deviations recorded also increased. The influence of voltage was not found to be as pronounced as feed rate because the standard deviation calculated for scaffolds produced at different voltages all fit within a similar range.

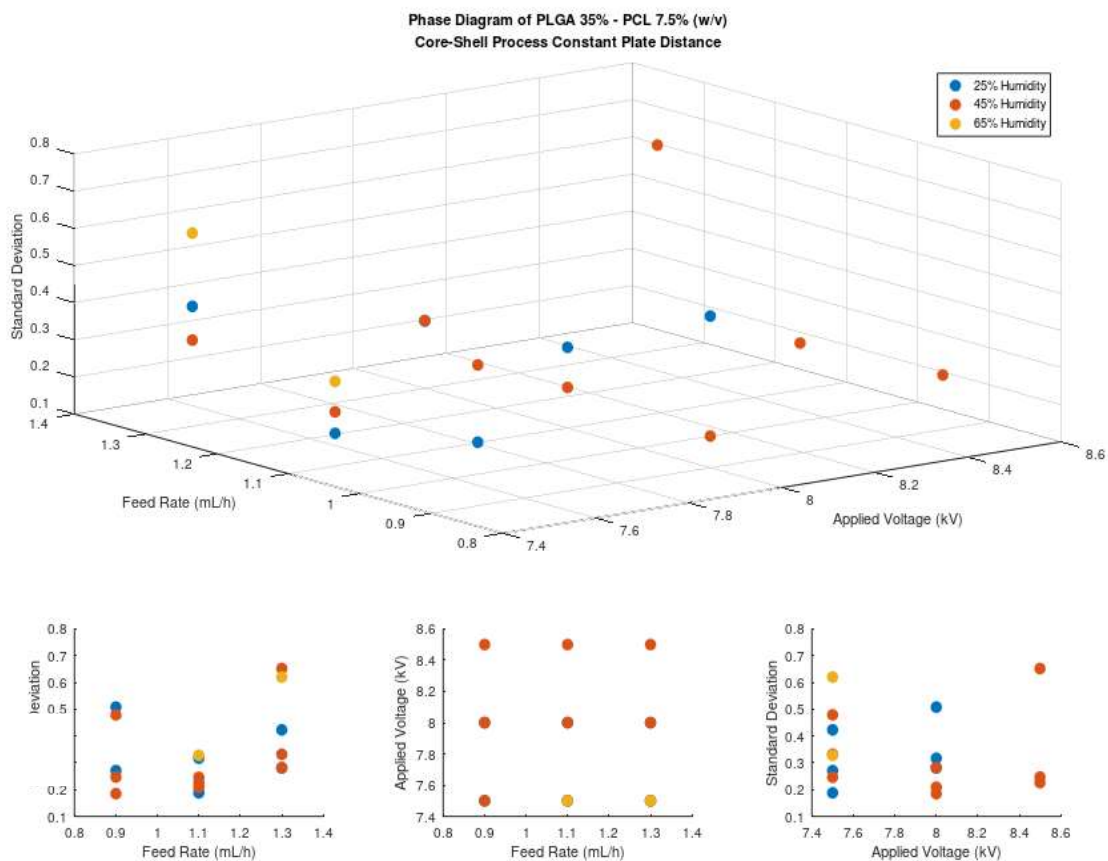


Figure 40 Phase diagram of core-shell process with a 10 cm plate distance

Figure 41 is a second phase diagram that was created; the data collected in Figure 41 represents all experiments run with a 15 cm plate distance that produced stable Taylor cones and a fibrous morphology. From the phase diagram, humidity had a clear impact on the standard deviation of the fibers measured. With all other variables kept constant, the change in humidity caused a scaffold with a different standard deviation to be created. The subplots below the phase diagram show that as feed rate was increased, the range of recorded standard deviations was also increased. The subplots also show that at a 7.5 kV applied voltage, the range of standard deviations was much higher than the range found for 8 kV and 8.5 kV applied voltage scaffolds.

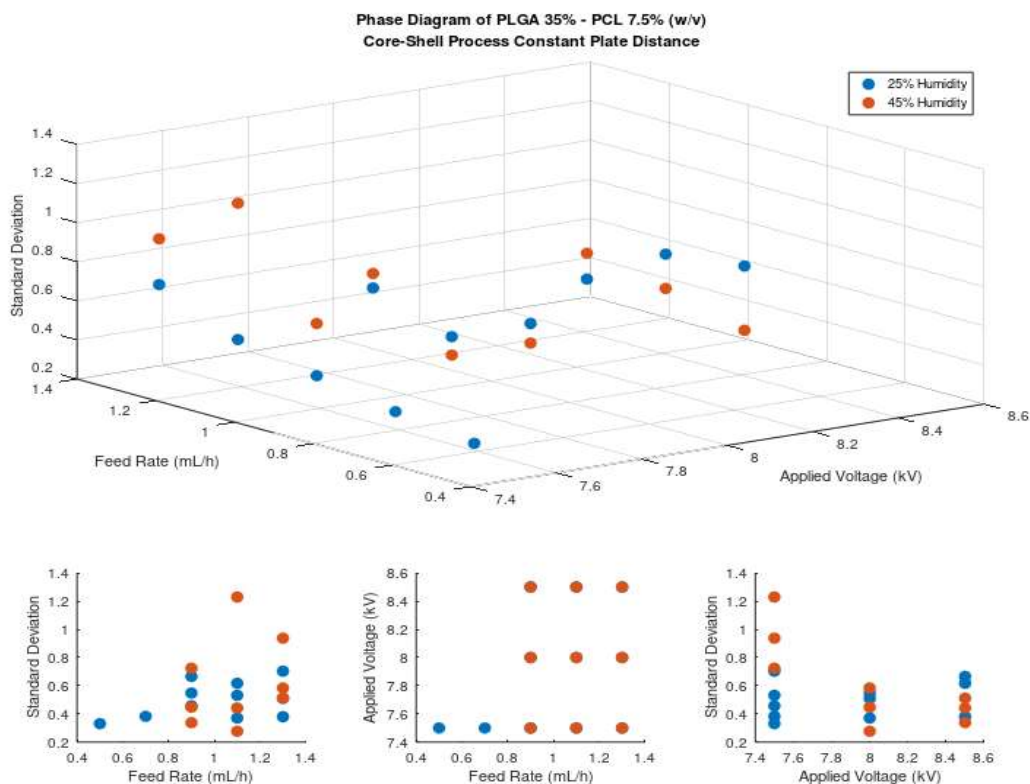


Figure 41 Phase diagram of core-shell process with a 15 cm plate distance

5.2.2 ATR-FTIR Bond Analysis

ATR-FTIR was conducted to determine the bonds present in the scaffold to ensure the scaffold was in no way tainted and had not reacted with the environment. Figure 42 shows the resulting plot from FTIR analysis of the core-shell PLGA-PCL scaffold. The spikes at 1300 and 1700 are indicative of PCL. The initial spike at 2800 was also found in ATR-FTIR of monoaxial PCL fibers. Comparing the FTIR results of the core-shell structure to the results of ATR-FTIR conducted on monoaxial PCL fibers, the results are nearly identical. This demonstrates a complete outer layer of PCL shell has formed, encasing the PLGA entirely.

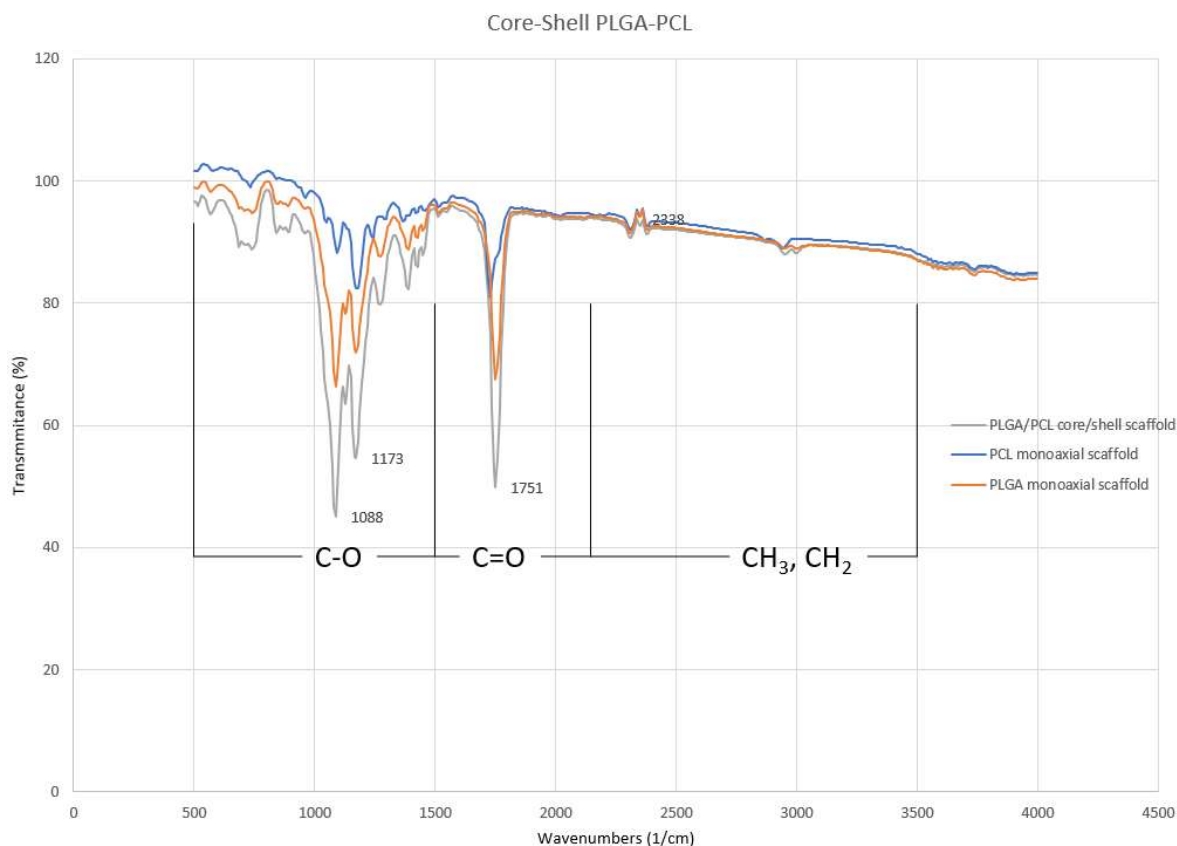


Figure 42 ATR-FTIR of core-shell PLGA-PCL

5.2.3 TEM

Figure 43 shows TEM images taken of core-shell fibers; Figure 43 A shows a TEM image taken as 100x magnification. At this magnification, the orientation of fibers electrospun on the copper grid can be observed. The random orientation of fibers is similar to the fibers imaged under SEM. The 1.1 mL/h core feed (Figure 43 B) rate and 0.7 mL/h (Figure 43 C) core feed rate were chosen for TEM imagery to show what effect, if any, core feed rate has on shell layer thickness. Figure 43 B shows a fiber from the scaffold imaged at 20k magnification; here a clear and distinct layer can be seen. The lighter layer is the PCL shell and the inner layer is the

PLGA core; the contact region between the layers was enhanced to further show the regions.

Figure 43 C shows TEM of fibers at 20k magnification with a 0.7 mL/h core feed rate; with the lower core feed rate a thicker shell layer formed. This is due to the fiber having a lesser volume of PLGA electrospun inside of it.

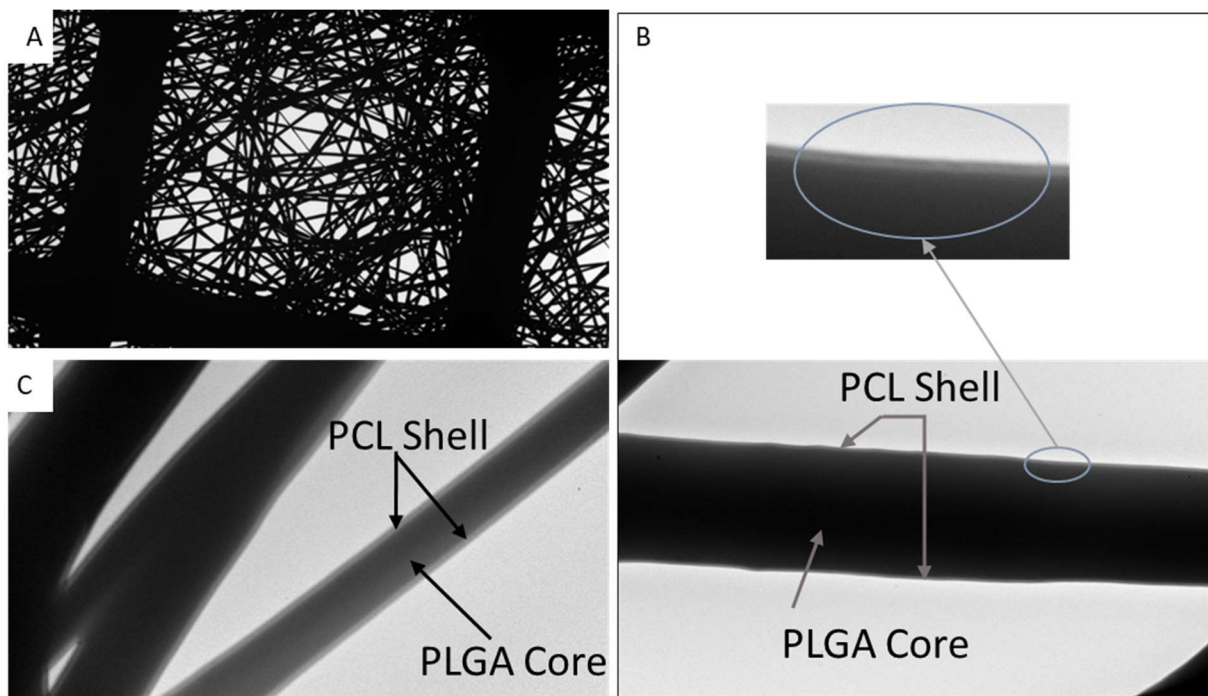


Figure 43 TEM images A) 100 magnification B) 20k magnification 1.1 mL/h core feed rate C) 20k magnification 0.7 mL/h core feed rate

5.3 Discussion

Provided the differences in average fiber diameter and standard deviation between scaffolds meeting the optimized criteria are not found to be statistically significant, the parameters will be considered as an optimized range. This optimized range will then be used in future experiments on core-shell electrospinning.

5.3.1 Impact of feed rate

The impact of core feed rate on average fiber diameter was found for core-shell electrospinning at 7.5 kV and 8 kV at both 10 cm and 15 cm plate distances and at 8.5 kV at a 15 cm plate distance. The impact of feed rate on average fiber diameter was inconclusive through all of the experiments run. Research done on the impact of core feed rate on PLC and gelatin-blended core-shell fibers found that changes in core feed rate had a significant impact on the diameter of the core layer but were inconclusive on the effects of core feed rate on the total fiber diameter [126]. This agrees with the scaffolds produced with 8 kV at a 10 cm plate distance, 8 kV at a 15 cm plate distance, and 8.5 kV at a 15 cm plate distance. The scaffolds from these parameters did not have a statistically significant change in total average fiber diameter with changing core feed rates. The scaffolds produced from 7.5 kV at a 10 cm plate distance and from 7.5 kV at a 15 cm plate distance did have statistically significant changes in total average fiber diameter with changes in core feed rate.

Looking at 7.5 kV at a 10 cm plate distance, the total average fiber diameter decreased very significantly from 0.5 mL/h core feed rate to 0.9 mL/h core feed rate and increased very significantly from 0.5 mL/h core feed rate to 1.1 mL/h core feed rate. This change from decreasing to increasing average fiber diameter does not clearly demonstrate the impact the change in core feed rate may have had and instead suggests external factors played a role. Scaffolds produced from 7.5 kV at a 15 cm plate distance showed a significant increase in fiber diameter comparing the 0.5 mL/h core feed rate scaffold to the 0.7 mL/h and 1.3 mL/h core feed rate scaffolds. The 0.7 mL/h and 1.1 mL/h core feed rate scaffolds did not show significant changes in fiber diameters compared to the 0.5 mL/h core feed rate scaffold. Research done on

the coaxial electrospinning of PVB found that when the concentration of polymer in solution is constant, the increase of core feed rate does not have a significant influence over the fiber diameter [127]. The findings in this experiment appear to agree with the literature that no clear correlation between core feed rate and total fiber diameter can be drawn. Even in the case of 7.5 kV at 10 cm and 15 cm plate distances, the significant changes in total fiber diameter found are not consistent with the other core feed rates tested at those parameters.

5.3.2 Impact of voltage

The impact of voltage on core-shell fiber diameter has been researched using poly(methyl methacrylate) (PMMA) core and polyacrylonitrile (PAN) shell [128]. The research found that attempting to electrospin a core-shell solution at a lower voltage resulted in a buildup of solution on the nozzle before the magnetic field was strong enough to induce a Taylor cone. This resulted in scaffolds composed of fibers with beads and inconsistent diameters. Higher voltage was also tested and resulted in the fibers reaching the collector before the solvent had fully dissolved, resulting in fibers being stuck closely together and causing inconsistent fiber diameters. In the experiments conducted, no bead formation was observed in the core-shell structure. Inconsistent fiber diameters were noticed in scaffolds electrospun with an 8.5 kV applied voltage, a 15 cm plate distance and 1.1 mL/h and 0.9 mL/h core feed rates. Scaffolds created using a 7.5 kV applied voltage, a 15 cm plate distance, and a 1.3 mL/h core feed rate also had inconsistent fiber diameter, characterized by a high standard deviation. In all three of the scaffolds produced when electrospun at 8.5 kV or 7.5 kV, the standard deviation increased when compared to the scaffolds produced at 8 kV. This agrees with published literature that found voltages greater or lesser than the optimized applied voltage produced scaffolds with a wider range of fiber diameters.

5.3.3 Impact of humidity

Humidity was found to have a very significant impact on average fiber diameter. As the relative humidity was increased from 25% to 65%, the average fiber diameter increased. The opposite trend was found in literature examining the monoaxial electrospinning of polyvinyl alcohol and poly(ethylene oxide), where increasing the relative humidity resulted in smaller diameter fibers [129]. The reason given for this trend is the impact relative humidity has on the rate the solvent evaporates. When the relative humidity is low, the high rate of solvent evaporation can cause an increase in polymer concentration at the exposed solution. It was also found in this literature that as relative humidity increased, the length of the jet from the Taylor cone increased to the point where at very high humidity the jet made contact with the collector plate. In the literature, PVA was dissolved in water and PEO was dissolved in 3% acetic acid; the different solvents could explain why the trend found is the opposite of what was observed in this research [129]. For core-shell electrospinning research conducted on polylactic acid (PCL) and polyethylene glycol (PEG) found that increasing the relative humidity resulted in smaller fiber diameters [130]. Due to relative humidity not being a parameter the lab could control, it is likely external environmental factors led to the increase in fiber diameter despite the increase in relative humidity. Another likely cause for the discrepancy is two different solutions had to be used to gather results at two different humidity levels because the experiment relied on the environment to produce the relative humidity.

5.3.4 Fiber diameter

Core-shell fibers are quantified by their diameters, core-shell structure, and fiber morphology. The diameters found in this research are in agreement with established literature.

The trend of increased fiber diameter of core-shell structured fibers opposed to their monoaxial structure outlined with poly(caprolactone)-poly(glycerol-sebacate) PCL-PGS and nylon-6-PU core-shell fibers [131], [132]. The diameter of the total fiber increased by 0.3532 μm at 7.5kV compared to 1.1-1.5mL/h PLGA-PCL to 1.5mL/h PCL and by 0.5239 μm at 8kV compared 1.1-1.5mL/h PLGA-PCL to 1.5mL/h PCL. Nylon-6-PU observed an increase in fiber diameter ranging from 0.47 μm to 2.112 μm comparing 8 wt.% PU to various concentrations of Nylon-6-PU core-shell fibers [132]. Looking at monoaxial PLGA electrospun at 1.1mL/h PCL-PGS, core-shell fibers noticed a 0.580 μm increase in diameter from pure PCL. In the research conducted, the PLGA core increased by 0.7756 and 0.1473 μm at 7.5kV and 8kV, respectively compared to monoaxial PCL fibers electrospun under the same parameters.

5.3.5 Core-shell integrity

ATR-FTIR conducted on the core-shell fibers resulted in a graph that greatly resembles that of pure PCL. This phenomenon was also found in research on PU/Cs/PEO core-shell fibers with PU as the core and a Cs/PEO blend as the shell [133]. The TEM imagery showing the formation of different core and shell layers is similar to the TEM conducted on PDT-PEO core-shell fibers. The lighter region shows the shell layer and the darker region shows the core layer. In research, the diameter of the core layer had some inconsistencies in it, being measured at 0.150 and 0.222 μm at different points on the same fiber [134]. It was found that FTIR of the core-shell fibers greatly resembled the FTIR of the Cs/PEO blend. The TEM conducted on PCL-PLGA fibers appears consistent throughout; diameter measurements were not taken because the TEM electron beam was capable of melting the polymer fibers, and as such, any measurements would incur a high degree of uncertainty.

5.3.6 Degradation

The degradation rate of core-shell fibers must take into account the degradation rates of the individual polymers in each layer. The degradation of thermoplastic PGA/PCL and PLA/PCL has been studied as a way to isolate the impact each component of PLGA has on degradation. It was found that PGA/PCL degrades much more rapidly and became fragile after two weeks and brittle after 16. PLA/PCL degraded much slower and 80% of its original mass remained after 25 weeks [125]. In the paper it was stated that the likely cause for the rapid degradation of PGA/PCL was the combination results in a less crystalline plastic. When determining degradation rates of core-shell fibers it is assumed that only the shell layer has contact with its surroundings and must degrade before the core is exposed to the outside environment. Controlling for fiber thickness, the degradation of PCL should be unchanged as there is no blending of polymers on the outermost surface of the shell layer. As the shell degrades and the exposed layer is closer to the PLGA core, some blending of core and shell polymers may exist. Any blending would increase the degradation rate similar to what was found in research [125]. By encapsulating the less crystalline (50:50) PLGA it is expected that the core-shell fiber will have a slower degradation time than the monoaxial (50:50) PLGA fibers. PLGA-based polyurethanes with a (50:50) LA:GA ratio electrospun at 18 kV with a 8 cm plate distance and a .02-.04 mL/h feed rate were studied over a four-week period. After a four-week degradation study there was less than 20% of the original fiber mass remaining [135]. With the PCL shell layer, the core-shell fibers are expected to have a significantly lower degradation rate than pure PLGA.

5.3.7 Drug release

Monoaxial PCL has been used to load and release drugs in *in vitro* and *in vivo* experiments. As discussed in Chapter 2 the drug release of FITC-dextran-loaded PCL reached just 10 % while PCL-O released over 40% [96]. The poor drug encapsulation and release properties of pure PCL demonstrate the advantage the core-shell fiber can have. By loading PLGA, the loading and release of the drug will be dependent on the ratio of LA:GA. Discussed in Chapter 3, the drug encapsulation of glial cell-line-derived neurotrophic factor (GDNF)-loaded (50:50) PLGA was found to be around 86%. The PLGA fibers then achieved sustained *in vitro* release over 42 days, which resulted in over 60% cumulative release of GDNF [119]. It was stated by the researchers that burst release could further be reduced by increasing the fiber diameter. The core-shell fibers produced take advantage of the high encapsulation efficiency and cumulative release of PLGA while also increasing the fiber diameter with a PCL shell layer. The more hydrophobic PCL will also further impede the burst release of the drug as it will have to permeate through the shell layer.

5.4 Summary

In synopsis, the production of a core-shell PLGA(50:50)/PCL scaffold was successful. The results indicate that the produced scaffolds are consistent throughout and can be produced on a voltage range from 7-8kV with a core feed rate of 0.9-1.3 mL/h, depending on the desired fiber. The best core-shell fibers were produced at 8 kV and a 10 cm plate distance with a 1.1 mL/h core feed rate and a 1.5 mL/h shell feed rate. The 10 cm plate distance was found to be superior based on the smaller average fiber diameter and standard deviation. The smaller plate distance also led to a more focused Taylor cone depositing fibers in a smaller area on the plate.

The 1.1 mL/h core feed rate resulted in more consistent fibers and allowed a thicker shell layer that could be used to reduce burst release. An 8 kV applied voltage resulted in good fiber morphology and a very consistent electrospinning process. Electrospinning with 8 kV and a 1.1-1.5 mL/h core-shell feed rate with a 15 cm plate distance also produced consistent fibers with a slightly larger average diameter. The impact of humidity was found to have a very significant impact on fiber diameter. Increasing the voltage at which core-shell fibers were electrospun was shown to have a significant impact on fiber diameter. Changes in feed rate showed a significant impact on fiber diameter when reduced from 1.1 to 0.9 mL/h. The impact of plate distance was found to be inconclusive. The successful electrospinning of these core-shell fibers opens future research to investigate the impact electrospinning parameters have on the mechanical, drug release, and degradation properties of PLGA-PCL core-shell fibers.

5.5 Future work

The impact of core feed rate on total average fiber diameter should be further investigated, as the published literature in the area is scarce. An experiment to determine the impact of core feed rate would require all other electrospinning conditions be held constant as the feed rate is increased from a low point to a high point by a set interval.

The impact of voltage observed in this research should be repeated with a larger incremental step. The 0.5 kV increment was used to optimize fiber production; however, the standard increment used in research on the influence of applied voltage is typically 5 kV.

Humidity could not be controlled in this research; while the impact of humidity was able to be investigated, the trends observed do not agree with literature. Further research on humidity

and coaxial electrospinning should take place in a climate-controlled environment where more humidity levels can be tested over a short period of time.

The drug release capabilities of a core-shell PLGA-PCL scaffold should be examined using doxycycline as a test drug due to its usefulness as a post-surgery antibiotic. Both the drug loading and release should be tested to determine if the scaffolds produced in this research meet the criteria for further study in this field.

The degradation of the scaffolds should also be determined in future work both with *in vivo* and *in vitro* studies. Rats are a commonly used mammal in degradation studies, but simulated body fluids have also been used to great success.

Each of the proposed future experiments addresses a void in the current knowledge base and understanding of electrospinning. Experiments involving the degradation, drug loading, or mechanical properties of scaffolds may have a more immediate impact on the application of electrospun scaffolds in tissue engineering. However, more precisely determining and understanding the impact of humidity, voltage, and core feed rate on core-shell fibers can reduce the time needed to optimize new solutions.

References

- [1] Nair, L., Laurecin, C., 2006, “Polymers as Biomaterials for Tissue Engineering and Controlled Drug Delivery” *Advances in Biochemical Engineering/Biotechnology*, **102**, pp 47-90.
- [2] Thomas, S., Balak, P., and Sadasivan, S., 2018, *Fundamental Biomaterials: Ceramics*, Elsevier Science.
- [3] Helsen, J., and Breme, J., 1998, *Metals as Biomaterials*, Wiley.
- [4] Park, J., and Lakes, R., 2010, *Biomaterials An Introduction*, Springer, New York
- [5] Huebsch, N., and Mooney, D., 2009, “Inspiration and application in the evolution of biomaterials”, *Nature*, **462**, pp 426-432.
- [6] Burg, K., and Orr, D., *An overview of bioresorbable materials*, Woodhead, Chap 1.
- [7] Kuhn, L., 2005, *Introduction to Biomedical Engineering*, 2nd ed., Academic Press, Chap 6
- [8] Ha, T., Quan, T., Nguyen, D., and Si, D., 2013, *Naturally Derived Biomaterials: Preparation and Application*, IntechOpen
- [9] Ruys, A., 2013, *Biomimetic biomaterials Structure and applications*, 1st ed., Woodhead
- [10] NIH, 2017, “Biomaterials”, from <https://www.nibib.nih.gov/science-education/science-topics/biomaterials#:~:text=Biomaterials%20play%20an%20integral,tissue%20or%20a%20biological%20function.>

- [11] Parida, P., Behera, A., and Mishra, S., 2012, "Classification of Biomaterials used in Medicine", **1**(3).
- [12] Dhandayuthapani, B., Yoshida, Y., Maekawa, T., and Kumar, S., 2011 "Polymeric Scaffolds in Tissue Engineering Application: A Review", *International Journal of Polymer Science*, pp 1687-9422.
- [13] NIH, "Tissue Engineering and Regenerative Medicine", from <https://www.nibib.nih.gov/science-education/science-topics/tissue-engineering-and-regenerative-medicine>.
- [14] Smith, L., Liu, X., and Ma, P., 2008, "Tissue engineering with nano-fibrous scaffolds", *Soft Matter*.
- [15] He, M., Storr-Paulsen, T., Wang, A., Ghezzi, C., Wang, S., Fullana, M., Karamichos, D., Uthem, T., Islam, R., Griffith, M., Islam, M., Hodges, R., Wnek, G., Kaplan, D., and Dartt, D., 2016, "Artificial Polymeric Scaffolds as Extracellular Matrix Substitutes for Autologous Conjunctival Goblet Cell Expansion", *Invest Ophthalmol Vis. Sci.*, **57**(14).
- [16] Karageorgiou, V., and Kaplan, D., 2005, "Porosity of 3D biomaterial scaffolds and osteogenesis", *Biomaterials*, **26**(27).
- [17] Eltom, A., Zhong, G., and Muhammad, A., 2019, "Scaffold Techniques and Designs in Tissue Engineering Functions and Purposes: A Review", *Advances in Materials Science and Engineering*.

- [18] Bosworth, L., and Downes, S., 2011, *Electrospinning for Tissue Regeneration*, Science Direct.
- [19] Jun, I., Hyung-Seop, H., Edwards, J., and Jeon, H., 2018, “Electrospun Fibrous Scaffolds for Tissue Engineering: Viewpoints on Architecture and Fabrication”, *International Journal of Molecular Sciences*.
- [20] Abdullah, M., and Nuge, T., 2008, “Core-Shell Fibers: Design, Roles, and Controllable Release Strategies in Tissue Engineering and Drug Delivery”, *Polymers*, **11**(12).
- [21] Piccirillo, G., Carvajal Berrio, D., Laurita, A., Pepe, A., Bochicchio, B., Schenke-Layland, K., and Hinderer, S., 2019, “Controlled and tuneable drug release from electrospun fibers and a non-invasive approach for cytotoxicity testing”, *Scientific Reports*.
- [22] Cam, M., Yildiz, S., Alenezi, H., Cesur, S., Ozcan, G., Erdemir, G., Edirisinghe, U., Akakin, D., Kuruca, D., Kabasakal, L., Gunduz, O., and Edirisinghe, M., 2020, “Evaluation of burst release and sustained release of pioglitazone-loaded fibrous mats on diabetic wound healing: an *in vitro* and *in vivo* comparison study”, *Journal of the Royal Society Interface*.
- [23] Yao, J., Wang, Y., Ma, W., Dong, W., Zhang, M., and Sun, D., 2019, “Dual-Drug-Loaded Silk Fibroin/PLGA Scaffolds for Potential Bone Regeneration Applications”, *Journal of Nanomaterials*.
- [24] Wang, C., Lu, W., and Wang, M., 2020, “Multifunctional fibrous scaffolds for bone regeneration with enhanced vascularization”, *Journal of Materials Chemistry B*.

- [25] Prabha, R., Kraft, D., Harkness, L., Melsen, B., Varma, H., Nair, P., Kjems, J., and Kassem, M., 2017, “Bioactive nano-fibrous scaffold for vascularized craniofacial bone regeneration”, *Journal of Tissue Engineering Regenerative Medicine*.
- [26] Chocholata, P., Kulda, V., and Babuska, V., 2019, “Fabrication of Scaffolds for Bone-Tissue Regeneration”, *Materials*.
- [27] Jansen, E., Sladek, R., Bahar, H., Yaffe, A., Gijbels, M., Kuijer, R., Bulstra, S., Guldmond, N., Binderman, I., and Koole, L., 2005, “Hydrophobicity as a design criterion for polymer scaffolds in bone tissue engineering”, *Biomaterials*.
- [28] Chen, V., Smith, L., and Ma, P., 2006, “Bone regeneration on computer-designed nano-fibrous scaffolds”, *Biomaterials*.
- [29] Vesely, I., 2005 “Heart valve tissue engineering”, *Circulation Research*, **97**(8).
- [30] Shin, M., Ishii, O., Sueda, T., and Vacanti, J., 2004, “Contractile cardia grafts using a novel nanofibrous mesh”, *Biomaterials*, **25**(17), pp 3717-3723.
- [31] Du, M., Gu, J., Wang, J., Xue, Y., Ma, Y., Mo, X., and Xue, S., 2019, “Silk fibroin/poly(L-lactic acid-co- ϵ -caprolactone) electrospun nanofibrous scaffolds exert a protective effect following myocardial infarction”, *Experimental and Therapeutic Medicine*.
- [32] Hoveizi, E., Nabiuni, M., Parivar, K., Rajabi-Zeleti, S., and Tavakol, S., 2013, “Functionalisation and surface modification of electrospun polylactic acid scaffold for tissue engineering”, *Cell Biology International*.

- [33] Ravichandran, R., Venugopal, J., Sundarrajan, S., and Mukherjee, S., 2012, "Composite poly-L-lactic acid/poly-(α,β)-DL-aspartic acid/collagen nanofibrous scaffolds for dermal tissue regeneration", *Materials Science and Engineering: C*, **32**(6).
- [34] Bacakova, M., Pajorova, J., Stranska, D., Hadraba, D., Lopot, F., Riedel, T., Brynda, E., Zaloudkova, M., and Bacakova, L., 2017, "Protein nanocoatings on synthetic polymeric nanofibrous membranes designed as carriers for skin cells", *International Journal of Nanomedicine*, **12**.
- [35] Shimauchi, H., Nemoto, E., Ishihata, H., and Shimomura, M., 2013, "Possible functional scaffolds for periodontal regeneration", *Japanese Dental Science Review*.
- [36] Park, C., Rios, H., Jin, Q., Bland, M., Flanagan, C., Hollister, S., and Giannobile, W., 2010, "Biomimetic Hybrid Scaffolds for Engineering Human Tooth-Ligament Interfaces", *Biomaterials*.
- [37] Nicolae, A., and Grumezescu, A., 2019, *Materials for Biomedical Engineering*, Elsevier, Chap 1.
- [38] Nam, Y., and Park, T., 1999, "Biodegradable polymeric microcellular foams by modified thermally induced phase separation method", *Biomaterials*.
- [39] Packwood, D., Han, P., and Hitosugi, T., 2017, "Chemical and entropic control on the molecular self-assembly process", *Nature communications*.
- [40] Beachley, V., and Wen, X., 2010, "Polymer nanofibrous structures: Fabrication, biofunctionalization, and cell interactions", *Progress in Polymer Science*.

- [41] Geoffrey Taylor, 1964, "Disintegration of Water Drops in an Electric Field", Royal Society.
- [42] Shin, Y., Hohman, M., Brenner, M., and Rutledge, G., 2001, "Experimental characterization of electrospinning: the electrically forced jet and instabilities", *Polymer*, **42**(25).
- [43] Gatford, J., 2008, The New Zealand Institute for Plant and Food Research Ltd.
- [44] Haider, A., Haider, S., and Kang, I., 2018, "A comprehensive review summarizing the effect of electrospinning parameters and potential applications of nanofibers in biomedical and biotechnology", *Arabian Journal of Chemistry*, **11**(8).
- [45] Clarke, J., and Jayasinghe, S., 2008, "Bio-electrosprayed multicellular zebrafish embryos are viable and develop normally", *Biomedical Materials*.
- [46] Yeo, L., Gagnon, Z., and Change, H., 2005, "AC electro spray biomaterials synthesis", *Biomaterials*.
- [47] Koenig, K., Beukenberg, K., Langensiepen, F., and Seide, G., 2019, "A new prototype melt-electrospinning device for the production of biobased thermoplastic sub-microfibers and nanofibers", *Biomaterials Research*.
- [48] Leach, M., Feng, Z., Tuck, S., and Corey, J., 2011, "Electrospinning Fundamentals: Optimizing Solution and Apparatus Parameters", *Journal of Visualized Experiments*.
- [49] Ko, J., Mohtaram, N., Lee, P., Willerth, S., and Jun, M., 2013, Parametric studies of melt electrospinning poly-ε-(caprolactone) fibers for tissue engineering applications. In: 8th ICOMM, 25–28 March 2013, pp 526–531.

- [50] Ogata, N., Yamaguchi, S., Shimada, N., Lu, G., Iwata, T., Nakane, K., and Ogihara, T., 2007, "Poly(lactide) nanofibers produced by a melt-electrospinning system with a laser melting device", *Journal of Applied Polymer Science*.
- [51] Williams, G., Raimi-Abraham, B., and Luo, C., 2019, *Nanofibres in Drug Delivery*, UCL Press.
- [52] Xu, C., Inai, R., Kotaki, M., and Ramakrishna, S., 2004, "Electrospun nanofiber fabrication as synthetic extracellular matrix and its potential for vascular tissue engineering", *Tissue Engineering*.
- [53] Zhang, X., Wang, X., Keshav, V., Wang, X., Johanas, J., Leisk, G., and Kaplan, D., "Dynamic Culture Conditions to Generate Silk-Based Tissue-Engineered Vascular Grafts", *Biomaterials*, **30**(19).
- [54] Kumar, P., 2012, "Effect of Collector on Electrospinning to Fabricate Aligned Nanofiber", B.S. thesis, Bio-medical engineering, National Institute of Technology, Rourkela.
- [55] El-hadi, A., and Al-Jabri, F., "Influence of Electrospinning Parameters on Fiber Diameter and Mechanical Properties of Poly(3-Hydroxybutyrate) (PHB) and Polyanilines (PANI) Blends", *Polymers*.
- [56] Royal Society of Chemistry, "Composite materials," [Online]. From: <https://www.rsc.org/Education/Teachers/Resources/Inspirational/Resources/4.3.1.pdf>.
- [57] Samerender, N., and Smitha, M., "Multi-Functional Electrospun Nanofibers from Polymer Blends for Scaffold Tissue Engineering", *Fibers*, **7**(7).

- [58] Chaparro, F., Presley, K., Coutinho da Silva, M., Mandan, N., Colachis, M., Posner, M., Arnold, R., Fan, F., Moraes, C., and Lannutti, J., 2019, “Sintered electrospun poly(ϵ -caprolactone)–poly(ethylene terephthalate) for drug delivery”, *Journal of Applied Polymer Science*.
- [59] Hu, X., Liu, S., Zhou, G., Huang, Y., Xie, Z., and Jing, X., 2014, “Electrospinning of polymeric nanofibers for drug delivery applications”, *Journal of Controlled Release*, **185**.
- [60] Razavizadeh, B., and Niazmand, R., 2020, “Characterization of polyamide-6/ propolis blended electrospun fibers”, *Heliyon*.
- [61] Xu, T., Binder, K., Albanna, M., Dice, D., Zhao, W., Yoo, J., and Atala, A., 2013, “Hybrid printing of mechanically and biologically improved constructs for cartilage tissue engineering applications”, *Biofabrication*, **5**(1).
- [62] Wright, L., Young, R., Andric, T., and Freeman, J., 2010, “Fabrication and mechanical characterization of 3D electrospun scaffolds for tissue engineering”, *Biomedical materials*, **5**(5).
- [63] Hong, J., Bang, J., Xu, G., Lee, J., Kim, Y., Lee, H., Kim, H., and Kwon, S., 2015, “Thickness-controllable electrospun fibers promote tubular structure formation by endothelial progenitor cells”, *International Journal of Nanomedicine*, **10**(10), pp. 1189-1200.
- [64] Agarwal, S., and Shaohua, J., 2015, *Encyclopedia of Polymeric Nanomaterials*, Springer, pp. 1323-1337.

- [65] Zhao, P., Jiang, H., Pan, H., Zhu, K., and Chen, W., 2007, “Biodegradable fibrous scaffolds composed of gelatin coated poly(ϵ -caprolactone) prepared by coaxial electrospinning”, *Journal of Biomedical Materials Research*, **38A**(2), pp. 372-382.
- [66] Hang, Y., Zhang, Y., Jin, Y., Shao, H., and Hu, X., 2012, “Preparation of regenerated silk fibroin/silk sericin fibers by coaxial electrospinning”, *International Journal of Biological Macromolecules*, **51**(5).
- [67] Charkraborty, S., Liao, I., Adler, A., and Leong, K., 2009, “Electrohydrodynamics: A facile technique to fabricate drug delivery systems”, *Advanced Drug Delivery Reviews*, **61**(12), pp. 1043-1054.
- [68] Li, F., Zhao, Y., and Song, Y., 2010, *Nanofibers*, IntechOpen,
- [69] Alam, H., Dalgic, A., Tezcaner, A., Ozen, C., and Keskin, D., 2019, “A comparative study of monoaxial and coaxial PCL/gelatin/Pluronic 188 scaffolds for bone tissue engineering”, *International Journal of Polymeric Materials and Polymeric Biomaterials*, **69**(6), pp. 339-350.
- [70] Nagiah, N., Murdock, C., Bhattacharjee, M., Nair, L., and Laurencin, C., 2020, “Development of Tripolymeric Triaxial Electrospun Fibrous Matrices for Dual Drug Delivery Applications”, *Scientific Reports*, **10**(609).
- [71] Milosevic, M., Stojanovic, D., Simic, V., Grkovic, M., Bjelovic, M., Uskokovic, P., and Kojic, M., 2020, “Preparation and modeling of three-layered PCL/PLGA/PCL fibrous scaffolds for prolonged drug release”, *Scientific Reports*, **10**(11126).

- [72] Farkhondehnia, H., Tehran, M., and Zamani, F., 2018, “Fabrication of Biocompatible PLGA/PCL/PANI Nanofibrous Scaffolds with Electrical Excitability”, *Fibers and Polymers*, (9).
- [73] Peng, C., Zheng, J., Chen, D., Zhang, X., Deng, L., Chen, Z., and Wu, L., 2018, “Response of hPDLSCs on 3D printed PCL/PLGA composite scaffolds in vitro”, *Molecular Medicine Reports*, **18**(2), pp. 1335-1344.
- [74] Hiep, N., and Lee, B., 2010, “Electro-spinning of PLGA/PCL blends for tissue engineering and their biocompatibility”, **21**(6), pp. 1967-1978.
- [75] Makadia, H., and Siegel, S., 2011, “Poly Lactic-co-Glycolic Acid (PLGA) as Biodegradable Controlled Drug Delivery Carrier”, *Polymers*, **3**(3), pp. 1377-1397.
- [76] Deshmukh, K., Ahamed, M., Deshmukh, R., Pasha, S., Bhagat, P., and Chidambaram, K., 2017, *Biopolymer Composites in Electronics*, Elsevier, pp. 27-128, Chap. 3.
- [78] Vinolas, S., Engel, E., and Mateo-Timoneda, M., 2019, *Bone Repair Biomaterials*, Woodhead, pp. 179-197, Chap. 7.
- [79] Gaaz, T., Sulong, A., Akhtar, M., Kadhum, A., Mohamad, A., and Al-Amiery, A., 2015, “Properties and Applications of Polyvinyl Alcohol, Halloysite Nanotubes and Their Nanocomposites”, *Molecules*, **20**(12).
- [80] Filip, P., and Peer, P., 2019, “Characterization of Poly(Ethylene Oxide) Nanofibers— Mutual Relations between Mean Diameter of Electrospun Nanofibers and Solution Characteristics”, *Processes*, **7**(12).

- [81] Mochane, M., Motseoneng, T., Sadiku, E., and Teboho, M., 2019, “Morphology and Properties of Electrospun PCL and Its Composites for Medical Applications: A Mini Review”, *Applied Sciences*, **9**(11).
- [82] Sun, H., Mei, L., Song, C., Cui, X., and Wang, P., 2006, “The in vivo degradation, absorption and excretion of PCL-based implant”, *Biomaterials*, **27**(9).
- [83] Jiang, T., Zhang, G., He, W., Li, H., and Jin, X., 2014, “The Tissue Response and Degradation of Electrospun Poly(ϵ -caprolactone)/Poly(trimethylene-carbonate) Scaffold in Subcutaneous Space of Mice”, *Journal of Nanomaterials*, **2014**.
- [84] Silva-Cunba, A., Fialbo, S., Naud, M., and Behar-Coben, F., 2009, *Investigative Ophthalmology and Visual Science*, **50**(5).
- [85] Javan, R., Soleimani, M., Divsalar, A., and Eidi, A., 2013, “Biological behavior study of gelatin coated PCL nanofibrous electrospun scaffolds using fibroblasts”, *Journal of Paramedical Sciences*, **5**.
- [86] Ghobeira, R., Asadian, M., Vercruyssen, C., Declercq, H., Geyter, N., and Morent, R., 2018, “Wide-ranging diameter scale of random and highly aligned PCL fibers electrospun using controlled working parameters”, *Polymer*, **157**, pp. 19-31.
- [87] Fridrikh, S., Yu, J., Brenner, M., and Rutledge, G., “Controlling the fiber diameter during electrospinning”, *Physical Review Letters*, **90**(14).
- [88] Bate, T. S. R., Forbes, S. J., and Callanan, A., 2020, “Controlling Electrospun Polymer Morphology for Tissue Engineering Demonstrated Using hepG2 Cell Line”, *J. Vis. Exp.*, (159).

- [89] Gevorkyan, A., Shter, G., Shmueli, Y., and Buk, A., 2014, "Branching Effect and Morphology Control in Electrospun $\text{PbZr}_{0.52}\text{Ti}_{0.48}\text{O}_3$ Nanofibers", *Journal of Materials Research*, **29**(16).
- [90] Baker, S., Banerjee, S., Bonin, K., and Guthold, M., 2016, "Determining the mechanical properties of electrospun poly- ϵ -caprolactone (PCL) nanofibers using AFM and a novel fiber anchoring technique", *Materials Science and Engineering: C*, **59**, pp. 203-212.
- [91] Marting, J., Johnson, J., Cooper, A., 2006, "Mechanical Properties of Polymers: The Influence of Molecular Weight and Molecular Weight Distribution", *Journal of Macromolecular Science Part C*, **8**(1).
- [92] Wong, S., Baji, A., Leng, S., 2008, "Effect of fiber diameter on tensile properties of electrospun poly(ϵ -caprolactone)", *Polymer*, **49**(21).
- [93] Shamsah, A., Cartmell, S., Richardson, S., and Bosworth, L., 2020, "Material Characterization of PCL:PLLA Electrospun Fibers Following Six Months Degradation In Vitro", *Polymers*, **12**(3), p. 700.
- [94] Cunha-Reis, C., TuzlaKoglu, K., Baas, E., Yang, Y., El Haj, A., and Reis, R., 2007, "Influence of porosity and fibre diameter on the degradation of chitosan fib(re-mesh scaffolds and cell adhesion", *Journal of Materials Science. Materials in Medicine*, **18**(2), pp. 195-200.
- [95] Bala Balakrishnan, P., Gardella, L., Forouharshad, M., Pellegrino, T., and Monticelli, O., 2018, "Star poly(ϵ -caprolactone)-based electrospun fibers as biocompatible scaffold for doxorubicin with prolonged drug release activity", *Colloids and surfaces*, **161**, pp. 488-496.

- [96] Tarvainen, T., Karjalainen, T., Malin, M., Perakorpi, K., Tuominen, J., Seppala, J., and Jarvinen, K., 2002, "Drug release profiles from and degradation of a novel biodegradable polymer, 2,2-bis(2-oxazoline) linked poly(ϵ -caprolactone)", *European Journal of Pharmaceutical Sciences*, **16**(4-5), pp. 323-331.
- [97] Gentile, G., Chiono, V., and Carmagnola, I., 2014, "An Overview of Poly(lactic-co-glycolic) Acid (PLGA)-Based Biomaterials for Bone Tissue Engineering", *International Journal of Molecular Sciences*, **15**(3).
- [98] Pohanka, M., "D-Lactic Acid as a Metabolite: Toxicology, Diagnosis, and Detection", *Biomedical Research International*.
- [99] Liu, X., Baldursdottir, S.G., Aho, J., Qu, H., Christensen, L., Rantanen, J., and Yang, M., 2017, "Electrospinnability of Poly Lactic-co-glycolic Acid (PLGA): the Role of Solvent Type and Solvent Composition", *Pharm Res*, **34**, pp. 738–749.
- [100] Alnuman, N., Al-Jafary, R., Manna, F., and Almuhtaseb, R., 2018, "Fabrication and Characterization of Electrospun 75:25 PLGA Nanofibers for Skin Tissue Engineering", *IEEE-EMBS Conference on Biomedical Engineering and Sciences (IECBES)*.
- [101] Chor, A., Goncalves, R., Machado Costa, A., Farina, M., Ponche, A., Sirelli, L., Schrodj, G., Gree, S., Rodrigues de Andrade, L., Anselme, K., and Lopes Dias, M., 2020, "In Vitro Degradation of Electrospun Poly(Lactic-Co-Glycolic Acid) (PLGA) for Oral Mucosa Regeneration", *Polymers*, **12**(8).

[102] Ma, X., Oyamada, S., Wu, T., Robich, M.P., Wu, H., Wang, X., Buchholz, B., McCarthy, S., Bianchi, C.F., Sellke, F.W., Laham, R., 2011, "In vitro and in vivo degradation of poly(D, L-lactide-co-glycolide)/amorphous calcium phosphate copolymer coated on metal stents", *Journal of Biomedical Materials Research A.*, **96**(4), pp. 632-638.

[103] Hedelin, H., Hebelka, H., Brisby, H., and Laine, T., 2020, "MRI evaluation of resorbable poly lactic-co-glycolic acid (PLGA) screws used in pelvic osteotomies in children-a retrospective case series", *Journal of Orthopedic Surgery Research*, **15**(1), p. 329.

[104] Marques, D., Santos, L., Schopf, L., and Fraga, J., 2013, "Analysis of Poly(Lactic-co-Glycolic Acid)/Poly(Isoprene) Polymeric Blend for application as biomaterial", *Polímeros*, **23**(5).

[105] Fallahi, D., Rafizadeh, M., Mohammadi, N., and Vahidi, B., 2009, "Effects of feed rate and solution conductivity on jet current and fiber diameter in electrospinning of polyacrylonitrile solutions", *e-Polymers*, **9**(1).

[106] Oteyaka, M.O., Ozel, E., and Yildirim, M., 2011, "The Effects of Power and Feeding Rate on Production of Polyurethane Nanofiber with Electrospinning Process", *International Congress on Advances in Applied Physics and Materials Science*, **1400**, pp. 216-221.

[107] Sener, A.G., Altay, A.S., and Altay, F., 2011, "Effect of voltage on morphology of electrospun nanofibers", *Electrical and Electronics Engineering (ELECO)*.

[108] Zhu, G., Zhao, L., Zhu, L., Deng, X., and Chen, W., 2017, "Effect of Experimental Parameters on Nanofiber Diameter from Electrospinning with Wire Electrodes", *IOP Conference Series: Materials Science and Engineering*, **230**.

- [109] Beachley, V., and We, X., 2009, “Effect of electrospinning parameters on the nanofiber diameter and length”, *Materials Science and Engineering: C*, **29**(3), pp. 663-668.
- [110] Huan, S., Liu, G., Han, G., Cheng, W., Fu, Z., Wu, Q., and Wang, Q., 2015, “Effect of Experimental Parameters on Morphological, Mechanical and Hydrophobic Properties of Electrospun Polystyrene Fibers”, *Materials*, **8**.
- [111] Yu C.C., Chen Y.W., Yeh P.Y., Hsiao Y.S., Lin W.T., Kuo C.W., Chueh D.Y., You Y.W., Shyue J.J., Chang Y.C., and Chen P., 2019, “Random and aligned electrospun PLGA nanofibers embedded in microfluidic chips for cancer cell isolation and integration with air foam technology for cell release”, *Journal of Nanobiotechnology*, **17**(1).
- [112] Carmagnola, I., Chiono, V., Ruocco, G., Scalzone, A., Gentile, P., Taddei, P., Ciardelli, G., 2020, “PLGA Membranes Functionalized with Gelatin through Biomimetic Mussel-Inspired Strategy”, *Nanomaterials*, **10**.
- [113] Zhang, H., 2011, 2011, “Effects of electrospinning parameters on morphology and diameter of electrospun PLGA/MWNTs fibers and cytocompatibility in vitro”, *Journal of Bioactive and Compatible Polymers*, **26**(6), pp. 590-606.
- [114] Shin H.J., Lee C.H., Cho I.H., Kim Y.J., Lee Y.J., Kim I.A., Park K.D., Yui N., and Shin J.W., “Electrospun PLGA nanofiber scaffolds for articular cartilage reconstruction: mechanical stability, degradation and cellular responses under mechanical stimulation in vitro”, *Journal Biomaterials Science Polymer Ed.*, 2006, **17**(1-2), pp.103-19.

- [115] Jazi, R., Rafienia, M., Rozve, H., Karamian, E., and Sattery, M., 2017, "Fabrication and characterization of electrospun poly lactic-co-glycolic acid/zeolite nanocomposite scaffolds using bone tissue engineering", *Journal of Bioactive and Compatible Polymers*, **33**(1), pp. 63-78.
- [116] El Khatib, M., Mauro, A., Di Mattia, M., Wyrwa, R., Schweder, M., Ancora, M., Lazzaro, F., Berardinelli, P., Valbonetti, L., Di Giacinto, O., Polci, A., Cammà, C., Schnabelrauch, M., Barboni, B., and Russo, V., 2020, "Electrospun PLGA Fiber Diameter and Alignment of Tendon Biomimetic Fleece Potentiate Tenogenic Differentiation and Immunomodulatory Function of Amniotic Epithelial Stem Cells", *Cells*, **9**.
- [117] Keles, H., Naylor, A., Clegg, F., and Sammon, C., 2015, "Investigation of factors influencing the hydrolytic degradation of single PLGA microparticles", *Polymer Degradation and Stability*, **119**, pp. 228-241.
- [118] Mekala, N., Baadhe, R., Parcha, S., and Yalavarthy, P., 2013, "Physical and degradation properties of PLGA scaffolds fabricated by salt fusion technique.", *Journal of Biomedical Research*, **27**(4).
- [119] Liu, C., Wang, C., Zhao, Q., Li, X., Xu, F., Yao, X., and Wang, M., 2018, "Incorporation and release of dual growth factors for nerve tissue engineering using nanofibrous bicomponent scaffolds", *Biomedical Materials*.
- [120] Sperling, L., Reis, K., Pranke, P., and Wendorff, J., 2016, "Advantages and challenges offered by biofunctional core-shell fiber systems for tissue engineering and drug delivery", *Drug Discovery Today*, **21**(8), pp. 1243-1256.

- [121] Yu, D., Wang, X., Li, X., Chain, W., Li, Y., and Liao, Y., 2013, “Electrospun biphasic drug release polyvinylpyrrolidone/ethyl cellulose core/sheath nanofibers”, *Acta Biomaterialia*, **9**(3), pp. 5665-5672.
- [122] Liu, J., Wang, C., Wang, J., Ruan, H., and Fan, C., 2011, “Peripheral nerve regeneration using composite poly(lactic acid-caprolactone)/nerve growth factor conduits prepared by coaxial electrospinning”, *Journal of Biomedical Materials Research A*, **96**(1), pp. 13-20.
- [123] Goncalves, R., Fernandes, F., Picciani, P., Dias, M., 2015, “Morphology and Thermal Properties of Core-Shell PVA/PLA Ultrafine Fibers Produced by Coaxial Electrospinning”, *Materials Sciences and Applications*, **6**(2), pp. 189-199.
- [124] Li, S., Sun, B., Li, X., and Yuan, X., 2008, “Characterization of electrospun core/shell poly(vinyl pyrrolidone)/poly(L-lactide-co-epsilon-caprolactone) fibrous membranes and their cytocompatibility in vitro”, *Journal of Biomaterials Science. Polymer Ed.*, **19**(2), pp. 245-258.
- [125] Vieira, A., Vieira, J., Guedes, R., and Marques, A., 2010, “Degradation and viscoelastic properties of PLA-PCL, PGA-PCL, PDO and PGA fibres”, *Materials Science Forum*.
- [126] Drexler, J., and Powell, H., 2010, “Regulation of electrospun scaffold stiffness via coaxial core diameter”, *Acta Biomaterialia*, **7**(3), pp. 1133-1139.
- [127] Yi, L., Wang, Y., Fang, Y., Zhang, M., Yao, J., Wang, L., and Marek, J., 2019, “Development of core–sheath structured smart nanofibers by coaxial electrospinning for thermo-regulated textiles”, *Royal Society of Chemistry*, **9**, pp. 21844-21851.

- [128] Kaerkitcha, N., Chuangchote, S., and Sagawa, T., 2016, “Control of physical properties of carbon nanofibers obtained from coaxial electrospinning of PMMA and PAN with adjustable inner/outer nozzle-ends”, *Nanoscale Research Letters*, **11**, p. 186.
- [129] Palipenko, J., Kristl, J., Jankovic, B., Baugartner, S., and Kocbec, P., 2013, “The impact of relative humidity during electrospinning on the morphology and mechanical properties of nanofibers”, *International Journal of Pharmaceutics*, **456**(1), pp. 125-134.
- [130] Golin, A., 2014, “Humidity Effect on the Structure of Electrospun Core-Shell PCL-PEG Fibers for Tissue Regeneration Applications”, M.S. thesis, Chemical and Biochemical Engineering, University of Western Ontario
- [131] Hou, L., Zhang, X., Mikael, P., Lin, L., Dong, W., Zheng, Y., Simmons, T., Zhang, F., and Linhardt, R., 2017, “Biodegradable and Bioactive PCL-PGS Core-Shell Fibers for Tissue Engineering”, *ACS Omega*, **2**(10), pp. 6321-6328.
- [132] Han, X., Huang, Z., He, C., and Liu, L., 2007, “Preparation and Characterization of Core—Shell Structured Nanofibers by Coaxial Electrospinning”, *High Performance Polymers*, **19**(2), pp. 147-159.
- [133] Maleknia, L., Dilamian, M., Pilehrood, M., Sadeghi-Aliabadi, H., and Hekmati, A., 2018, “Preparation, process optimization and characterization of core-shell polyurethane/chitosan nanofibers as a potential platform for bioactive scaffolds”, *Research in Pharmaceutical Sciences*, **13**(3), pp. 273-282.

[134] Huang, Z., Wu, J., Wong, S., Qu, J., and Srivatsan, T., 2017, “The technique of electrospinning for manufacturing core-shell nanofibers”, *Materials and Manufacturing Processes*, **33**(2).

[135] Blakney, A., Simonovsky, F., Suydam, I., Ratner, B., and Woodrow, K., 2016, “Rapidly Biodegrading PLGA-Polyurethane Fibers for Sustained Release of Physicochemically Diverse Drugs”, *ACS Biomater. Sci. Eng.*, **2**(9), pp. 1595-1607.

APPENDIX

ELECTROSPINNING SOP

Table of Contents

	Page
A.1 Safety	140
A.2 Maintenance	140
A.2.1 Electrical.....	140
A.2.2 Hardware	140
A.3 Solution Preparation	142
A.4 Electrospinning Procedure.....	146
A.4.1 Parts of the Electrospinner	146
A.4.2 Safe use of the NanoSpinner	149
A.4.3 Electrospinning Quick Start.....	149
A.4.4 Monoaxial Electrospinning.....	151
A.4.5 Coaxial Electrospinning	152

List of Figures

Figure A.1 Overview image of NanoSpinner	147
Figure A.2 Close-up image of NanoSpinner LCD screen	148

A.1 Safety

The NanoSpinner NS1 should be operated in a well vented area, gloves, masks, and lab coats must be worn during operation and cleaning. Always check the safety procedures for the solvent and solute being used and adhere to any requirements for those materials. For questions please refer to the [NIU Division of Research and Innovation Partnerships Laboratory Safety](https://www.niu.edu/divresearch/compliance/safety/index.shtml) [<https://www.niu.edu/divresearch/compliance/safety/index.shtml>]

For safety information specific to the NS1 please refer to the User's Manual NS1 Starter Kit version: AEM.01 .01.19. A physical copy of this document is kept in EB 254B with the NS1. The document is also available online [here](https://niuits-my.sharepoint.com/:b:/g/personal/z1814815_students_niu_edu/EQX1TyzDc-5KoT3XMC-MDxsBXE_Gl--sRdVxtNSGwTC4IQ?e=JOD9T3). [https://niuits-my.sharepoint.com/:b:/g/personal/z1814815_students_niu_edu/EQX1TyzDc-5KoT3XMC-MDxsBXE_Gl--sRdVxtNSGwTC4IQ?e=JOD9T3]

A.2 Maintenance

A.2.1 Electrical

The electrospinner is a very delicate machine. Proper maintenance must be performed to ensure the equipment continues to function. Defective electrical equipment or wiring must be immediately replaced and repaired. In the event that an electrical fault has been detected the machine must not be operated until proper repairs have been made and the machine has been reset.

A.2.2 Hardware

Gloves must be worn when interacting within the plexiglass shield. This is to prevent grease and other debris from collecting inside the electrospinner. Prior to running an experiment,

the collector must be moved up and down on the rail to ensure there are no obstructions. The electrospinner must be cleaned thoroughly after every experiment. This cleaning is necessary to prevent polymer buildup on the rail and collector. The proper way to clean the electrospinner is to use the same solvent that was used in the experiment and wipe down the entire testing area inside the plexiglass shield. This includes the plastic flooring, the metal rail, the collector used, the nozzle, the plastic upright that holds the nozzle, and the syringe mounts. If proper cleaning is not done polymer solution may begin to build up and affect future experiments. If the solvent used in the previous experiment cannot be used for cleaning, then acetone may be used instead. If acetone is used extra care must be taken to ensure the entire electrospinner has been wiped down properly as the polymer may not dissolve as easily. The nozzle can be disassembled and placed in a 10 mL beaker that is full of 3 parts acetone/solvent and 7 parts water such that the nozzle assembly is fully submerged. This should be left for 24 hours to dissolve any polymer on the inside of the nozzle. If after 24 hours some polymer remains inside the nozzle assembly, it can be gently rubbed off using a gloved hand. After the nozzle has been removed from the 10 mL beaker and any remaining polymer has been gently rubbed off each component should be carefully dried using a paper towel. To properly dry the nozzle components, take one component in a gloved hand and gently roll it on a dry paper towel for 1 minute. After rolling for 1 minute inspect the component, if there are still visible water droplets on the component repeat the rolling process. Once all water droplets have been removed place the component on a dry paper towel and let it sit for 24 hours. After sitting for 24 hours reinspect the component for any polymer residue. If polymer residue remains first, try to gently rub the polymer off the component with a gloved hand. If the polymer cannot be gently rubbed off repeat the cleaning process by placing

the component in a 10 mL beaker consisting of 3 parts acetone/solution 7 parts water. A sonication step may also be performed. The benefits of sonication were not found to significantly improve the cleaning time for polycaprolactone dissolved in 1,1,1,3,3,3 hexafluoro-2-propanol at 7.5% (w/v).

A.3 Solution preparation

1. Each solution was characterized by the weight of solute to volume of solvent (w/v) see equation 2

$$\frac{\textit{weight}}{\textit{volume}} \% = \frac{\textit{weight of solute}}{\textit{volume of solution}} \times 100 \quad (2)$$

2. The desired amount of solid polymer particulate was massed out into weigh paper at the Biology building using a scale to the nearest thousandths
3. The weigh paper was then carefully folded and sealed using masking tape to prevent any spilling
4. The polymer was protected from any contact with water while being transported from the Biology building to the Engineering building
5. A clean 10 mL glass beaker was then taken and placed under the fume hood in the Materials Lab (EB 143)
6. The fume hood was then turned on
7. A 6.35 mm x 10.32 mm (1/4" x 13/32") magnetic stir bar was then carefully placed inside the 10 mL glass beaker
8. The polymer particulate was then transferred from the weigh paper to the 10 mL glass beaker under the fume hood
 - a. If some of the polymer particulate became stuck to the side of the glass ware or to the weigh paper a gentle nudge with a gloved finger was done to dislodge the polymer

9. The desired volume of solvent was then pipetted into a 10 mL graduated cylinder to measure the volume of solvent
10. The solvent was then slowly added to the 10 mL glass beaker
11. Two 2.5"x2.5" sheets of parafilm were cut from the box of parafilm in EB 254B
12. The first sheet of cut parafilm was placed on top of the 10 mL glass beaker such that the entire opening is covered
13. The parafilm was then gently pulled over the lip of the glass beaker and stretched tightly clockwise around the glass ware
14. The second sheet of cut parafilm was then placed on top of the first sheet such that it meets the same criteria outlined in step 12
15. The parafilm was then gently pulled over the lip of the glass beaker and stretched tightly counterclockwise around the glass ware
16. A magnetic stir plate was then carefully placed under the fume hood in EB 143
17. The magnetic stir plate was plugged in to the electrical outlet located on the left side of the fume hood when facing the south wall
 - a. Take extra precaution to make sure the cable does not knock over any equipment in the fume hood
18. Carefully place the 10 mL beaker in the center of the magnetic stir plate
19. Keeping all arms and hands clear from the magnetic stir plate switch the stir function to level 1
20. Observe the stirring of the polymer solution if the beaker moves in anyway carefully stabilize the beaker and gently push it back to the center of the magnetic stir plate with a gloved hand
21. Once the beaker is centered and is no longer moving the stir level may be increased up to level 3 if desired
 - a. After each increase in level repeat steps 19-21

22. The stirring may take up to an hour. While the beaker may be left unattended for intermittent periods of up to 10 minutes, if possible constant supervision should be maintained
23. Every 15 minutes the beaker should be checked for any polymer particulate stuck to the sides
 - a. If polymer particulates have become stuck carefully pick up the 10 mL beaker with a gloved hand and gently tap the side of the beaker with another gloved hand to dislodge the polymer
24. Once no visible polymer particulate remains a timer should be set for 15 minutes to ensure the solution is homogenous
25. At the end of the 15-minute timer the magnetic stir plate can be turned off
26. The 10 mL beaker can now be removed from the stir plate and should be placed on the counter under the fume hood
27. A 10 mL syringe should be taken from EB 254B to load the solution
28. Any wrapping or container around the syringe should be removed
29. The syringe should now be placed on the counter in the fume hood such that the hub does not touch any of its surroundings
30. Carefully remove each layer of parafilm from the 10 mL glass beaker with a gloved hand
31. Holding the glass beaker in one gloved hand pick up the 10 mL syringe with another gloved hand
32. Carefully insert the hub of the syringe into the polymer solution in the 10 mL glass beaker
33. Slowly pull the plunger out from the syringe to collect as much polymer solution as possible
 - a. It may be helpful to slightly tilt the 10 mL glass beaker in one direction to force the polymer solution to collect on one side of the glass ware
34. When all the polymer solution has been collected in the syringe carefully place the 10 mL beaker on the counter in the fume hood

35. With the syringe in one hand adjust your grip so the syringe hub is pointing up to check for any air bubbles in the syringe
 - a. If there are any air bubbles in the syringe wait for them to shift to the hub and then carefully push on the plunger until all the air has been ejected
36. When there is no air left in the syringe it may be moved from EB 143 to EB 254B

A.4 Electrospinning procedure

A.4.1 Parts of the electrospinner

The Inovenso NanoSpinner is located on the lab bench in room EB 254B. The operation and cleaning of the machine is laid out in this document. An overview of the different feature and buttons is provided in Figure A.1 and Figure A.2.

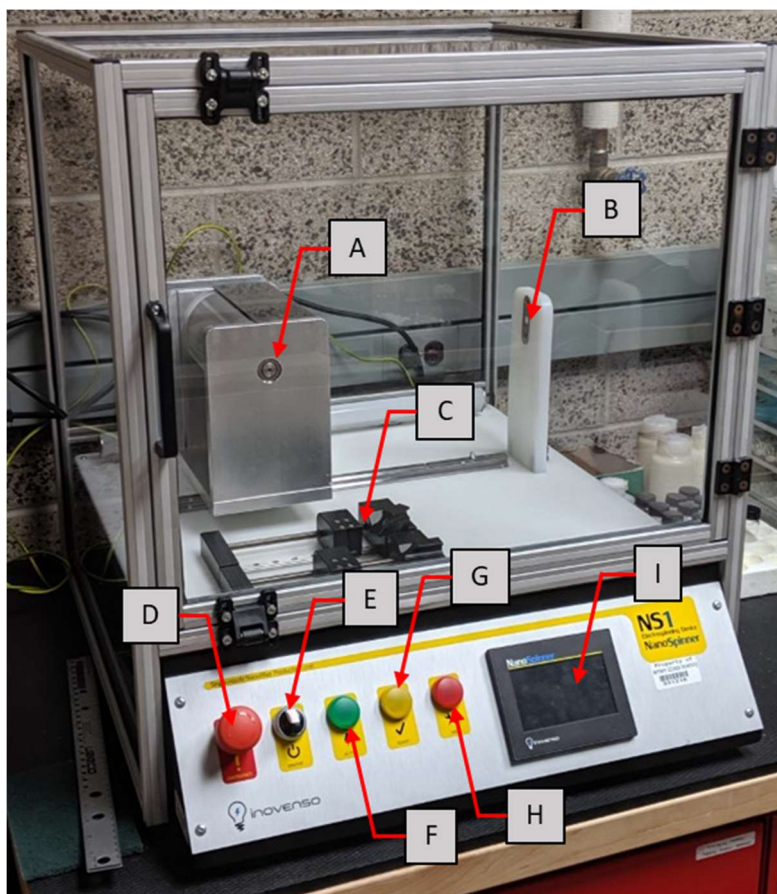


Figure A.1 Overview image of NanoSpinner

Index	Description
A	Collector plate/Roller
B	Nozzle Holder
C	Syringe Holder and ejection
D	Emergency shut-off
E	Power switch
F	Voltage active indicator
G	Ready for voltage indicator
H	Maintenance indicator
I	LCD settings display



Figure A.2 Close-up image of NanoSpinner LCD screen

Index	Description
A	Turn on roller
B	Adjust respective units for various operations
C	Turn on/off back light
D	Turn on syringe 1 (closest to collector)
E	Input syringe parameters for syringe 1
F	Turn on syringe 2 (closest to operator)
G	Maintenance button
H	Turn on voltage
I	Adjust values for various operations ex. increase/decrease voltage

A.4.2 Safe use of the NanoSpinner

1. Ensure the NanoSpinner is off open the Plexiglas shield and check to make sure the NanoSpinner has been properly cleaned
 - a. If the NanoSpinner has not been properly cleaned contact the last researcher to operate the NanoSpinner for information on proper cleaning or contact Dr. Vahabzadeh
2. Once the NanoSpinner has been properly cleaned determine whether the experiment requires the use of the roller collector (See Fig. A.1 callout A for location).
 - b. If the roller collector is desired remove the plate collector by sliding it upwards out of the grooves. Place the plate collector on top of the Plexiglas shield.
 - c. If the plate collector is desired ensure it is appropriately inserted into the slot see Fig. A.1. It may be desirable to cover the plate in aluminum foil to make retrieval of the fibers easier.
3. Determine what nozzle is appropriate for the experiment, either single or coaxial Continue following the steps under the appropriate section, for Monoaxial NanoSpinning see subsection *Monoaxial NanoSpinning* for Coaxial NanoSpinning see *Coaxial NanoSpinning*

A.4.3 Electrospinning quick start

1. Load the 10 mL syringe into the syringe holder and ejection zone C
2. Fix the plastic syringe to tube adapter to the hub of the syringe
3. Load the plastic tubing into the adapter and make a generous cut to ensure there will be enough tubing to reach the nozzle that will be placed at B
4. Turn on the electrospinner using the on/off switch D
5. Adjust the appropriate syringe ejector block so it only slightly contacts the syringe plunge using the on-screen buttons that should be displayed I. Figure D or F and the associated arrows in Figure I will adjust the ejector blocks location
6. Assemble the nozzle and place it firmly in the nozzle holding zone B
7. Connect the tubing to the nozzle

8. Set the collector distance manually and set all electrospinning parameters using the touch screen I and Figure
9. Close the plexiglass door
10. Turn on the voltage by pressing the voltage button Figure H
 - a. A warning message should pop up informing you that a high voltage is about to be applied use this time to double check all settings and the electrospinning setup. Once everything has been checked make sure the plexiglass door is closed and confirm the message
11. Electrospinning has now begun
12. At the end of the experiment turn off the electrospinner using the on/off switch D and follow the cleaning protocol

For a more detailed guide see 3.4 Monoaxial Electrospinning or 3.5 Coaxial Electrospinning

A.4.4 Monoaxial electrospinning

1. Assemble the nozzle by screwing the tube adapter to the chosen nozzle.
2. Once the nozzle is assembled insert tubing into the nozzle by pressing down on the black outer ring and pushing the nozzle into the hole, the nozzle should insert a few millimeters.
3. Determine which Syringe holder and ejector you will use and cut the tubing to size. (See Fig. A.1 callout *C* for location).
4. Insert the nozzle into the holding tower by pushing it through the back side such that the nozzle points towards the collector and the tubing comes out towards the Plexiglas shield. (See Fig. A.1 callout *B* for location).
5. Position the Collector by sliding it on the rail mount, using a ruler measure from the tip of the nozzle and place the front edge of the collector at the desired distance
6. Carefully load the syringe with the desired amount of solution, be sure to remove any air bubbles that enter the syringe.
7. Turn on the Nanospinner by twisting the power dial clockwise. (See Fig. A.1 callout *E* for location).
8. Once the NanoSpinner is on check to make sure the LCD display is identical to Fig. A.2.
9. Press either Fig. A.2 callout *D* if the syringe will be placed in the holder closest to the collector or callout *F* if the syringe will be placed in the holder closest to the operator.
10. Press and hold down the arrow pointing to the left, on the same row as the nozzle see Fig. A.2 callout *I* until enough space has been cleared so the syringe can be inserted
11. Place the syringe in the Syringe holder such that the Barrel flange is snug against the holder and lock it in place.
12. Press and hold down the arrow pointing to the right, on the same row as the nozzle see Fig. A.2 callout *I* until the block is close to but not yet touching the syringe
13. Check all the units for each variable see Fig. A.2 callout *B*. To adjust the units, press the box that should be changed and follow the on-screen instructions.

14. Once all the units have been correctly set ensure the syringe diameter has been properly set by checking the custom section of Fig. A.2 callout *E*. The syringes currently in stock (1/6/2020) have a custom value of 14.25. If the value is incorrect and needs to be changed press on the custom box and follow the onscreen instructions. NOTE callout *E* is for the syringe holder closest to the collector, to adjust the values for the other holder see the identical layout below Fig. A.2 callout *E*
15. Set the appropriate values for each variable by pressing the yellow box next to the variable intended to be set and following on-screen instructions, refer to Fig. A.2 for what each symbol represents.
16. Double check to ensure all the values have been properly set, if the Plexiglas shield is still open close it at this time. Turn on the electromagnetic field by pressing the lightning symbol See Fig. A.2 callout *H*
17. Enable the syringe feeding by pressing the appropriate syringe symbol Fig. A.2 callout *D* if the syringe is in the holder closest the collector or Fig. A.2 callout *F*
18. The NanoSpinner is now engaged in the spinning process watch the fluid from the syringe progress through the tubing, this may take some time. When the fluid reaches the nozzle observe the cone and adjust feed rate/voltage if needed to achieve a proper Taylor cone
19. Once the experiment has completed Turn off the voltage by again pressing the lighting symbol See Fig. A.2 callout *H*. Carefully remove the fibers and begin the cleaning process using the same solvent used in aqueous solution. Adhere to all material specific guidelines

A.4.5 Coaxial electrospinning

1. Assemble the nozzle by screwing the tube adapter to the chosen nozzle.
2. Once the nozzle is assembled insert tubing into the nozzle by pressing down on the black outer ring and pushing the nozzle into the hole, the nozzle should insert a few millimeters. This must be completed for two separate tubes as both will be used
3. For coaxial NanoSpinning both Syringe holders will be used determine which solution will be the outer layer and which will be the inner layer. Use the syringe holder closest

to the collector for the inner layer and the syringe holder closest to the operator for the outer layer. (See Fig. A.1 callout *C* for location).

4. Insert the nozzle into the holding tower by pushing it through the back side such that the nozzle points towards the collector and the tubing comes out towards the Plexiglas shield. (See Fig. A.1 callout *B* for location).
5. Position the Collector by sliding it on the rail mount, using a ruler measure from the tip of the nozzle and place the front edge of the collector at the desired distance
6. Carefully load the syringes with the desired amount of solution, be sure to remove any air bubbles that enter the syringe.
7. Turn on the Nanospinner by twisting the power dial clockwise. (See Fig. A.2 callout *E* for location).
8. Once the NanoSpinner is on check to make sure the LCD display is identical to Fig. A.2
9. Press either Fig. A.2 callout *D* for the syringe loaded with the inner solution and callout *F* for the syringe loaded with the outer solution.
10. Press and hold down the arrow pointing to the left, on the same row as the nozzle see Fig. A.2 callout *I* until enough space has been cleared so the syringe can be inserted
11. Place the syringe in the Syringe holder such that the Barrel flange is snug against the holder and lock it in place.
12. Press and hold down the arrow pointing to the right, on the same row as the nozzle see Fig. A.2 callout *I* until the block is close to but not yet touching the syringe. Repeat Steps 12-15 for the remaining holder.
13. Check all the units for each variable see Fig. A.2 callout *B*. To adjust the units, press the box that should be changed and follow the on-screen instructions.
14. Once all the units have been correctly set ensure the syringe diameter has been properly set by checking the custom section of Fig. A.2 callout *E*. The syringes currently in stock (1/6/2020) have a custom value of 14.25. If the value is incorrect and needs to be changed press on the custom box and follow the onscreen instructions. Repeat this for the identical box directly below Fig. A.2 callout *E*

15. Set the appropriate values for each variable by pressing the yellow box next to the variable intended to be set and following on-screen instructions, refer to Fig. A.2 for what each symbol represents.
16. Double check to ensure all the values have been properly set, if the Plexiglas shield is still open close it at this time. Turn on the electromagnetic field by pressing the lightning symbol See Fig. A.2 callout *H*
17. Enable the syringe feeding by pressing the appropriate syringe symbol Fig. A.2 callout *D* and Fig. A.2 callout *F*
18. The NanoSpinner is now engaged in the spinning process watch the fluid from the syringe progress through the tubing, this may take some time. When the fluid reaches the nozzle observe the come and adjust feed rate/voltage if needed to achieve a proper Taylor cone
19. Once the experiment has completed Turn off the voltage by again pressing the lighting symbol See Fig. A.2 callout *H*. Carefully remove the fibers and begin the cleaning process using the same solvent used in aqueous solution. Adhere to all material specific guidelines